Abstract

Abstract of thesis entitled 'Stress Intensity Factors for Cracks at or Close to and Parallel to an Interface'

submitted by Wai-Man Grace, So

for the Degree of Master of Philosophy.

at The Hong Kong Polytechnic University in December 2001.

The problems concerning cracks at or close to the interface of two dissimilar materials are gaining importance for their applications in the use of advanced and composite materials, and in electronic packaging. In this work, methods for determining the complex stress intensity factors for cracks on an interface were examined and improved, while conventional stress intensity factors for cracks close to and parallel to an interface are also determined, with a view of designing a test specimen for studying such cracks.

In the case of interfacial cracks, plates and beams of various thickness and modulus ratios are modeled for finite element analysis and the complex stress intensity factors of interfacial cracks are obtained by a new modified stiffness derivative method. This new method made use of the strain energies of near-crack-tip elements before and after a virtual crack extension. The cumbersome need for computing element stiffnesses in the originally and commonly adopted procedure is removed. Accuracy of the method was verified for central cracks, edge cracks and the four-point bending specimen configuration.

In the case of cracks close and parallel to the interface, a bimaterial four point bending specimen is developed. Finite element analysis is employed to determine specimen configurations that produce constant strain energy release rates.

A crack surface displacement method is employed to find the stress intensity factors for beams of different thickness ratios and modulus ratios, different crack lengths and for cracks at various distances from the interface. Displacements on the crack surface are then used in conjunction with a semi-infinite-crack crack model to solve for the opening mode and the shearing mode stress intensity factors. Basing on the strain energy release rate and stress intensity factor plots, recommendations for support spacing and specimen heights are made. Due to the large number of parameters involved, a special way for normalizing the stress intensity factor values is implemented by using values from a beam of the same dimension but consisting of one material only. These normalized values are curve-fitted using a combination of power and polynomial terms in the distance between the crack and the interface. The use of these curves is demonstrated by an application to cracks near solder/copper, Ni/MgO, and Si/Cu interfaces. Finally the relationship between the conventional stress intensity factors for a crack close to and parallel to the interface and the complex stress intensity factors of a corresponding interfacial crack is studied. The validity of a closed-form relationship is established within a certain range of crack-interface separation distance.

Stress Intensity Factors for Cracks at or Close to and Parallel to an Interface

by

Wai-Man Grace, So

A thesis submitted to.
The Hong Kong Polytechnic University
for the Degree of
Master of Philosophy

2001

Department of Mechanical Engineering
The Hong Kong Polytechnic University

Declaration

I declare that this thesis contains no material, which has previously been presented for the award of any other degree or diploma in any other University or Institute. To the best of my knowledge, the material is original except where due reference is made in the text of the thesis.

Signed by :

Wai-Man Grace, So

Acknowledgements

I would like to express my deepest gratitude towards my supervisors Dr. K.J. Lau and Dr. P.C. Tse for their patience and guidance throughout the research project. It will not be successful without their support and enlightenment.

I would like to thank all the staff and technicians in the laboratories and offices for their support.

I would also like to thank my family and my friends for their love and care during my study.

All the work described in this study has been supported by the Research Grants Council of Hong Kong, China (Project no. PolyU 5122/98E).

Nomenclature

A

A $= \frac{K_1^2 + K_2^2}{H}$, defined in Equation …(3.6)

a half crack length for embedded cracks and cracks on the four point bend specimen (interfacial or subinterfacial); and whole crack length for edge cracks

A $= \frac{1}{1 + 4\eta + 6\eta^2 + 3\eta^3}$, found in Equation …(4.7)

A_n Coefficient for normalization (coeffcient of the power term)

B

$\boldsymbol{B}$ $= \frac{(K_1 + \Delta K_1)^2 + K_2^2}{H}$, defined in Equation …(3.7)

B width of the four point bend specimen

B_n Coefficient for normalization (power of the power term)

b the length of crack surface on which a pressure p is applied

b_{root} solution (length of crack surface with applied pressure) of semi-infinite crack model in determining the stress intensity factor

C

$\boldsymbol{C}$ $= \frac{\Delta K_1^2}{H}$, defined in Equation …(3.12)

C_n Coefficient for normalization (coeffcient of the 3rd order polynomial term)

C_1 $= \frac{1}{(1/\eta) + 1}$

C_2 $= \frac{6/\eta}{[(1/\eta) + 1]^3}$

C_3 $= \frac{1}{[(1/\eta)+1]^3}$.

c power of tenths which bounds the solution for the semi-infinite crack model i.e. soltuion exists between 10^c and 10^{c-1} (found in Appendix I)

D

D $= \frac{K_1^2 + (K_2 + \Delta K_2)^2}{H}$, defined in Equation ...(3.15)

D_n Coefficient for normalization (coeffcient of the 2nd order polynomial term)

d horizontal distance between the inner and outer load points of the four point bend specimen

dA change of crack length

ds an infinitesimal length along the path Γ.

dU change of strain energy

E

E $= \frac{\Delta K_2^2}{H}$, defined in Equation ...(3.16)

E Young's modulus

E_1 Young's modulus of material 1

E_2 Young's modulus of material 2

E_j Young's modulus of material j

E_n Coefficient for normalization (coeffcient of the 1st order polynomial term)

E^* $= \left[\frac{1}{2}\left(\frac{1}{\overline{E_1}} + \frac{1}{\overline{E_2}}\right)\right]^{-1}$

$\overline{E_j}$ $= E_j$ for plane stress and

$= \frac{E_j}{1-\nu_j^2}$ for plane strain

e the quarter point element size

e/a relative quarter point element size in terms of ratio of quarter point element size to the (half) crack length

F

F_{iref} Reference value from which reference complex stress intensity factors can be detemined

F_n Coefficient for normalization (the constant term)

F_T equivalent tensile load applied on the beam with thickness T in Appendix IV

F_{T+t} original tensile load applied on the beam with thickness $T+t$ in Appendix IV

f_{x1} , f_{y1} , f_{x2} and f_{y2} displacement functions for interface cracks in Appendix II

G

G strain energy release rate

G_3 strain energy release rate of 3-layered beam defined by Equation ...(4.1)

G_c critical strain energy release rate when fracture occurs

G_{ss} Steady state strain energy release rate

H

H $=E^* \cdot \cosh^2(\pi\varepsilon)$, a material constant

H_1 thickness of the upper layer of the four point bend specimen, i.e. material 1, where the crack exists

H_2 thickness of the lower uncracked layer of the four point bend specimen, i.e. material 2

H_3 total thickness of the four point bend specimen, i.e. $H_3=H_1+H_2$

h vertical distance of the crack from the interface in the subinterfacial crack specimen

I

I $= \frac{1}{12\left(1+\eta^3\right)}$, found in Equation ...(4.7)

I_2 moment of inertia of the cracked thinner portion of the 3-layered beam

I_3 moment of inertia of the uncracked thicker portion of the 3-layered beam

I_T moment of inertia of a beam with thickness T in Appendix IV

$I_{(T+t)}$ moment of inertia of a beam with thickness $T+t$ in Appendix IV

J

j material index

K

$\boldsymbol{K}$ $= K_1 + iK_2$, complex stress intensity factor

K_1 real part of complex stress intensity factor

K_{1CSD} real part of complex stress intensity factor obtained by crack surface displacements

K_{1ref} real part of complex stress intensity factor of reference value

K_2 imaginary part of complex stress intensity factor

K_{2CSD} imaginary part of complex stress intensity factor obtained by crack surface displacements

K_{2ref} imaginary part of complex stress intensity factor of reference value

K_c critical stress intensity factors (i.e. stress intensity factors at onset of crack propagation)

K_I the stress intensity factor under mode I loading

K_{I0} the eventual denominator for the normalization procedure for K_I

K_{II} the stress intensity factor under mode II loading

K_{II0} the eventual denominator for the normalization procedure for K_{II}

L

L half distance between two inner load points of the four-point bend speicmen

L_Q length of the quarter point element side

L_T the size of the transition element

l characteristic length taken for normalization in determining complex stress intensity factors

M

M bending moment applied on the specimen

M^* equivalent bending moment of the system with M_1, M_2 and M_3 applied to the half specimen

M^{**} resultant of M^*

M_o the resultant bending moment acting on the material 1 area of the full cross-section in front of the crack tip using elementary beam bending theory

M_1, M_2 and M_3 bending moments applied to the half specimen (divided along the plane of symmetry) along the neutral axis of the corresponding portion

M_T equivalent bending moment applied on the beam with thickness T in Appendix IV

M_{T+t} total bending moment applied on the beam with thickness $T+t$

m the geometric progression factor of element size from the crack-tip for meshing

N

N_1 the total number of crack-tip elements in application of SDM

$\mathbf{n}$ the outward drawn normal

n $= \overline{\frac{E_2}{E_1}}$, modulus ratio with consideration of plane stress/strain

P

P perpendicular force applied to the four point bend specimen

P^* equivalent tensile force of the system with P_1, P_2 and P_3 applied to the half specimen

P_o the resultant tensile force acting on the material 1 area of the full cross-section in front of the crack tip using elementary beam bending theory

P_1, P_2 and P_3 tensile forces applied in xy-plane at the ends of the half specimen (divided along the plane of symmetry) along the neutral axis of the corresponding portion

p opening pressure on the crack surface in the semi-infinite model

p_1 opening pressure on the crack surface in the semi-infinite model in terms of (x_1, v_{I1})

p_2 opening pressure on the crack surface in the semi-infinite model in terms of (x_2, v_{I2})

p_q the position of the mid-side node of the transistion element

p_{root} solution (pressure applied on crack surface) of semi-infinite crack model in determining the stress intensity factor

Q

q half the ratio of the quarter-point element size to the transition element size

q_s $= \left(\frac{1-\beta^2}{1+\alpha} \right)^{0.5}$, a material constant

R

r radius in polar coordinate with (0,0) at crack-tip

S

S the four point bend specimen length

$[S_j^{ct}]$ the element stiffness matrix of the crack-tip elements

T

T the traction vector on a plane defined by the outward drawn normal **n**

T thickness of lower portion of a beam taken for determination of equivalent tensile force and bending moment in Appendix IV

t thickness of upper portion of a beam in Appendix IV

U

u displacement in x-direction

U strain energy

$\boldsymbol{u}$ the displacement vector on a plane defined by the outward drawn normal vector **n**

u' nodal displacement on upper crack surface in x-direction

u'' nodal displacement on lower crack surface in x-direction

u_{II} decoupled sliding displacment of a particular node pair on the crack surface

u_n the current resulting displacement by the applied load

u_x displacement in x-direction

u_y displacement in y-direction

$\{u_j^{ct}\}$ the displacement matrix of the crack-tip elements

V

v displacement in y-direction

v' nodal displacement on upper crack surface in y-direction

v'' nodal displacement on lower crack surface in y-direction

v_I decoupled opening displacment of a particular node pair on the crack surface

W

w plate width

X

x, y and z Cartesian coordinates

Y

y_2 neutral axis of the thinner cracked portion with reference from the bottom and taking material 1 as reference material

y_3 neutral axis of the thicker uncracked portion with reference from the bottom and taking material 1 as reference material

Y_{KI} normalized stress intensity factor of K_I

Y_{KII} normalized stress intensity factor of K_{II}

Z

z a complex number with $z = x + i\,y$

Greek variables

α Dundur's elastic mismatch parameter

β Dundur's elastic mismatch parameter

Δa the absolute size of virtual crack extension

$\Delta a/e$ the relaive size of virtual crack extension per length of quarter point element' side

ΔK arbitrary perturbation of stress intensity factor

ΔK_1 arbitrary perturbation of stress intensity factor K_1

ΔK_2 arbitrary perturbation of stress intensity factor K_2

δ_x $= u(r,\pi) - u(r,-\pi)$, opening displacement in x-direction

δ_y $= v(r,\pi) - v(r,-\pi)$, opening displacement in y-direction

ε $= \frac{1}{2\pi} \ln\left[\frac{\kappa_1\mu_2 + \mu_1}{\kappa_2\mu_1 + \mu_2}\right]$, oscillatory constant

ϕ single dimensionless function of the elastic moduli $\phi(\alpha,\beta)$ found in Table X.1 in Appendix X.

Γ any arbitrary path enclosing the crack-tip starting from the bottom crack surface ending on the upper crack surface

γ_s surface energy per unit area

γ_p energy consumed on plastic deformations around the crack-tip per unit area

η the thickness ratio defined by $\eta = \frac{h}{H_1 - h}$

κ_j $= 3 - 4\nu_j$ for plane strain and

$= \frac{3 - \nu_j}{1 + \nu_j}$ for plane stress

μ_1 shear modulus of material 1

μ_2 shear modulus of material 2

ν_1 Poisson ratio of material 1

ν_2 Poisson ratio of material 2

ν_j Poisson ratio of material j

θ angle in polar coordinate with (0,0) at crack-tip

σ tensile stress

σ_{xb} the nominal flexural (x-direction) stresses in material 1 on the bottom layer (interface)

σ_{xt} the nominal flexural (x-direction) stresses in material 1 at the top layer (free surface)

τ shear stress

ω $\approx 52.1\text{-}3\eta$, with ω and η in degrees; defined as phase factor, which is a single dimensionless function of the elastic moduli $\omega(\alpha,\beta)$

ψ $= \arctan\left[\frac{K_2}{K_1}\right]$, phase angle

Table of Contents

Abstract i

Declaration v

Acknowledgements vi

Nomenclature vii

Table of Contents xvii

Chapter 1 Linear Elastic Fracture Mechanics 1

INTRODUCTION 1

1.1 THE STRAIN ENERGY RELEASE RATE G AND GRIFFITH THEORY 1

1.2 PLASTIC DEFORMATIONS AND IRWIN'S MODIFICATION 2

1.3 THE THREE MODES OF FRACTURE 3

1.4 THE STRESS INTENSITY FACTOR K AND THE CRITICAL STRESS INTENSITY FACTOR K_C 4

1.5 STRESS AND DISPLACEMENT FIELD IN THE VICINITY OF THE CRACK-TIP 5

1.6 THE RELATION BETWEEN K AND G 7

1.7 INTERFACIAL FRACTURE MECHANICS 8

Chapter 2 Finite Element Methods on Determination of Stress Intensity Factors 11

INTRODUCTION 11

2.1 CRACK-TIP SINGULARITY MODELLING 12

2.2 INTERPRETATION OF THE FINITE ELEMENT RESULTS 14

2.2.1 Displacement-Based Stress Intensity Factor Computation Techniques *14*

2.2.1.1 The Semi-Infinite Crack Model 15

2.2.1.2 The Displacement Correlation Technique (DCT) and Quarter Point Displacement Technique (QPDT) 17

2.2.2 Energy-Based Stress Intensity Factor Computation Techniques *19*

2.2.2.1 The J-integral 19

2.2.2.2 Stiffness Derivative Method (SDM) 21

Chapter 3 Determination of Complex Stress Intensity Factors of Interface Cracks by FEA 23

3.1 INTRODUCTION 23

3.2 THE FEA METHOD ON DETERMINING COMPLEX STRESS INTENSITY FACTORS 25

3.2.1 Modified SDM by Ng and Lau (2000) *26*

3.2.2 Wu's (1994) method on extracting the complex stress intensity factors *27*

3.2.3 Combination of Ng and Lau's (2000) SDM with Wu's (1994) Method *31*

3.3 VALIDATION OF THE COMBINED METHOD 34

3.3.1 Interface Crack in Infinite Plate under Biaxial Loading *36*

3.3.1.1 Effect of Quarter Point Element Size *e* 39

3.3.1.2 Effect of the Geometric Progression Factor *m* 43

3.3.1.3 Effect of the Virtual Crack Extension Length Δa 47

3.3.1.4 Effect of Variation of Material Properties 49

3.3.2 Center Interface Crack in Finite Bimaterial Plate *51*

3.3.3 Single Edge Interface Crack in Finite Bimaterial Plate *54*

3.3.4 Interface Cracks in Four-Point Bend Specimen *57*

3.4 CONCLUSION 60

Chapter 4 Design of a Four Point Bend Specimen for Subinterfacial Crack Studies 61

4.1 INTRODUCTION 61

4.2 FOUR-POINT BENDING SPECIMEN FOR SUB-INTERFACIAL CRACK DETERMINATION 63

4.3 DETERMINATION OF STRESS INTENSITY FACTORS FOR CRACKS PARALLEL TO AN INTERFACE 66

4.3.1 The Normalization Procedure *69*

4.3.2 Verification of the Preliminary Results *73*

4.3.3 The Relation of Steady State to the Crack Length *74*

4.3.4 Curvefitting for Normalization of K_I and K_{II} *83*

4.3.5 Applications of the Tables 4.2 and 4.3 ..... *94*

4.4 RELATION OF SUBINTERFACIAL CRACKS TO INTERFACIAL CRACKS 99

4.5 CONCLUSION 103

Chapter 5 Preliminary Experimentation and Suggestions for Further Studies 104

5.1 SPECIMEN WITHOUT "INTERFACIAL PROPERTIES" 104

5.2 CHARACTERISTICS AND APPLICATIONS OF THE SPECIMEN 106

Chapter 6 Conclusion 111

Reference List 113

Appendix I Solving Algorithm of (p,b) and (τ,b) A-1

Appendix II The Displacement Functions for Interface Cracks A-4

Appendix III Tables of Results in Chapter 3 ..... A-5

Appendix IV Superposition for Beams A-8

Appendix V Equilibrium in Beams A-10

Appendix VI Plots of Stress Intensity Factors Against Crack Length for Specimens with Subinterfacial Cracks A-14

Appendix VII Steady State Regions of Extreme Cases A-23

Appendix VIII Tables of Stress Intensity Factors for Subinterface Crack Specimen A-27

Appendix IX The Stress Intensity Plots against the Penetration Ratio A-35

Appendix X Table of ϕ and the plots of Section 4.4 ..... A-40

Chapter 1 Linear Elastic Fracture Mechanics

INTRODUCTION

Cracks and flaws are minute discontinuities naturally present in solid bodies. The presence of these cracks may lead to failure of the component within operating loads. The purpose of fracture mechanics studies is to define a measurable and employable material property to parameterize fracture resistance of bodies containing cracks. Efforts have lead to two important parameters that serve this purpose : the strain energy release rate G and the stress intensity factor K . Cracks in isotropic media and cracks along an interface are separated into different families of fracture studies with different definitions of the strain energy release rate and stress intensity factor. Both studies are based on the assumption that the plastic deformations are only confined to small scales close to the crack-tip comparing to the smallest dimension of the system. This class of study on small scale plastic zone is called the Linear Elastic Fracture Mechanics (LEFM). This chapter includes the definitions of the strain energy release rate and the stress intensity factor for cracks in isotropic bodies and for interfacial cracks. In the next chapter, the methods of their determinations by finite element analysis (FEA) will be introduced.

I.I THE STRAIN ENERGY RELEASE RATE G AND GRIFFITH THEORY

The concept of fracture toughness was first developed by Griffith (1920). He proved experimentally that the fracture resistance of ideally brittle materials could be measured by comparing the strain energy release rate G to the work done in forming newly cracked surfaces of the material. The strain energy release rate G is

defined as the release of strain energy $-dU$ per unit increment in crack area dA in case the crack advances and thus relaxes the body, i.e.

$$G = -\frac{dU}{dA} \qquad \ldots(1.1)$$

It is a function of geometrical parameters, material parameters and loading configuration of the solid body containing the crack. The work done to create new surfaces per unit area is equal to the surface energy γ_s. The condition for a crack to propagate is :

$$G \geq G_c \qquad \ldots(1.2)$$

The critical strain energy release rate G_c, which is one of the fracture toughness parameters, is defined as the critical value of G when the crack starts to propagate. It is a material property similar to the surface energy. Thus for ideally brittle materials :

$$G_c = 2\gamma_s \qquad \ldots(1.3)$$

This is the Griffith theory of fracture.

1.2 Plastic Deformations and Irwin's Modification

Irwin (1936), with the support of Orowan's (1949) findings and his observations on ductile fracture of metals, modified the decrease in strain energy to account for energy consumed on plastic deformations around the crack-tip, γ_p, as well. Then the critical strain energy release rate is given by :

$$G_c = 2\gamma_s + \gamma_p \qquad \ldots(1.4)$$

And for ductile materials, this energy is far greater than the energy spent on forming new surfaces.

$$G_c \cong \gamma_p \qquad \ldots(1.5)$$

Since then, the Griffith approach can be applied on metals as well. This modified Griffith theory is valid only for cracks with small region of plastic deformations comparing to the smallest dimensions of the cracked body. This condition is the basic assumption of LEFM whenever it is applied. All our discussions following on will be based on small scale plastic deformations.

1.3 THE THREE MODES OF FRACTURE

The loading condition and deformation of a crack can be classified into three modes, with respect to the movement of the fracture surfaces, as shown in Figure 1.1. The modes will be denoted by Roman subscripts (I, II, III) for cracks in isotropic bodies and by Arabic subscripts (1, 2, 3) for interface cracks. Mixed mode fracture happens when a crack is subjected to a combination of two or more modes.

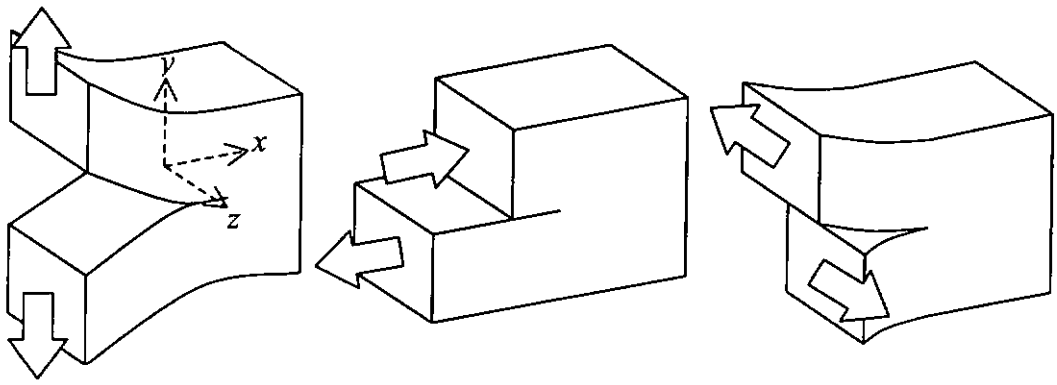

a) Mode I b) Mode II c) Mode III

Figure 1.1 The Three Modes of Fracture : a) Opening Mode I ; b) Shearing Mode II ; c) Tearing Mode III

a) Opening mode I : crack surfaces pulled apart from each other in the y-direction ;

b) Shearing mode II : crack surfaces slide over each other in the x-direction ; and

c) Tearing mode III : crack surfaces slide over each other in the z-direction.

1.4 THE STRESS INTENSITY FACTOR K AND THE CRITICAL STRESS INTENSITY FACTOR K_C

It has been shown (e.g. Sneddon (1946)) that the stresses in the vicinity of the crack-tip, under mode I loading, has the general form, for all loading and geometrical configurations of the body:

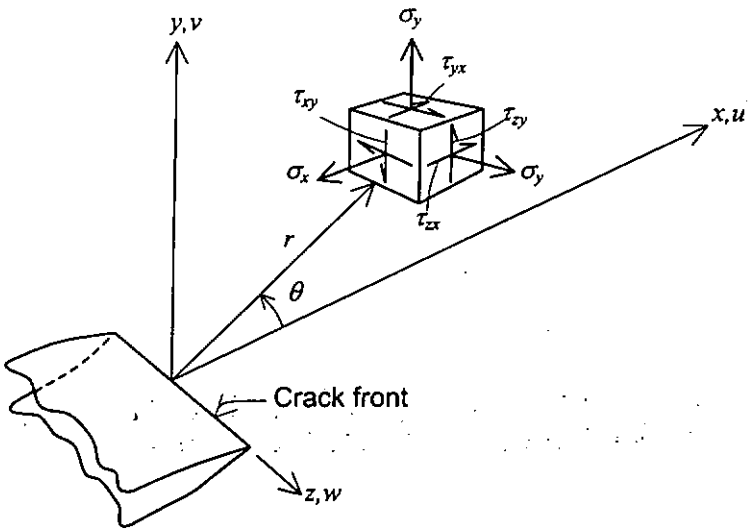

Figure 1.2 Three-dimensional crack-tip coordinate and stress systems

$$\sigma_x = \frac{K_I}{\sqrt{2\pi r}}\cos\left(\frac{\theta}{2}\right)\left[1-\sin\left(\frac{\theta}{2}\right)\sin\left(\frac{3\theta}{2}\right)\right] + \text{non-singular terms}$$

$$\sigma_y = \frac{K_I}{\sqrt{2\pi r}}\cos\left(\frac{\theta}{2}\right)\left[1+\sin\left(\frac{\theta}{2}\right)\sin\left(\frac{3\theta}{2}\right)\right] + \text{non-singular terms}$$

$$\tau_{xy} = \frac{K_I}{\sqrt{2\pi r}}\cos\left(\frac{\theta}{2}\right)\sin\left(\frac{\theta}{2}\right)\cos\left(\frac{3\theta}{2}\right) + \text{non-singular terms} \qquad \ldots(1.6)$$

where (r,θ) are polar coordinates from the right hand crack-tip and the stresses are shown in Figure 1.2. Note that all stresses approaches infinity as r tends to zero. This is referred to as the stress singularity. K_I is named the stress intensity factor under

mode I loading and measures the magnitude of the crack tip stress singularity. The stress intensity factor, K, is a function of geometry and loading conditions of the cracked body. The critical stress intensity factor K_c is also defined as the value of K on the onset of crack propagation. Similar to G_c, K_c is also a material property and is another fracture toughness parameter.

1.5 STRESS AND DISPLACEMENT FIELD IN THE VICINITY OF THE CRACK-TIP

The stress and displacement fields are represented in magnitude by the stress intensity factor and have a general form for each mode of loading and deformation. They can be treated by superposition for mixed mode problems. As mentioned in Section 1.4, the stresses will tend to infinity as its position gets closer to the crack-tip therefore allowing one to simplify the expressions by neglecting the non-singular terms. Under plane strain they are given by Equation ...(1.7) and Equation ...(1.8). For plane stress, the expressions can be obtained by putting $\sigma_z = 0$ and replacing ν by $\frac{\nu}{1+\nu}$.

Mode I (plane strain) :

$$\sigma_x = \frac{K_I}{\sqrt{2\pi r}}\cos\left(\frac{\theta}{2}\right)\left[1-\sin\left(\frac{\theta}{2}\right)\sin\left(\frac{3\theta}{2}\right)\right]$$

$$\sigma_y = \frac{K_I}{\sqrt{2\pi r}}\cos\left(\frac{\theta}{2}\right)\left[1+\sin\left(\frac{\theta}{2}\right)\sin\left(\frac{3\theta}{2}\right)\right]$$

$$\tau_{xy} = \frac{K_I}{\sqrt{2\pi r}}\cos\left(\frac{\theta}{2}\right)\sin\left(\frac{\theta}{2}\right)\cos\left(\frac{3\theta}{2}\right) \qquad \ldots(1.7)$$

$$\sigma_z = \nu(\sigma_x + \sigma_y), \qquad \tau_{xz} = \tau_{yz} = 0$$

$$u = \frac{K_I}{\mu}\sqrt{\frac{r}{2\pi}}\cos\left(\frac{\theta}{2}\right)\left[1-2\nu+\sin^2\left(\frac{\theta}{2}\right)\right]$$

$$v = \frac{K_I}{\mu}\sqrt{\frac{r}{2\pi}}\sin\left(\frac{\theta}{2}\right)\left[2-2\nu-\cos^2\left(\frac{\theta}{2}\right)\right]$$

$$w = 0$$

where μ is the shear modulus of elasticity,

ν the Poisson's ratio and

$$K_I = \sqrt{2\pi r}\lim_{r\to 0}\sigma_y$$

Mode II (plane strain) :

$$\sigma_x = \frac{K_{II}}{\sqrt{2\pi r}}\sin\left(\frac{\theta}{2}\right)\left[2+\cos\left(\frac{\theta}{2}\right)\cos\left(\frac{3\theta}{2}\right)\right]$$

$$\sigma_y = \frac{K_{II}}{\sqrt{2\pi r}}\sin\left(\frac{\theta}{2}\right)\cos\left(\frac{\theta}{2}\right)\cos\left(\frac{3\theta}{2}\right)$$

$$\tau_{xy} = \frac{K_{II}}{\sqrt{2\pi r}}\cos\left(\frac{\theta}{2}\right)\left[1-\sin\left(\frac{\theta}{2}\right)\sin\left(\frac{3\theta}{2}\right)\right] \qquad \ldots(1.8)$$

$$\sigma_z = \nu(\sigma_x + \sigma_y), \qquad \tau_{xz} = \tau_{yz} = 0$$

$$u = \frac{K_{II}}{\mu}\sqrt{\frac{r}{2\pi}}\sin\left(\frac{\theta}{2}\right)\left[2-2\nu+\cos^2\left(\frac{\theta}{2}\right)\right]$$

$$v = \frac{K_{II}}{\mu}\sqrt{\frac{r}{2\pi}}\cos\left(\frac{\theta}{2}\right)\left[-1+2\nu+\sin^2\left(\frac{\theta}{2}\right)\right]$$

$$w = 0$$

where $K_{II} = \sqrt{2\pi r}\lim_{r\to 0}\tau_{xy}$

1.6 THE RELATION BETWEEN K AND G

For single mode fracture, it can be shown (Irwin (1957)) that :

$$G = \frac{K_I^{\,2}}{\overline{E}} \qquad \ldots(1.9)$$

where $\overline{E} = E$ for plane stress and

$\overline{E} = \dfrac{E}{1-\nu^2}$ for plane strain

E is the Young's modulus.

For mixed mode loading :

$$G = \frac{K_I^{\,2} + K_{II}^{\,2}}{\overline{E}} \qquad \ldots(1.10)$$

for cracks extending in a self-similar manner.

1.7 INTERFACIAL FRACTURE MECHANICS

One of the complications in interface fracture mechanics is that, due to the difference in moduli, the resulting stresses are in mixed mode even though single mode loading conditions are applied. The other complication is that the bimaterial

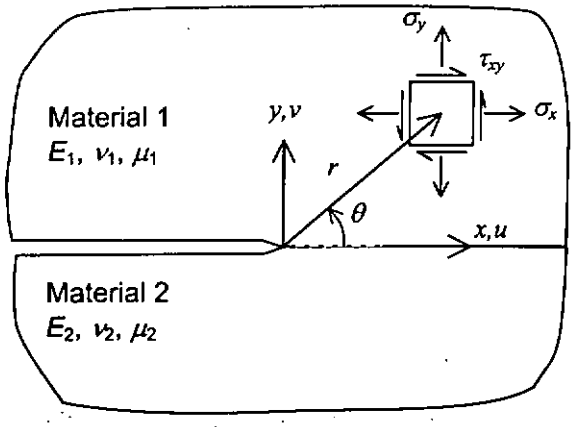

Figure 1.3 Geometry and conventions for an interface crack

constant ε (see Equation ...(1.12)) introduces an oscillatory singularity into the theoretical near crack-tip solution, which implies that crack face interpenetration occurs near the crack-tip. In practice, this really means crack closure. However, this contact is comparatively smaller than the crack-tip plastic zone and therefore can be neglected, (Hutchinson and Suo (1992)). Consider Figure 1.3, the coupled stress field along the interface ($\theta = 0$) and near the crack-tip is expressed (Murakami (1987)) in complex form :

$$\sigma_y + \mathrm{i}\,\tau_{xy} = \frac{K_1 + \mathrm{i}\,K_2}{\sqrt{2\pi r}} \left(\frac{r}{l}\right)^{\mathrm{i}\varepsilon} \qquad \ldots(1.11)$$

where $\mathrm{i} = \sqrt{-1}$; $\qquad r^{\mathrm{i}\varepsilon} = \cos(\varepsilon \ln r) + \mathrm{i}\sin(\varepsilon \ln r)$;

$l = 1$ for most of the cases here in our study, unless specified ;

$K_1 + iK_2 = \boldsymbol{K}$, the *complex stress intensity factor* and

$$\varepsilon = \frac{1}{2\pi}\ln\left[\frac{\kappa_1\mu_2 + \mu_1}{\kappa_2\mu_1 + \mu_2}\right] \qquad \ldots(1.12)$$

in which

$\kappa_j = 3 - 4\nu_j$ for plane strain and

$\kappa_j = \dfrac{3-\nu_j}{1+\nu_j}$ for plane stress

with μ_j and ν_j as the shear modulus and the Poisson's ratio of material j (j = 1, 2) respectively.

The complete expressions for the displacement field and stress field at ($\theta \neq \pm\pi$) and ($\theta \neq 0$) respectively can be found in Rice et al (1990).

The opening displacements δ_y and δ_x at ($\theta = \pi$) is given by :

$$\delta_y + i\delta_x = \frac{8(K_1 + \mathrm{i}K_2)}{(1+2\mathrm{i}\varepsilon)\cosh(\pi\varepsilon)E^*}\sqrt{\frac{r}{2\pi}}\left(\frac{r}{l}\right)^{i\varepsilon} \qquad \ldots(1.13)$$

with $\delta_y = v(r,\pi) - v(r,-\pi)$

$\delta_x = u(r,\pi) - u(r,-\pi)$

where

$$\frac{1}{E^*} = \frac{1}{2}\left(\frac{1}{\overline{E_1}} + \frac{1}{\overline{E_2}}\right) \qquad \ldots(1.14)$$

and $\overline{E_j} = E_j$ for plane stress and

$\overline{E_j} = \dfrac{E_j}{1-\nu_j^{\,2}}$ for plane strain

with E_j and ν_j are the Young's modulus and the Poisson's ratio of material j (j = 1, 2) respectively.

The strain energy release rate is related to $\boldsymbol{K}$ by :

$$G = \frac{|\boldsymbol{K}|^2}{H} \qquad \ldots(1.15)$$

where $$\frac{1}{H} = \frac{1}{E^* \cdot \cosh^2(\pi\varepsilon)} \qquad \ldots(1.16)$$

Another useful parameters defined for interface fracture mechanics are the Dundurs' elastic mismatch parameters α and β:

$$\alpha = \frac{\mu_1(\kappa_2+1) - \mu_2(\kappa_1+1)}{\mu_1(\kappa_2+1) + \mu_2(\kappa_1+1)} \quad \text{and} \quad \beta = \frac{\mu_1(\kappa_2-1) - \mu_2(\kappa_1-1)}{\mu_1(\kappa_2+1) + \mu_2(\kappa_1+1)} \qquad \ldots(1.17)$$

Alternatively, α and ε can be expressed as :

$$\alpha = \frac{\overline{E_1} - \overline{E_2}}{\overline{E_1} + \overline{E_2}} \quad \text{and} \quad \varepsilon = \frac{1}{2\pi}\ln\left(\frac{1-\beta}{1+\beta}\right) \qquad \ldots(1.18)$$

Chapter 2 Finite Element Methods on Determination of Stress Intensity Factors

INTRODUCTION

Analytical solutions for the stress intensity factors K and the strain energy release rate G are mostly limited to simple crack systems under infinite media. Examples of such solutions are recorded in stress intensity factor manuals (Tada et. al. (1985), Sih (1973) and Murakami(1987)). As long as the accuracy of the solution is dependent on the accuracy of boundary conditions, while the boundary conditions of cracks in finite medium are not well defined, the analytical approach to these problems are still not practical for most cases. Fortunately, with the use of the expressions of stress and displacement fields (Equation ...(1.7) and Equation ...(1.8)), alternative methods using finite element analysis (FEA) can be employed to determine indirectly the expressions for the stress intensity factors K and the strain energy release rate G. One of the advantages of using finite element analysis is that there are no restrictions to the loading configuration and to the dimension and shape of body containing the crack. With continuous propulsion in computer technology and improvements in accuracy of finite element methods on determining fracture toughness parameters K and G, the finite element method is becoming firmly established and growing popular. Some of the finite element methods applied in our study will be introduced here in this chapter.

2.1 CRACK-TIP SINGULARITY MODELLING

To model the $\frac{1}{\sqrt{r}}$ crack-tip singularity of cracks in isotropic media, special crack-tip elements are necessary. Employed here in our study surrounding the crack-tip are the isoparametric quarter point element and the transition element. Developed independently by Barsoum (1976) and Henshell and Shaw (1975), the isoparametric quarter point element is a collapsed eight-noded quadrilateral element with mid-side nodes, adjacent to the crack-tip, moved to the location shown in Figure 2.1.

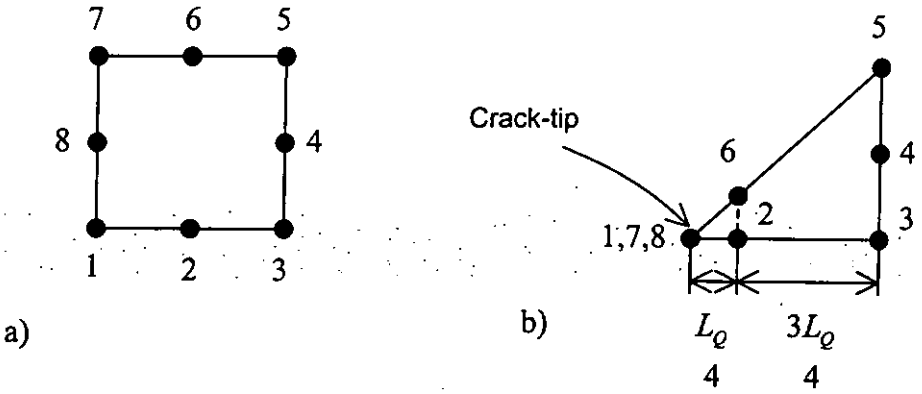

L_Q denotes the size of the quarter point element

Figure 2.1 a) Original eight-noded quadrilateral element ;
b) Modified to Isoparametric Quarter Point Element

The transition element, originated by Lynn and Ingraffea (1980), is the adjacent element of the quarter point element, see Figure 2.2. It derives the singularity by adjusting the location of the 'mid-side' node. The equation governing the position of the mid-side node p_q, is as follows:

$$p_q = \frac{(1-q) \pm \sqrt{(q^2 + 2q)}}{2} \qquad \ldots(2.1)$$

where q is half the ratio of the quarter-point element size to the transition element size.

More recent review on the application of the above elements can be found in Lim et al. (1993).

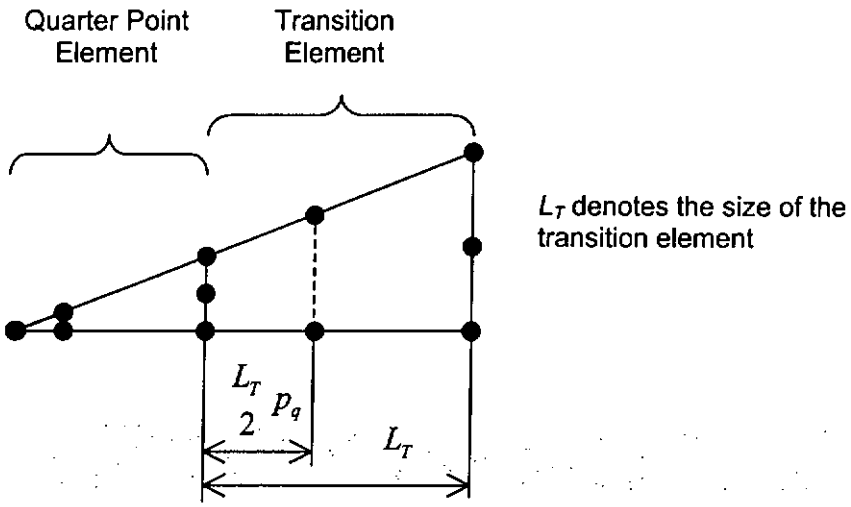

Figure 2.2 The position of midside nodes of transition element

Transition elements and quarter point elements are used throughout our study with $L_Q = L_T$.

2.2 INTERPRETATION OF THE FINITE ELEMENT RESULTS

In FEA, the model of the cracked body is meshed and the loading condition applied onto it. From these FEA results, the magnitude of displacements, stresses, strains and strain energies of the nodes and elements are obtained. From these numerical values, it is possible to determine the stress intensity factors and the strain energy release rate. One family of methods uses the displacements of the nodes to determine the fracture parameters, namely displacement-based stress intensity factor computation techniques. Such examples are the Displacement Correlation Technique (DCT) by Shih et al (1976) and Tracey (1977), the Quarter Point Displacement Technique (QPDT) and the Displacement Extrapolation Technique (DET) by Chan et al (1970). All the above are summarized in Lim et al (1992). Another class makes use of the strain energy around the crack-tip to determine the fracture parameters, namely energy-based stress intensity factor computation techniques. Methods applied in our study will be introduced here.

2.2.1 Displacement-Based Stress Intensity Factor Computation Techniques

The *semi-infinite crack model* (SICM), by Ng and Lau (1997), is adopted to extract stress intensity factors of cracks in isotropic condition in our study due to its accuracy and its consistent performance over a wide range of mesh variations. The *displacement correlation technique* (DCT), by Shih et al. (1976), and the *quarter point displacement technique* (QPDT), by Barsoum (1976), are used as rough checking for the results obtained.

2.2.1.1 The Semi-Infinite Crack Model

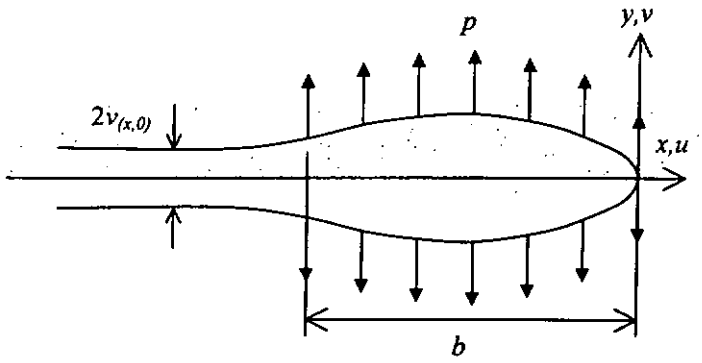

Figure 2.3 A semi-infinite crack under uniform partial crack surface pressure

Ng and Lau (1997) had mapped the cracked surface displacements into the semi-infinite-crack model (Tada et al. (1985)), shown in Figure 2.3, to obtain the stress intensity factor with great accuracy. The displacements (u',u'',v' and v'' shown in Figure 2.4) of the four nodes on the upper and lower crack surface immediately

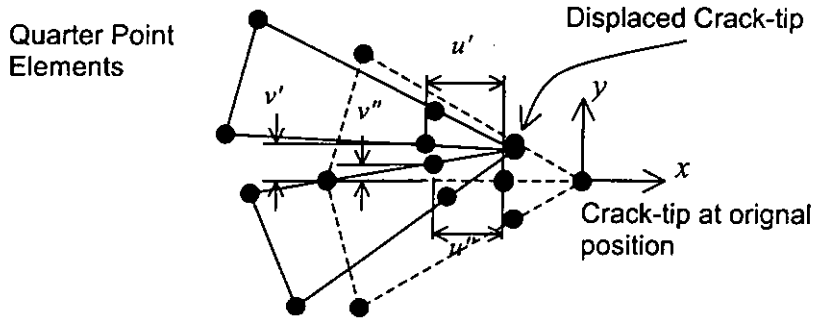

Figure 2.4 The definition of u',u'', v' and v''

adjacent to the crack-tip (with coordinates $\left(\frac{-L_Q}{4},0\right)$ and ($-L_Q$,0)), are first decoupled into mode I and mode II components according to Equation ...(2.2) and Equation ...(2.3). These nodes of the above location were shown to give highest accuracy.

The displacements are decoupled into Mode I and Mode II by :

$$\begin{Bmatrix} u_I \\ v_I \end{Bmatrix} = \frac{1}{2}\begin{Bmatrix} u'+u'' \\ v'-v'' \end{Bmatrix} \qquad \ldots(2.2)$$

$$\begin{Bmatrix} u_{II} \\ v_{II} \end{Bmatrix} = \frac{1}{2}\begin{Bmatrix} u'-u'' \\ v'+v'' \end{Bmatrix} \qquad \ldots(2.3)$$

Each pair of u_{II} and v_I are substituted to the close-form formula (Equation ...(2.5)-Equation ...(2.7) and Equation ...(2.9)-Equation ...(2.11)) of the semi-infinite-crack model and solved to obtain (p, b) and (τ, b) respectively. Finally the estimates for the stress intensity factors are determined by Equation ...(2.4) and Equation ...(2.8).

The closed form solution are as follows :

For Mode I, the stress intensity factor K_I is :

$$K_I = \frac{2\sqrt{2}}{\sqrt{\pi}} \cdot p\sqrt{b}, \qquad \ldots(2.4)$$

where p and b are determined by solving :

$$2\mu v_I\left(x,0\right)_{x\le 0} = \frac{\kappa+1}{\pi} pb\left[\sqrt{\frac{|x|}{b}} + \left(1+\frac{x}{b}\right)\cdot \tanh^{-1}\sqrt{\frac{|x|}{b}}\right] \quad -b < x \le 0, \qquad \ldots(2.5)$$

$$2\mu v_I\left(x,0\right)_{x\le 0} = \frac{\kappa+1}{\pi} pb\left[\sqrt{\frac{|x|}{b}} + \left(1+\frac{x}{b}\right)\cdot \coth^{-1}\sqrt{\frac{|x|}{b}}\right] \quad x < -b, \qquad \ldots(2.6)$$

$$2\mu v_I\left(-b,0\right) = \frac{\kappa+1}{\pi} pb \qquad x = -b, \qquad \ldots(2.7)$$

For Mode II, the stress intensity factor K_{II} is :

$$K_{II} = \frac{2\sqrt{2}}{\sqrt{\pi}} \cdot \tau\sqrt{b}, \qquad \ldots(2.8)$$

where τ and b are determined by solving :

$$2\mu u_{II}(x,0)_{x\le 0} = \frac{\kappa+1}{\pi}\tau b\left[\sqrt{\frac{|x|}{b}} + \left(1+\frac{x}{b}\right)\cdot \tanh^{-1}\sqrt{\frac{|x|}{b}}\right] \qquad -b < x \le 0, \qquad \ldots(2.9)$$

$$2\mu u_{II}(x,0)_{x<0} = \frac{\kappa+1}{\pi}\tau b\left[\sqrt{\frac{|x|}{b}} + \left(1+\frac{x}{b}\right)\cdot \coth^{-1}\sqrt{\frac{|x|}{b}}\right] \qquad x < -b, \qquad \ldots(2.10)$$

$$2\mu u_{II}(-b,0) = \frac{\kappa+1}{\pi}\tau b \qquad x = -b, \qquad \ldots(2.11)$$

The algorithm used to solve for (p,b) and (τ,b) are given in Appendix I.

2.2.1.2 The Displacement Correlation Technique (DCT) and Quarter Point Displacement Technique (QPDT)

The nomenclature in Lim et al. (1992) will be adopted for unity. The definitions for the displacements are found in Figure 2.5. Note that the displacements

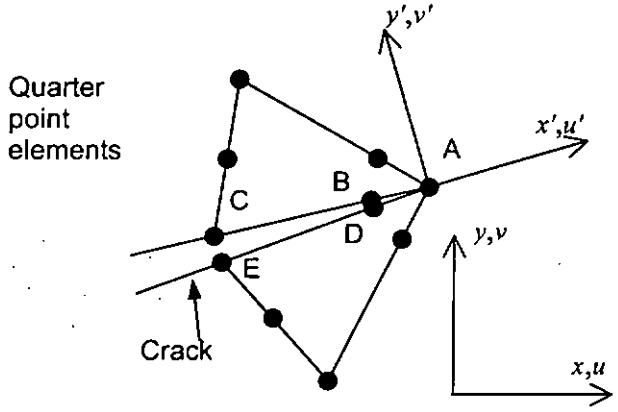

Figure 2.5 Nodal lettering for DCT and QPDT

are taken from local displacements along and normal to the crack axis. More details can be found in Lim et al. (1992).

Equations for determining the stress intensity factor using the *displacement correlation technique* (DCT), by Shih et al. (1976), are given as :

$$K_I^{DCT} = \frac{\mu}{\kappa+1}\sqrt{\frac{2\pi}{L_Q}}\{4(v'_B - v'_D) - (v'_C - v'_E)\},$$
$$K_{II}^{DCT} = \frac{\mu}{\kappa+1}\sqrt{\frac{2\pi}{L_Q}}\{4(u'_B - u'_D) - (u'_C - u'_E)\} \quad \ldots(2.12)$$

Shih et al. (1976) demonstrated accuracies up to 1.2% and 1.1% for the cases of double edge cracked strip and three point bending specimen respectively.

Equations for determining the stress intensity factor using the quarter point displacement technique (QPDT), by Barsoum (1976), are given as :

$$K_I^{QPDT} = \frac{2\mu}{\kappa+1}\sqrt{\frac{2\pi}{L_Q}}\{v'_B - v'_D\},$$
$$K_{II}^{QPDT} = \frac{2\mu}{\kappa+1}\sqrt{\frac{2\pi}{L_Q}}\{u'_B - u'_D\} \quad \ldots(2.13)$$

Lim et al. (1993) showed that accuracy up to 1% can be obtained with a special mesh.

2.2.2 Energy-Based Stress Intensity Factor Computation Techniques

Like the displacements, the strain energy U is also a basic output of finite element analysis. With the relations of G to U (Equation ...(1.1)) and K to G (Equation ...(1.9)), it is possible to derive the estimates of stress intensity factors K from finite element analysis. The relation of the strain energy to the stress intensity factor is therefore :

$$K = \sqrt{-\frac{\partial U}{\partial a} \cdot \overline{E}} \qquad \ldots(2.14)$$

The energy-based methods introduced here include the J-integral by Rice (1968) and the stiffness derivative method (SDM) originated by Parks (1974). Here SDM will be introduced in details. The modified SDM by Ng and Lau (2000) will be combined with Wu's (1994) technique in extracting the complex stress intensity factors in our study. The combined method will be presented in Chapter 3.

2.2.2.I The J-integral

With reference to Figure 2.6, the path-independent constant, J-integral, defined by Rice (1968) is :

$$J = \int_{\Gamma} \left(U \, \mathrm{d}y - \boldsymbol{T} \cdot \frac{\partial \boldsymbol{u}}{\partial x} \mathrm{d}s \right) \qquad \ldots(2.15)$$

where U is the strain energy per unit volume,

Γ is any arbitrary path enclosing the crack-tip starting from the bottom crack surface ending on the upper crack surface,

$\boldsymbol{T}$ and $\boldsymbol{u}$ are the traction vector and the displacement vector on a plane defined by the outward drawn normal **n** respectively.

ds is an infinitesimal length along the path Γ.

For elastic medium with small plastic zone,

$$J = G \qquad \ldots(2.16)$$

Therefore, the stress intensity factor K can be found by :

$$K = \sqrt{\frac{J}{E}} \qquad \ldots(2.17)$$

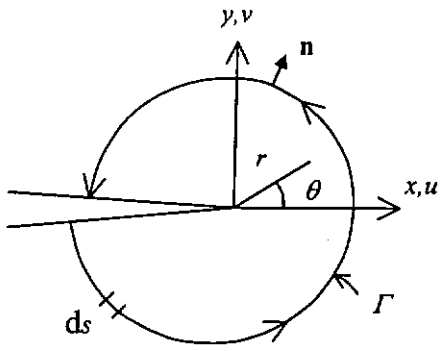

Figure 2.6 Coordinates and contour around crack-tip for evaluating the J-integral

However, this method is limited to single mode fracture problems and special procedures are needed to deal with mixed mode problems. Furthermore, for cracks in bimaterial interface, additional procedures are required to determine the complex stress intensity factors. One such modification of the J-integral is given in Matos et al. (1989).

2.2.2.2 Stiffness Derivative Method (SDM)

SDM applied with quarter point elements were shown by Banks-Sills and Sherman (1986) to be the most accurate methods in determining the stress intensity factors. Parks (1974) found that the stress intensity factors K for cracks in isotropic bodies can be determined from the finite element analysis by :

$$K = \left(-\frac{\overline{E}}{2} \sum_{j=1}^{N_1} \{u_j^{ct}\}^T \frac{\partial [S_j^{ct}]}{\partial a} \{u_j^{ct}\} \right)^{1/2} \quad \ldots(2.18)$$

where N_1 denotes the total number of crack-tip elements,

a denotes the crack length,

$\{u_j^{ct}\}$ denotes the displacement matrix of the crack-tip elements,

$[S_j^{ct}]$ denotes the element stiffness matrix of the crack-tip elements.

With the *virtual crack extension* (VCE), the partial derivative of the element stiffness matrix can be approximated by forward difference:

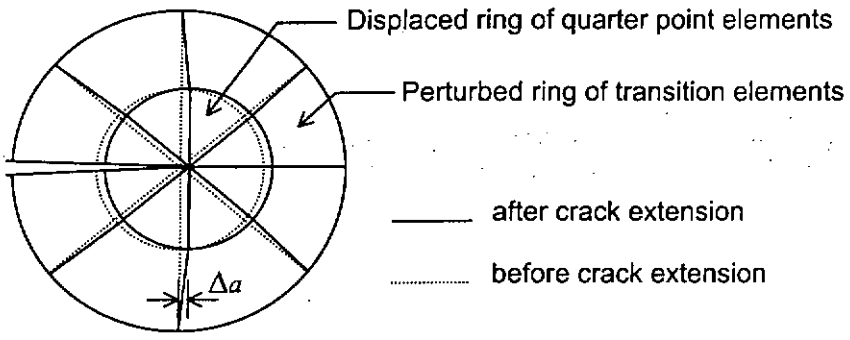

Figure 2.7 Crack-tip elements before and after crack extension

$$\frac{\partial[S_j^{ct}]}{\partial a} = \frac{1}{\Delta a}\left([S_j^{ct}]_{a+\Delta a} - [S_j^{ct}]_a\right) \qquad \ldots(2.19)$$

where Δa denotes the magnitude of the infinitesimal crack extension,

$[S_j^{ct}]_a$ and $[S_j^{ct}]_{a+\Delta a}$ denotes the element stiffness matrices of the crack-tip elements before and after the infinitesimal crack extension respectively, see Figure 2.7.

This method has the drawback of necessitating the extraction of the elements stiffness matrices which are not readily available in commercial finite element packages. Ng and Lau (2000) has suggested a modification to overcome this obstacle and will be shown in Chapter 3.

Chapter 3 Determination of Complex Stress Intensity Factors of Interface Cracks by FEA

3.1 INTRODUCTION

Early analytical studies on cracks in bimaterial interfaces dates back to the work of Williams (1959). Although development has since been continually reported, a systematic way of implementing engineering procedures for the analysis and prediction of interfacial crack failure is yet to be established. A complex stress intensity factor, $\boldsymbol{K} = K_1 + \mathrm{i}K_2$, is used to characterize the crack tip stresses, with K_1 relating to the effect of a remotely applied direct stress and K_2 relating to that of a remotely applied shear stress. K_1 and K_2, however, neither carry the same physical meaning nor have the same units as K_I and K_{II}. In fact the tensile and shear effects as characterized by this complex stress intensity factor is considered as intrinsically inseparable into analogues of classical opening (Mode I) and shearing (Mode II) conditions. Recent developments in this area are well documented in Rice (1988), Comninou (1990), Erdogan (1997) and Hutchinson and Suo (1992).

A numerical method to determine the complex stress intensity factors is attempted here. This numerical method which combines the modified SDM by Ng and Lau (2000) and Wu's (1994) method will be described in details in Section 3.2.3.

The verification and mesh optimization of this combined method will be given in Section 3.3. Mesh optimization will be performed to determine suitable meshing parameters by using the closed form solution of the interface crack in an

infinite plate. Verification of this method will be performed by comparing with reference complex stress intensity factors for the following cases presented in Murakami (1987) : edge crack along an interface on a finite plate, central interface crack on a finite plate and the four-point bend specimen.

3.2 THE FEA METHOD ON DETERMINING COMPLEX STRESS INTENSITY FACTORS

Many numerical methods in determining the complex stress intensity factors have evolved since Williams (1959) presented analytical solutions for interface cracks. These FEA methods includes Lin & Mar (1976), Matos et al. (1989), Naik and Crews Jr. (1994), Wu (1994), Chow & Atluri (1995), and Charalambides & Zhang (1996).). Good accuracy has been demonstrated for each procedure.

Among these methods Matos et al. (1989) suggested a method based on evaluation of the J-integral by the virtual crack extension method before and after the perturbation by small increments of the complex stress intensity factors K_1 and K_2. This approach can be implemented in a relatively straightforward manner but accuracy depends somewhat on the magnitude of the perturbation used. Wu (1994) modified the procedure to remove this dependence. However, in both methods, element stiffness matrices have to be extracted and their derivatives with respect to crack length evaluated for postprocessing purposes. Since commercial finite element codes usually do not include such matrices as standard outputs, special routines have to be written to select the elements involved and to reconstruct such matrices. Ng and Lau (2000) has proposed a new method for finding such derivatives for determining traditional stress intensity factors K_I and K_{II} in isotropic materials. Only nodal displacements and strain energies of the crack-tip elements are needed in the procedure. Since these are standard outputs in most finite element codes, the incorporation of this approach will remove this final barrier for the implementation of the virtual crack extension approach. The method is extended and combined with

the ΔK perturbation approach for the determination of the complex stress intensity factors for interfacial cracks.

3.2.I Modified SDM by Ng and Lau (2000)

Ng and Lau (2000) made use of the strain energy (basic outputs from commercial finite element packages) to replace the stiffness derivatives to extract the stress intensity factors. Substituting Equation ...(2. 19) into Equation ...(2.18), one gets :

$$K = \left[\frac{\bar{E}}{\Delta a} \left(\frac{1}{2} \sum_{j=1}^{N_1} \{u_j^{ct}\}^T [S_j^{ct}]_a \{u_j^{ct}\} - \frac{1}{2} \sum_{j=1}^{N_1} \{u_j^{ct}\}^T [S_j^{ct}]_{a+\Delta a} \{u_j^{ct}\} \right) \right]^{1/2} \quad \ldots(3.1)$$

The first term in bracket, named as U_a^{ct}, is the total strain energy of crack-tip elements before crack extension :

$$U_a^{ct} = \frac{1}{2} \sum_{j=1}^{N_1} \{u_j^{ct}\}^T [S_j^{ct}]_a \{u_j^{ct}\} \quad \ldots(3.2)$$

The second term, named as $U_{a+\Delta a}^{ct}$, is the total strain energy of crack-tip elements after crack extension :

$$U_{a+\Delta a}^{ct} = \frac{1}{2} \sum_{j=1}^{N_1} \{u_j^{ct}\}^T [S_j^{ct}]_{a+\Delta a} \{u_j^{ct}\} \quad \ldots(3.3)$$

In other words, U_a^{ct} is the sum of strain energy (readily available output from FEA) of the crack-tip elements before crack extension under prescribed loadings. Refering to Figure 2.7, $U_{a+\Delta a}^{ct}$ is the sum of strain energy of the displaced crack-tip elements under the nodal loading by the identical displacements of the crack-tip elements after crack extension. With this modification, Ng and Lau (2000) showed that the accuracy is comparable to the original SDM for isotropic cases.

3.2.2 Wu's (1994) method on extracting the complex stress intensity factors

So far, the energy-based methods discussed in Section 2.2.2 are based on cracks in isotropic media under single mode loading. These methods are not adequate for extracting stress intensity factors under mixed mode conditions and for interface cracks without some modifications. The method adopted in this study for interface cracks is from Wu (1994). He made use of the superposition of an addition of nodal displacements loading, which contribute to an arbitrary ΔK_1, on the crack-tip elements nodes to find K_1. Likewise, K_2 can be found. The algorithm for finding K_1 is as follows :

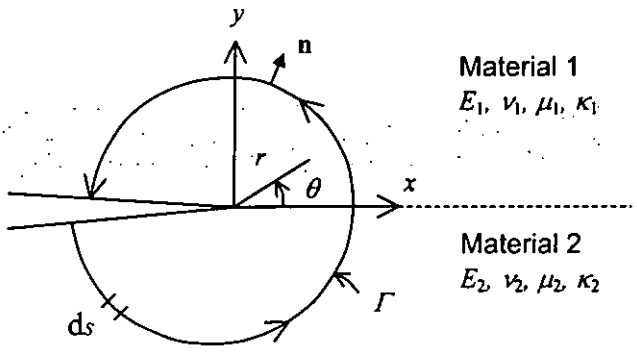

Figure 3.1 Coordinates and contour around crack-tip for evaluating the J-integral for interface cracks

The J-integral for interface cracks with complex stress intensity factor of $\boldsymbol{K} = K_1 + \mathrm{i}K_2$ is given by :

$$J = \frac{1}{H}\left(K_1^2 + K_2^2\right) \qquad \ldots(3.4)$$

and since :

$$J = \frac{1}{\Delta a}\left(U_a^{cl} - U_{a+\Delta a}^{cl}\right) \qquad \ldots(3.5)$$

therefore :

$$\frac{K_1^2 + K_2^2}{H} = \frac{1}{\Delta a}\left(U_a^{ct} - U_{a+\Delta a}^{ct}\right)_{u_n} = A \qquad \ldots(3.6)$$

For convenience, we denote this term as A. The subscript u_n denotes the current resulting displacement by the applied load. Thus this can be viewed as the J-integral of the body under pure nodal displacement vector u_n as loading. Then by superposition of another small values of nodal displacement vector $\Delta u_{K1} = \left(\Delta u_{x1}^j, \Delta u_{y1}^j\right)$, which are the displacements resulting from ΔK_1 and $\Delta K_2 = 0$, one gets :

$$\frac{\left(K_1 + \Delta K_1\right)^2 + K_2^2}{H} = \frac{1}{\Delta a}\left(U_a^{ct} - U_{a+\Delta a}^{ct}\right)_{u_n + \Delta u_{K1}} = B \qquad \ldots(3.7)$$

The additional crack-tip displacements for superposition are given by :

For extraction of K_1 :

With ΔK_1 acting alone, the displacements for superposition are :

$$\Delta u_{x1}^j = \frac{\Delta K_1}{2\mu_j}\sqrt{\frac{r}{2\pi}}\frac{e^{\pi\varepsilon}}{1+e^{2\pi\varepsilon}} f_{x1}\left(r,\theta,\varepsilon,\kappa_j\right), \quad \text{and}$$

$$\Delta u_{y1}^j = \frac{\Delta K_1}{2\mu_j}\sqrt{\frac{r}{2\pi}}\frac{e^{\pi\varepsilon}}{1+e^{2\pi\varepsilon}} f_{y1}\left(r,\theta,\varepsilon,\kappa_j\right) \qquad \ldots(3.8)$$

Likewise, for the extraction of K_2 later on:

With ΔK_2 acting alone, the displacements for superposition are :

$$\Delta u_{x2}^j = \frac{\Delta K_2}{2\mu_j}\sqrt{\frac{r}{2\pi}}\frac{e^{\pi\varepsilon}}{1+e^{2\pi\varepsilon}} f_{x2}\left(r,\theta,\varepsilon,\kappa_j\right), \quad \text{and}$$

$$\Delta u_{y2}^j = \frac{\Delta K_2}{2\mu_j}\sqrt{\frac{r}{2\pi}}\frac{e^{\pi\varepsilon}}{1+e^{2\pi\varepsilon}} f_{y2}\left(r,\theta,\varepsilon,\kappa_j\right) \qquad \ldots(3.9)$$

where Δu_{x1}^{j} and Δu_{y1}^{j} denotes the displacement in the direction of x-axis and y-axis for node j with cylindrical coordinates (r,θ) and material constant κ_j of corresponding node j under $\Delta K_1 \neq 0$ loading

Δu_{x2}^{j} and Δu_{y2}^{j} denotes the displacement in the direction of x-axis and y-axis for node j with cylindrical coordinates (r,θ) and material constant κ_j of corresponding node j under $\Delta K_2 \neq 0$ loading

f_{x1} , f_{y1} , f_{x2} and f_{y2} are functions of coordinates and material properties given in Appendix II.

The values of $\boldsymbol{A}$ and $\boldsymbol{B}$ are extracted by FEA with virtual crack extension. By rewriting $\boldsymbol{A}$ and $\boldsymbol{B}$ in terms of stiffness derivatives and introducing a new term $\boldsymbol{C}$:

$$\boldsymbol{A} = \frac{K_1^2 + K_2^2}{H} = -\frac{1}{2}\{u_n\}^{\mathrm{T}}\left(\frac{\partial[S]}{\partial a}\right)\{u_n\} \qquad \ldots(3.10)$$

$$\boldsymbol{B} = \frac{(K_1 + \Delta K_1)^2 + K_2^2}{H} = -\frac{1}{2}\{u_n + \Delta u_{K1}\}^{\mathrm{T}}\left(\frac{\partial[S]}{\partial a}\right)\{u_n + \Delta u_{K1}\} \qquad \ldots(3.11)$$

$$\boldsymbol{C} = \frac{\Delta K_1^2}{H} = -\frac{1}{2}\{\Delta u_{K1}\}^{\mathrm{T}}\left(\frac{\partial[S]}{\partial a}\right)\{\Delta u_{K1}\} \qquad \ldots(3.12)$$

Then by subtracting Equation ...(3.10) and Equation ...(3.12) from Equation ...(3.11), K_1 can be determined by:

$$K_1 = \frac{H}{2\Delta K_1}(\boldsymbol{B} - \boldsymbol{A} - \boldsymbol{C}) \qquad \ldots(3.13)$$

Or alternatively :

$$K_1 = -\frac{H}{2\Delta K_1}\{\Delta u_{K1}\}^{\mathrm{T}}\left(\frac{\partial[S]}{\partial a}\right)\{u_n\} \qquad \ldots(3.14)$$

Similarly K_2 can be found by first superimposing the displacements $\Delta u_{K2} = \left(\Delta u_{x1}^{j}, \Delta u_{y2}^{j}\right)$ of a small value of $\Delta K_2 \neq 0$ and perform FEA with virtual crack extension to determine $\boldsymbol{D}$:

$$\boldsymbol{D} = \frac{K_1^2 + \left(K_2 + \Delta K_2\right)^2}{H} = -\frac{1}{2}\left\{u_n + \Delta u_{K2}\right\}^{\mathrm{T}}\left(\frac{\partial [S]}{\partial a}\right)\left\{u_n + \Delta u_{K2}\right\} \qquad \ldots(3.15)$$

$$\boldsymbol{E} = \frac{\Delta K_2^2}{H} = -\frac{1}{2}\left\{\Delta u_{K2}\right\}^{\mathrm{T}}\left(\frac{\partial [S]}{\partial a}\right)\left\{\Delta u_{K2}\right\} \qquad \ldots(3.16)$$

Therefore :

$$K_2 = \frac{H}{2\Delta K_2}\left(\boldsymbol{D} - \boldsymbol{A} - \boldsymbol{E}\right) \qquad \ldots(3.17)$$

Or alternatively :

$$K_2 = -\frac{H}{2\Delta K_2}\left\{\Delta u_{K2}\right\}^{\mathrm{T}}\left(\frac{\partial [S]}{\partial a}\right)\left\{u_n\right\} \qquad \ldots(3.18)$$

This method was tested on bimaterial crack plate with central crack and claimed for high accuracy and less sensitive to mesh refinement around the crack-tip.

3.2.3 Combination of Ng and Lau's (2000) SDM with Wu's (1994) Method

In Wu's method, the determination of $\boldsymbol{A}$, $\boldsymbol{B}$ and $\boldsymbol{D}$ requires the extraction of stiffness derivatives $\frac{\partial[S]}{\partial a}$. While the modification of Ng and Lau's SDM (proved for isotropic cases) has improved to eliminate this trouble by replacing $\frac{\partial[S]}{\partial a}$ by the difference of strain energies before and after the virtiual crack extension, which are basic outputs readily given from FEA. This combined method will be verified here in this study for bimaterial cases.

The detailed procedures of the combined SDM are as follows :

[1] With quarter point elements and transition elements, the body containing an interface crack was meshed and loading conditions applied and solved.

[2] The resulting displacements (relative to the crack-tip) of all nodes on *transition elements* were recorded as $\{u_n\}$.

[3] The strain energy of all *transition elements* was summed as U_a^{ct}.

[4] The ring of *transition elements* was detached from the meshed body by deleting all nodes and elements except those of the *transition elements*.

[5] Virtual crack extension was applied onto the inner ring of nodes of the *transition elements* (coincident with the quarter point elements) by moving each node Δa in the direction of crack propagation as in Figure 2.7.

[6] The midside nodes (middle ring) of *transition elements* were shifted to their new position according to Equation ...(2.1).

[7] The recorded displacements $\{u_n\}$ were applied onto each nodes on the crack-tip elements and solved.

[8] The strain energy of the *transition elements* were summed as $U^{ct}_{a+\Delta a}$.

[9] The value of A can be found by ...(3.6).

[10] With an arbitrary small value of ΔK_1, the values of *transition elements* nodes displacements for superposition $\{\Delta u_{K1}\} = \{(\Delta u^j_{x1}, \Delta u^j_{y1})\}$ are found by ...(3.8) and are added to $\{u_n\}$ by pure addition to a new displacement vector $\{u_n + \Delta u_{K1}\}$.

[11] The displacement $\{u_n + \Delta u_{K1}\}$ were applied to the *transition elements* nodes on its original position and solved.

[12] The strain energy of *transition elements* was summed as $(U^{ct}_a)_{u_n+\Delta u_{K1}}$.

[13] The displacement $\{u_n + \Delta u_{K1}\}$ were applied to the *transition elements* nodes on its new position with virtual crack extension and solved.

[14] The strain energy of *transition elements* was summed as $(U^{ct}_{a+\Delta a})_{u_n+\Delta u_{K1}}$.

[15] The value of B can be found by ...(3.7).

[16] With C obtained by ...(3.12), the value of K_1 can be found in ...(3.13).

Similarly, K_2 can be found by :

[17] With an arbitrary small value of ΔK_2, the values of *transition elements* nodes displacements for superposition $\{\Delta u_{K2}\} = \{(\Delta u^j_{x2}, \Delta u^j_{y2})\}$ are found by ...(3.9) and are added to $\{u_n\}$ by pure addition to a new displacement vector $\{u_n + \Delta u_{K2}\}$.

[18] The displacement $\{u_n + \Delta u_{K2}\}$ were applied to the *transition elements* element nodes on its original position and solved.

[19] The strain energy of *transition elements* was summed as $(U^{ct}_a)_{u_n+\Delta u_{K2}}$.

[20] The displacement $\{u_n + \Delta u_{K2}\}$ were applied to the *transition elements* nodes on its new position with virtual crack extension and solved.

[21] The strain energy of *transition elements* was summed as $\left(U^{ct}_{a+\Delta a}\right)_{u_n+\Delta u_{K2}}$.

[22] The value of $\boldsymbol{D}$ can be found by similarly like $\boldsymbol{B}$ by replacing the stiffness derivatives in ...(3.15) with the difference of summed strain energies.

[23] With $\boldsymbol{E}$ obtained by ...(3.16), the value of K_2 can be found in ...(3.17).

It should be noted that the *transition elements* are used instead of quarter point elements. As stated in Wu (1994), quarter point elements should be avoided in this technique of determining complex stress intensity factors for interface cracks.

This combined method is validated in this study by several reference cases from the stress intensity factors manual by Murakami (1987) in the next section. The error is less than 1% for comparing with closed form solution of center interface crack in infinite plate when specific mesh parameters are applied. These mesh parameters are also determined. The stress intensity factors obtained by this method is also compared with those obtained from the crack surface displacements.

3.3 VALIDATION OF THE COMBINED METHOD

FEA with regular mesh pattern are constructed to test the proposed combined method. Circular quarter-point and transition crack-tip elements are employed in the analysis to account for stress singularity. 8- noded 2-D quadrilateral and 6-noded triangular elements filled the rest of the mesh. In the case of isotropic materials, the recommended size (L_Q) of the crack-tip element is about $a/50$ and the virtual crack extension (Δa) ranges between 10^{-5} and 10^{-3} of the crack-tip element size. A focused mesh at the crack-tip, with gradual enlargement of element size according to a geometric progression scheme, is usually employed. To ensure the circular crack-tip elements to progress smoothly into rectangular elements, the elements at the crack-tip are specially formed as shown in Figure 3.2. On the crack line the three elements on either side of the crack-tip are given the same length of side, e, while elements beyond are enlarged progressively using a factor equal to m.

The three objectives of this section are :

[1] The stress intensity factors obtained by the combined method is compared to four reference cases from the stress intensity manual by Murakami (1987) :

- interface crack in infinite plate with close form solution,
- edge interface crack in finite plate,
- center interface crack in finite plate, and
- Charalambides' (1989) results on interface cracks on four-point bend beams.

[2] Mesh optimization for interfacial crack studies is done by determining the mesh parameters, e and m, which characterize the mesh. The definition of mesh parameters is shown in Figure 3.2. e is the quarter point element size and m is

the factor of geometric progression of element size from the crack-tip. All crack-tip meshes are constructed in this manner.

[3] The size of virtual crack extension Δa, in relative terms of Δa/e, giving best accuracy will also be determined.

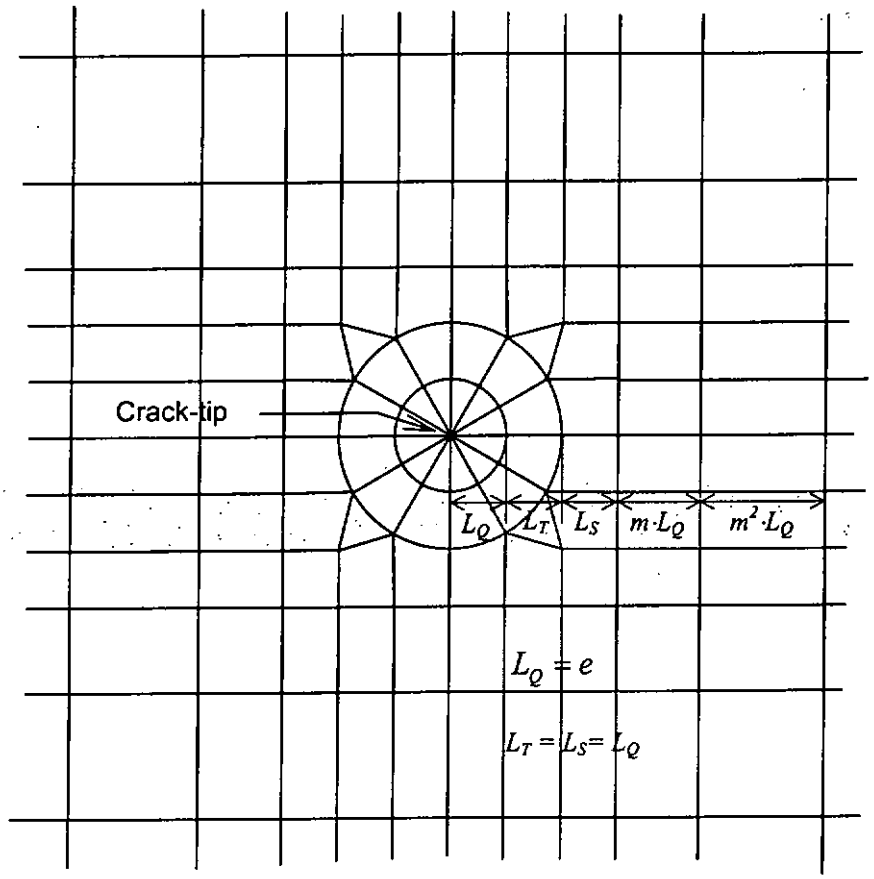

Figure 3.2 The crack-tip mesh and the definition of mesh parameters

3.3.1 Interface Crack in Infinite Plate under Biaxial Loading

More details of this solution is given in Rice (1965). The stress intensity factor of an embedded center interface crack (see Figure 3.3) is given by :

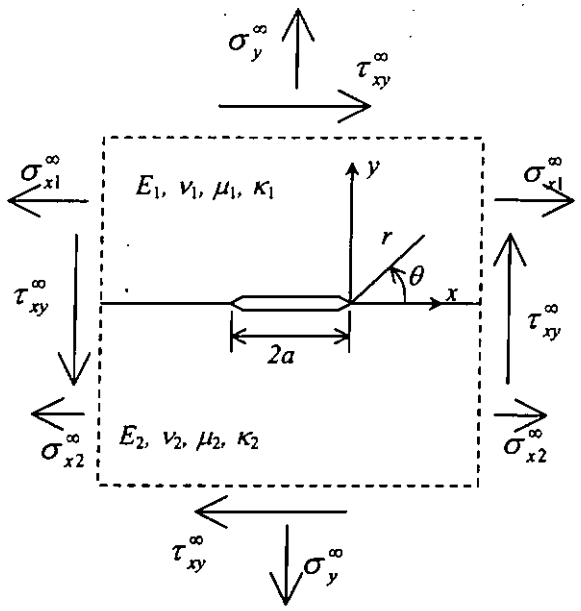

Figure 3.3 Center Interface Crack in an Infinite Plate

$$K_1 + iK_2 = (\sigma_y^\infty + i\tau_{xy}^\infty)(1+2i\varepsilon)\sqrt{\pi a}(2a)^{-i\varepsilon} \qquad \ldots(3.19)$$

while σ_{x2}^∞ is defined as :

$$\sigma_{x2}^\infty = \frac{1}{1+\kappa_2}\left[\frac{\mu_2}{\mu_1}(1+\kappa_1)\sigma_{x1}^\infty + \left\{3-\kappa_2 - \frac{\mu_2}{\mu_1}(3-\kappa_1)\sigma_y^\infty\right\}\right] \qquad \ldots(3.20)$$

The infinite plate was approximated by a 20×20 square units plate with center crack length 2 units. By symmetry, half of the plate was modeled. Plane stress conditions are applied. On all nodes along the lower edge $u_y = 0$ has been applied. And $u_x = 0$ applied on the node intersecting the line of symmetry and lower edge. The applied loads are $\sigma_y^\infty = \sigma_{x1}^\infty = \sigma = 1$ unit and $\tau_{xy}^\infty = 0$.

The reference values are calculated from Equation ...(3.19) to give :

$$K_{1ref} = \sigma\sqrt{\pi a}\cdot\left[\cos(\varepsilon \ln 2a) + 2\varepsilon\cdot\sin(\varepsilon \ln 2a)\right]$$

$$K_{2ref} = -\sigma\sqrt{\pi a}\cdot\left[\sin(\varepsilon \ln 2a) - 2\varepsilon\cdot\cos(\varepsilon \ln 2a)\right] \qquad \ldots(3.21)$$

A mesh is shown in Figure 3.4 with mesh parameters e/a = 1/6 and m = 1.5.

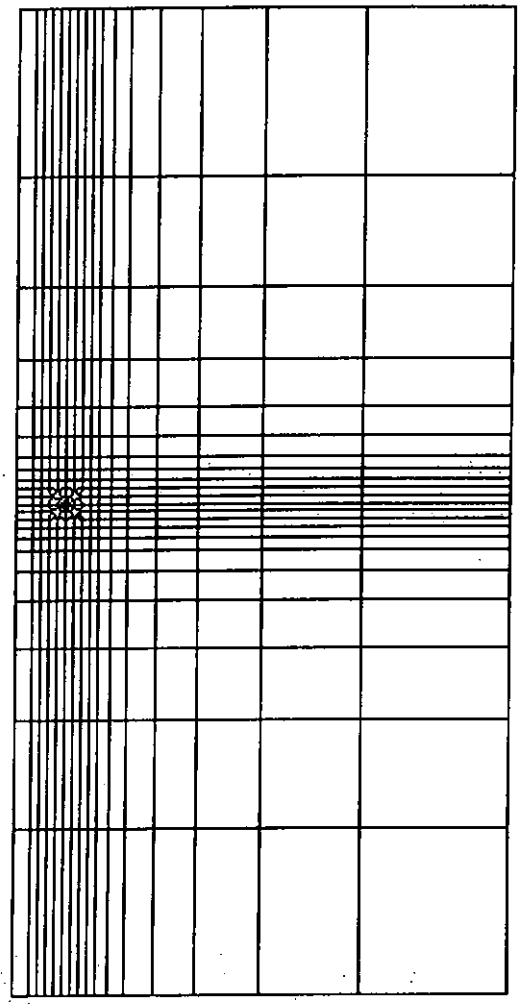

Figure 3.4 Half model of interface crack in infinite plate under biaxial loading with e/a = 1/6 and m = 1.5.

Plates of various mesh sizes and material properties were modeled. The arbitrary ΔK_1 and ΔK_2 were taken as 0.01 and 0.01 respectively. The complex stress intensity factors were obtained by the combined SDM.

Another method, for comparison purpose, makes use of the crack surface displacements, of the six pairs of closest crack surface nodes to the crack-tip, to determine the complex stress intensity factors. From Equation ...(1.13), the complex stress intensity factors can be expressed as :

$$K_{1CSD} = \frac{(\delta_y - 2\varepsilon\delta_x)\cos\left(\varepsilon \ln\frac{r}{l}\right) + (\delta_x + 2\varepsilon\delta_y)\sin\left(\varepsilon \ln\frac{r}{l}\right)}{const \cdot \sqrt{r}}$$

$$K_{2CSD} = \frac{(\delta_x + 2\varepsilon\delta_y)\cos\left(\varepsilon \ln\frac{r}{l}\right) - (\delta_y - 2\varepsilon\delta_x)\sin\left(\varepsilon \ln\frac{r}{l}\right)}{const \cdot \sqrt{r}} \qquad \ldots(3.22)$$

where

$$const = \frac{8}{\cosh(\pi\varepsilon)\cdot E^* \cdot \sqrt{2\pi}}$$

with $\delta_y = v(r,\pi) - v(r,-\pi)$ and $\delta_x = u(r,\pi) - u(r,-\pi)$

The stress intensity factors obtained with the minimum deviation from the reference values, K_{1ref} and K_{2ref}, will be taken. For convenience, this method will be denoted as CSD.

3.3.I.I Effect of Quarter Point Element Size *e*

The ratio, *e/a*, of the quarter point element size L_Q to the half crack length *a*, was varied from a coarse value of 1/4 to a fine value of 1/10000. The other parameters were fixed : $\Delta a/e$ = 1/500 and m = 1.5 . The number of elements and nodes varied from 292 to 3252 and 937 to 10017 respectively. The material properties are E_1 = 1000, E_2 =10, ν_1 = 0.3, ν_2 = 0.3 which gives K_{1ref} and K_{2ref} as 1.79874 and -0.262529 respectively. A large number of significant figures are used taking advantage of the closed-form solution.

The graph of absolute percentage deviation of the obtained complex stress intensity factors from the reference values is shown in Figure 3.5. The table of the corresponding numerical values is given in Table III.1 of Appendix III.

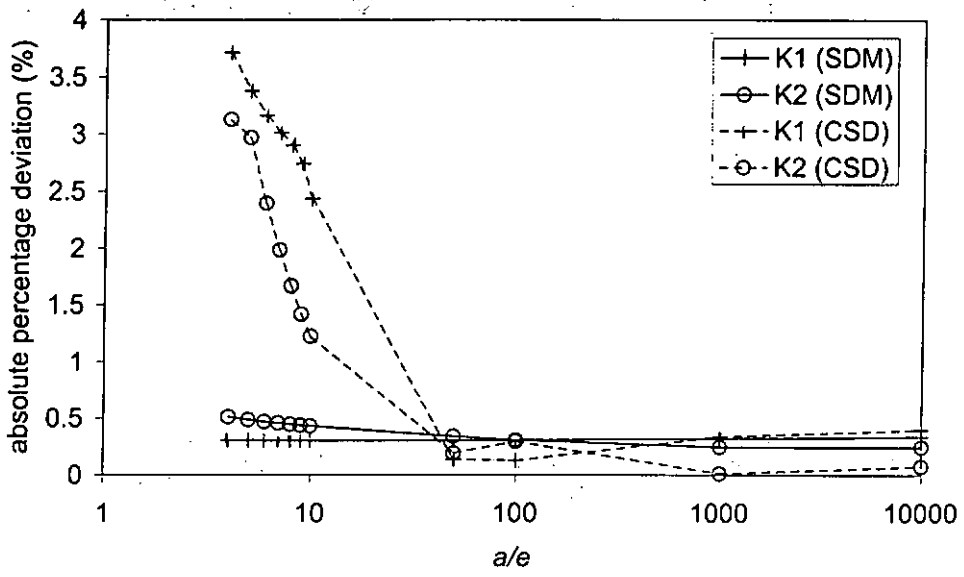

Figure 3.5 Comparison of the two methods : (combined SDM and CSD) in response to the change of quarter point element size

Given that the mesh have mild geometric progression (m =1.5), the combined SDM gives quite stable results, with percentage errors less than 0.6% despite the very large quarter point element, i.e. 1/4 of the crack length. The stress intensity factors are approximately the same for e/a = 1/4 throughout to e/a = 1/10000. Which means the size of the quarter point element do not affect the stress intensity factors under mild geometry progression. From Figure 3.5, it is clear that the accuracy of CSD depends on the element size. The smaller the elements, the more accurate it is. The corresponding numerical values of the graphs are in Table III.1 of Appendix III.

Therefore, it can be implied that the combined SDM is insensitive to the element size provided that the geometric progression is mild. High accuracy can be achieved with coarse element meshes.

Shown in Figure 3.6 and Figure 3.7 are the percentage deviation of the K-values obtained by CSD from the reference Ks. For CSD, the accuracy depends on the distance r from the crack-tip of the crack surface node pair, which was taken to calculate the complex K-values. When the quarter point element size e varies, the

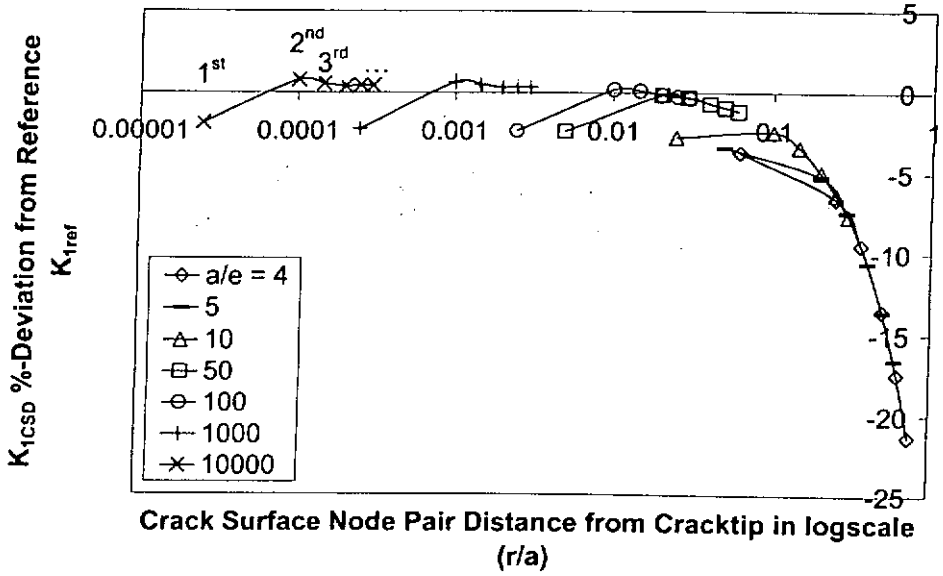

Figure 3.6 Deviation of K_{1CSD} from K_{1ref} of the first 6 node pairs on crack surface in relation to its distance from the crack-tip through changing the crack-tip element size e/a

distance r of the surface nodes from crack-tip also varies. Each line is taken from the first 6 node pairs from the crack-tip on the crack surface for one value of relative quarter point element size e/a.

Refering to Figure 3.6 for the results of K_{1CSD} : at $e/a \leq 1/50$ (represented by the lines marked with ×, +, O and □), apart from the 1st node pair, i.e. the quarter point element 'mid-side' node, all node pairs gives similar %-deviation less than 1%. Decreasing the element size does not improve the accuracy.

For $e/a \geq 1/50$, the errors are large indicating that the crack-tip element size is too large.

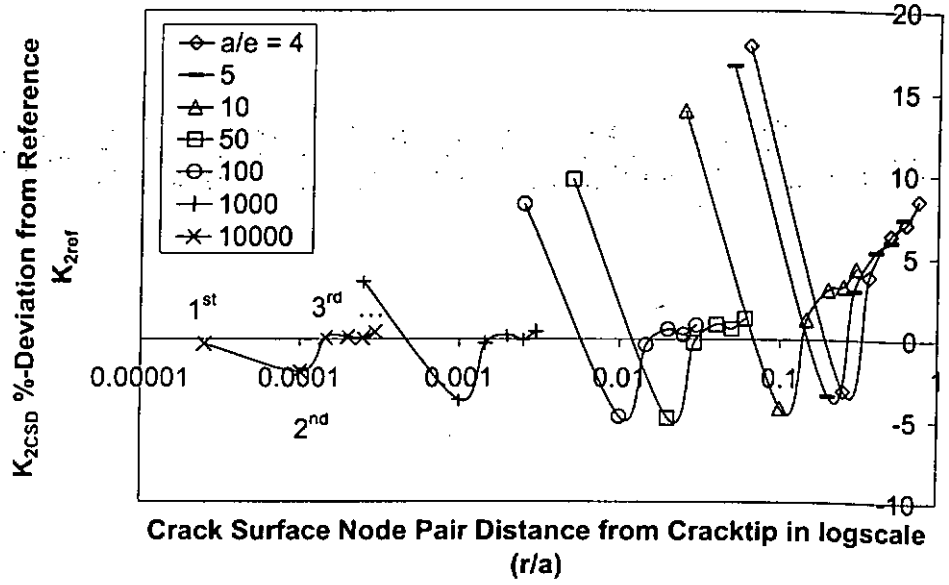

Figure 3.7 Deviation of K_{2CSD} from K_{2ref} of the first 6 node pairs on crack surface in relation to its distance from the crack-tip through changing the relative crack-tip element size e/a

In Figure 3.7, similar to the K_{1CSD} results, when $e/a \leq 1/50$ (represented by the lines marked with ×, +, O and □), the results of K_{2CSD} from 3rd to 6th node pair gives close accuracy of within 1.3%. The magnitude of deviation however is much

larger than that of K_{1CSD}. There is still room for improvement in accuracy if $e/a \leq 1/10000$.

When using CSD to determine the complex stress intensity factors, it is recommended to mesh with $e/a \leq 1/50$ and then take the 3rd node pair on the crack surface from the crack-tip, i.e. the 'mid-side' node of the transition element to calculate the K-values. The deviation will be less than 1%. For this case, the percentage deviation of the 3rd pair is less than 0.6% and 0.4% for K_{1CSD} and K_{2CSD} respectively.

3.3.1.2 Effect of the Geometric Progression Factor *m*

Keeping the material properties same as before, the reference complex stress intensity factors are also the same as before, with K_{1ref} and K_{2ref} as 1.79874 and -0.262529 respectively. The geometric progression factor m was varied from 1.2 to 5. The other parameters were fixed : e/a = 1/100, $\Delta a/e$ = 1/500. The number of elements varied from 3340 to 252. The results are given in Table 3.1 and those from CSD are taken from the 3rd pair of nodes from the crack-tip.

e/a =1/100	Combined SDM		CSD		
m	K_{1SDM} (% deviation)	K_{2SDM} (% deviation)	K_{1CSD} 3rd pair (% deviation)	K_{2CSD} 3rd pair (% deviation)	No. of elements
1.2	1.80429 (0.309)	-0.263339 (0.308)	1.80099 (0.125)	-0.263306 (0.296)	3340
1.5	1.80428 (0.308)	-0.263336 (0.308)	1.80098 (0.125)	-0.263300 (0.294)	1128
2	1.80417 (0.302)	-0.263372 (0.321)	1.80086 (0.118)	-0.263331 (0.305)	610
2.5	1.80374 (0.278)	-0.263726 (0.456)	1.80040 (0.092)	-0.262046 (-0.184)	430
4	1.80289 (0.231)	-0.265946 (1.302)	1.79940 (0.037)	-0.264087 (0.593)	300
5	1.79954 (0.045)	-0.280893 (6.995)	1.79475 (-0.222)	-0.279094 (6.310)	252

Table 3.1 Comparison of the two methods : (combined SDM and CSD) in response to the change of geometric progression m with e/a = 1/100

Both methods are comparable in accuracy under small element size with e/a = 1/100. Deviation less than 1% for combined SDM and CSD are maintained if $m \leq$ 2.5 and $m \leq 4$ respectively.

Effects on changing the mesh by varying the geometric progression factor m and the crack length to quarter point element ratio e/a altogether are shown in Table 3.2 to Table 3.4. Keeping the same series of m, the element size is increased gradually by e/a = 1/10, 1/5 and 1/4. The K_1 and K_2 results of CSD are taken from the best node pair : 1st and 3rd node pair.

e/a =1/10	Combined SDM		CSD		No. of elements
m	K_{1SDM} (% deviation)	K_{2SDM} (% deviation)	K_{1CSD} 1st pair (% deviation)	K_{2CSD} 3rd pair (% deviation)	
1.2	1.80420 (0.303)	-0.263661 (0.431)	1.74922 (-2.753)	-0.265749 (1.227)	1132
1.5	1.80419 (0.303)	-0.263659 (0.430)	1.74921 (-2.754)	-0.265749 (1.226)	532
2	1.80413 (0.300)	-0.263652 (0.428)	1.74915 (-2.757)	-0.265737 (1.222)	332
2.5	1.80379 (0.281)	-0.263724 (0.455)	1.74881 (-2.776)	-0.265782 (1.239)	236
4	1.80277 (0.224)	-0.264235 (0.650)	1.74777 (-2.834)	-0.266157 (1.382)	180
5	1.80267 (0.219)	-0.264284 (0.668)	1.74767 (-2.839)	-0.266192 (1.395)	180

Table 3.2 Comparison of the two methods : (combined SDM and CSD) in response to the change of geometric progression with e/a = 1/10

e/a =1/5 m	Combined SDM		CSD		No. of elements
	K_{1SDM} (% deviation)	K_{2SDM} (% deviation)	K_{1CSD} 1st pair (% deviation)	K_{2CSD} 3rd pair (% deviation)	
1.2	1.80424 (0.306)	-0.263809 (0.488)	1.73792 (-3.381)	-0.270328 (2.971)	684
1.5	1.80424 (0.306)	-0.263808 (0.487)	1.73791 (-3.382)	-0.270329 (2.971)	364
2	1.80420 (0.304)	-0.263805 (0.486)	1.73788 (-3.383)	-0.270327 (2.970)	264
2.5	1.80412 (0.299)	-0.263804 (0.486)	1.73780 (-3.388)	-0.270321 (2.968)	220
4	1.80378 (0.280)	-0.263849 (0.503)	1.73747 (-3.406)	-0.270277 (2.951)	166
5	1.80193 (0.178)	-0.264554 (0.771)	1.73560 (-3.510)	-0.270627 (3.085)	132

Table 3.3 Comparison of the two methods : (combined SDM and CSD) in response to the change of geometric progression with $e/a = 1/5$

e/a =1/4 m	Combined SDM		CSD		No. of elements
	K_{1SDM} (% deviation)	K_{2SDM} (% deviation)	K_{1CSD} 1st pair (% deviation)	K_{2CSD} 3rd pair (% deviation)	
1.2	1.80428 (0.308)	-0.263878 (0.514)	1.73194 (-3.713)	-0.272538 (3.813)	582
1.5	1.80427 (0.307)	-0.263877 (0.514)	1.73194 (-3.714)	-0.272537 (3.812)	292
2	1.80421 (0.304)	-0.263873 (0.512)	1.73188 (-3.717)	-0.272530 (3.810)	204
2.5	1.80403 (0.294)	-0.263878 (0.514)	1.73171 (-3.727)	-0.272519 (3.805)	166
4	1.80297 (0.235)	-0.264158 (0.621)	1.73064 (-3.786)	-0.272602 (3.837)	132
5	1.80289 (0.231)	-0.264188 (0.632)	1.73055 (-3.791)	-0.272614 (3.841)	132

Table 3.4 Comparison of the two methods : (combined SDM and CSD) in response to the change of geometric progression with $e/a = 1/4$

Observations are : the values of K_{2SDM} are affected more than K_{1SDM} by the element size as it increases. The accuracy of the combined SDM is stable within 1% for all cases despite with coarse mesh of large elements and large geometric progression. For stable results it is recommended that e/a = 1/100 and m = 1.5. These parameter values will be applied in company with the combined SDM in determining complex stress intensity factors.

However, for CSD, it is obviously dependent on the mesh size since the deviation increases to 4% when the element size increases. The dependence of CSD accuracy on element size is a feature of displacement-based methods. For almost equal number of elements, it is better to choose a smaller element size but a larger geometric progression. It should be noted that by redesigning the element mesh in areas away from the crack tip, the number of elements used could have been considerably reduced in the majority of cases, especially cases with small *e*-values. Since computing time and hardware requirements are not critical in the present study, taking into account the range of element size and number involved, an optimal mesh is not actively pursued.

3.3.1.3 Effect of the Virtual Crack Extension Length Δa

On the account of its definition, the virtual crack extension is an infinitesimal crack propagation. Therefore the length of virtual crack extension cannot be too large. Moreover, it cannot be too small, due to the round off errors during computation. Therefore an optimized length should be determined. The length of virtual crack extension Δa, is expressed in terms of relative length of virtual crack extension to the quarter point element size $\Delta a/e$.

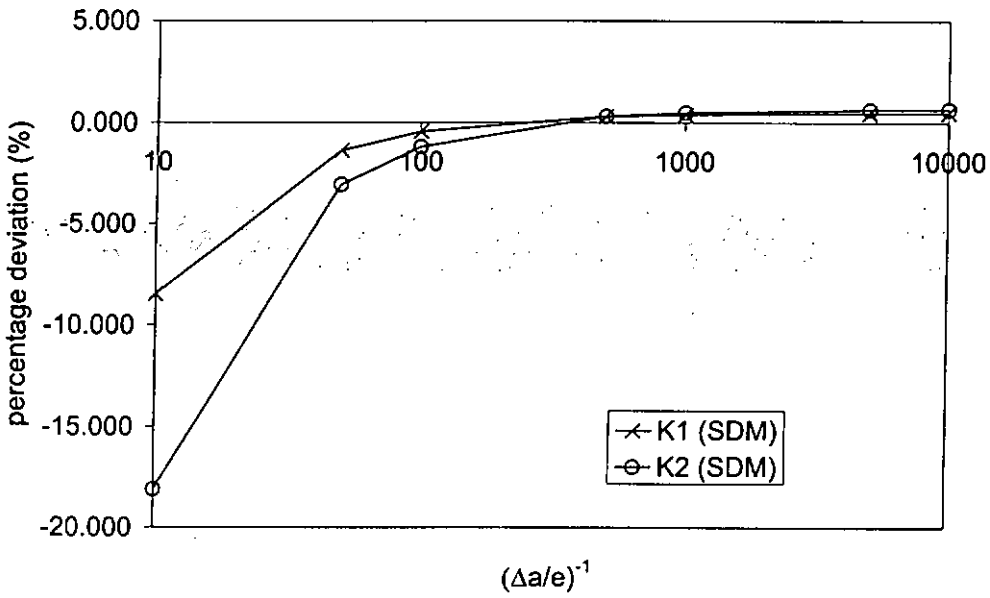

Figure 3.8 The percentage deviation of SDM results in response to variation of relative virtual crack extension length $\Delta a/e$

To consider the effect of virtual crack extension size, an infinite plate with an interface crack is analyzed, with e/a = 1/100, m = 1.5 and a total of 1132 elements. With the same material properties as before, the reference values for K_{1ref} and K_{2ref} are 1.79874 and -0.262529 respectively. Shown in Figure 3.8 is the dependence of combined SDM's accuracy on the relative size of virtual crack

extension length. The corresponding numerical values are given in Table III.2 of Appendix III. Basing on these results it is recommended that $\Delta a/e$ should be about 1/500 to 1/1000 to ensure that deviations are below 0.5%. $\Delta a/e$ will be kept to 1/500 for the rest of our study.

3.3.1.4 Effect of Variation of Material Properties

The accuracy and stability of the combined SDM is also verified on changing the material properties. The same infinite plate with central crack is again employed, with e/a = 1/100, m = 1.5 and a total of 1132 elements. The relative virtual crack extension length is kept to $\Delta a/e$ = 1/500. Different material properties are applied onto the plate by varying the E_1/E_2 ratio and Poisson's ratio, ν_1 and ν_2. The results are shown in Table 3.5 to Table 3.8 with the reference values on the right hand side.

For E_1 = 1000 and E_2 = 10, i.e. E_1/E_2 = 100 :

ν_1	ν_2	K_{1SDM} (% deviation)	K_{2SDM} (% deviation)	K_{1ref}	K_{2ref}
0.30	0.30	1.80428 (0.308)	-0.263336 (0.308)	1.79874	-0.262529
0.30	0.35	1.80002 (0.290)	-0.242924 (0.268)	1.79481	-0.242275
0.30	0.12	1.82312 (0.370)	-0.340110 (0.429)	1.81641	-0.338658

Table 3.5 Accuracy of combined SDM in response of change of Poisson's ratio for E_1/E_2 = 100

For E_1 = 100 and E_2 = 10, i.e. E_1/E_2 = 10 :

ν_1	ν_2	K_{1SDM} (% deviation)	K_{2SDM} (% deviation)	K_{1ref}	K_{2ref}
0.30	0.30	1.79837 (0.451)	-0.217886 (0.598)	1.79030	-0.216592
0.30	0.35	1.79517 (0.432)	-0.199720 (0.561)	1.78745	-0.198606
0.30	0.12	1.81247 (0.518)	-0.285456 (0.712)	1.80313	-0.283438

Table 3.6 Accuracy of combined SDM in response of change of Poisson's ratio for E_1/E_2 = 10

The deviation is within 0.8% for all cases.

It can be concluded that the combined SDM is accurate and stable to 1% when the parameters are kept to $e/a = 1/100$, $m = 1.5$ and $\Delta a/e = 1/500$.

The values obtained with same mesh by the CSD are as follows :

For $E_1 = 1000$ and $E_2 = 10$, i.e. $E_1/E_2 = 100$:

ν_1	ν_2	K_{1CSD} 3rd pair (% deviation)	K_{2CSD} 3rd pair (% deviation)	K_{1ref}	K_{2ref}
0.30	0.30	1.80098	-0.261662	1.79874	-0.262529
		(0.027)	(-0.330)		
0.30	0.35	1.79667	-0.241565	1.79481	-0.242275
		(0.028)	(-0.293)		
0.30	0.12	1.82008	-0.337545	1.81641	-0.338658
		(0.023)	(-0.329)		

Table 3.7 Accuracy of CSD in response of change of Poisson's ratio for $E_1/E_2 = 100$

For $E_1 = 100$ and $E_2 = 10$, i.e. $E_1/E_2 = 10$:

ν_1	ν_2	K_{1CSD} 3rd pair (% deviation)	K_{2CSD} 3rd pair (% deviation)	K_{1ref}	K_{2ref}
0.30	0.30	1.79506	-0.216734	1.79030	-0.216592
		(0.032)	(0.066)		
0.30	0.35	1.79186	-0.198869	1.78745	-0.198606
		(0.033)	(0.132)		
0.30	0.12	1.80934	-0.283385	1.80313	-0.283438
		(0.029)	(-0.019)		

Table 3.8 Accuracy of CSD in response of change of Poisson's ratio for $E_1/E_2 = 10$

The deviation is within 0.4%.

3.3.2 Center Interface Crack in Finite Bimaterial Plate

A finite plate shown in Figure 3.9 was taken for verification. The detailed solution is given in Yuuki and Cho (1989a and 1989b) and is collected concisely in Murakami (1987).

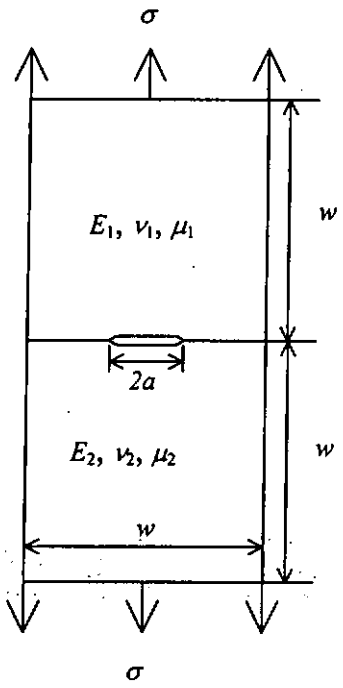

Figure 3.9 A center interface crack in finite bimaterial plate under tension

The accuracy of the numerical results are claimed to be better than 0.2%. With the definition of the stresses same as Equation ...(1.11) and normalization through taking $l = 2a$ for center cracks, the numerical solution for plates under plane stress with $\nu_1 = \nu_2 = 0.3$ are given as :

	2a/w				
	0.1	0.2	0.3	0.4	0.5
E_1/E_2					
2.0	0.999	1.021	1.055	1.106	1.183
	(-0.072)	(-0.070)	(-0.068)	(-0.066)	(-0.066)
4.0	0.991	1.013	1.046	1.096	1.170
	(-0.131)	(-0.126)	(-0.122)	(-0.120)	(0.118)
10.0	0.978	1.000	1.032	1.079	1.149
	(-0.218)	(-0.173)	(-0.168)	(-0.163)	(-0.161)

Table 3.9 Reference values of nondimensional stress intensity factors for center interface crack in finite plate with

Upper value = F_{iref}, Lower value in ( ) = $\left[\frac{K_2}{K_1}\right]_{ref}$

The reference values of complex stress intensity factor are therefore given by :

$$K_{1ref} = F_{iref} \cdot \left(\sigma\sqrt{\pi a}\right) \cdot \sin\left(\tan^{-1}\left[\frac{K_2}{K_1}\right]_{ref}\right)$$

$$K_{2ref} = F_{iref} \cdot \left(\sigma\sqrt{\pi a}\right) \cdot \cos\left(\tan^{-1}\left[\frac{K_2}{K_1}\right]_{ref}\right) \qquad \ldots(3.23)$$

The cases above in Table 3.9 are modeled in FEA with w = 10 units. The mesh parameters are e/a = 1/100 and m = 1.5 and number of elements vary from 1252 to 876 depending on the size of crack. The relative virtual crack extension length is kept to $\Delta a/e$ = 1/500. Plane stress and applied loading conditions are : a) symmetry along the plane of symmetry , b) $u_y = 0$ on the bottom edge and c) $\sigma = 1$ unit along the top edge. The combined SDM is applied to derive the complex stress intensity factors. The results and accuracy from the derived reference values are shown in Table 3.10. The combined SDM is accurate with deviation within 0.7%.

2a/w (no. of elements)	E_1/E_2	K_{1SDM} (% deviation)	K_{2SDM} (% deviation)	K_{1ref}	K_{2ref}
0.1	2	1.251	-0.090	1.249	-0.090
		(0.21)	(0.30)		
(1252)	4	1.235	-0.162	1.232	-0.161
		(0.27)	(0.13)		
	10	1.211	-0.218	1.206	-0.217
		(0.36)	(0.55)		
0.2	2	1.803	-0.126	1.805	-0.126
		(-0.12)	(-0.46)		
(1092)	4	1.780	-0.225	1.781	-0.224
		(-0.10)	(0.21)		
	10	1.746	-0.303	1.747	-0.302
		(-0.06)	(0.37)		
0.3	2	2.280	-0.155	2.285	-0.155
		(-0.22)	(-0.41)		
(998)	4	2.250	-0.276	2.254	-0.275
		(-0.18)	(0.34)		
	10	2.206	-0.371	2.209	-0.371
		(-0.14)	(-0.14)		
0.4	2	2.761	-0.184	2.766	-0.183
		(-0.20)	(0.63)		
(964)	4	2.722	-0.326	2.728	-0.327
		(-0.19)	(-0.30)		
	10	2.666	-0.436	2.669	-0.435
		(-0.12)	(0.24)		
0.5	2	3.300	-0.218	3.308	-0.218
		(-0.25)	(-0.21)		
(876)	4	3.250	-0.385	3.256	-0.384
		(-0.21)	(0.22)		
	10	3.176	-0.511	3.179	-0.512
		(-0.11)	(-0.12)		

Table 3.10 The results from combined SDM for center interface crack in finite plate

3.3.3 Single Edge Interface Crack in Finite Bimaterial Plate

A finite plate with edge interface crack shown in Figure 3.10 was taken for verification. The detailed solution is given in Yuuki and Cho (1989a and 1989b) and is collected in Murakami (1987) concisely.

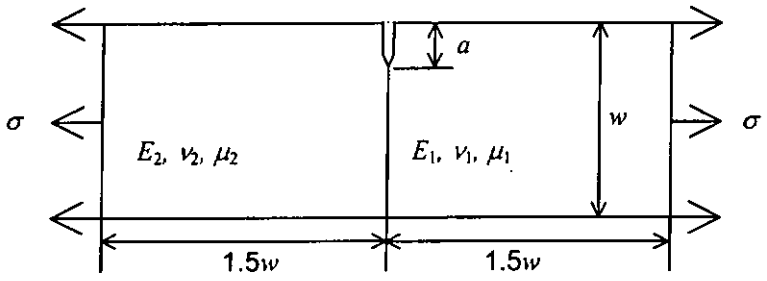

Figure 3.10 A single edge interface crack in finite bimaterial plate under tension

The accuracy of the numerical results are claimed to be better than 0.2%. With the definition of the stresses same as Equation ...(1.11) and normalization through taking $l = 2a$ for edge cracks, the numerical solution for plates under plane stress with $\nu_1 = \nu_2 = 0.3$ are given as :

	a/w				
	0.05	0.1	0.2	0.3	0.4
E1/E2					
2.0	1.147	1.195	1.373	1.664	2.117
	(-0.114)	(-0.108)	(-0.100)	(-0.095)	(-0.094)
4.0	1.201	1.224	1.410	1.678	2.130
	(-0.210)	(-0.198)	(-0.183)	(-0.174)	(0.171)
10.0	1.281	1.266	1.411	1.693	2.146
	(-0.292)	(-0.277)	(-0.255)	(-0.242)	(-0.237)

Table 3.14 Reference values of nondimensional stress intensity factors for single edge interface crack in finite plate with

Upper value = F_{iref}, Lower value in ( ) = $\left[\frac{K_2}{K_1}\right]_{ref}$

The reference values of complex stress intensity factor are calculated from Equation ...(3.23).

The cases above in Table 3.14 are modeled in FEA with w = 10 units. The mesh parameters are e/a = 1/100 and m = 1.5 and number of elements vary from 1398 to 908 depending on the size of crack. The relative virtual crack extension length is kept to $\Delta a/e$ = 1/500. Plane stress and applied loading conditions are : a) u_y = 0 on the bottom edge and u_x = 0 on its remote corner and b) σ = 1 unit along the top edge. The combined SDM is applied to derive the complex stress intensity factors. The results and accuracy from the derived reference values are shown in Table 3.12. The combined SDM is accurate with deviation within 1.6 %.

2a/w (no. of elements)	E_1/E_2	K_{1SDM} (% deviation)	K_{2SDM} (% deviation)	K_{1ref}	K_{2ref}
0.05	2	1.445	-0.163	1.428	-0.163
		(1.17)	(0.22)		
(1398)	4	1.493	-0.309	1.473	-0.309
		(1.36)	(-0.12)		
	10	1.563	-0.451	1.541	-0.450
		(1.39)	(0.30)		
0.1	2	2.113	-0.228	2.106	-0.227
		(0.35)	(0.20)		
(1190)	4	2.138	-0.423	2.128	-0.421
		(0.46)	(0.32)		
	10	2.174	-0.600	2.163	-0.599
		(0.51)	(0.22)		
0.2	2	3.420	-0.342	3.425	-0.342
		(-0.13)	(-0.10)		
(1092)	4	3.421	-0.626	3.477	-0.636
		(-1.59)	(-1.54)		
	10	3.424	-0.874	3.427	-0.874
		(-0.08)	(0.01)		
0.3	2	5.079	-0.485	5.086	-0.483
		(-0.14)	(0.42)		
(998)	4	5.066	-0.884	5.075	-0.883
		(-0.18)	(0.06)		
	10	5.050	-1.224	5.052	-1.223
		(-0.04)	(0.09)		
0.4	2	7.455	-0.701	7.472	-0.702
		(-0.22)	(-0.25)		
(908)	4	7.428	-1.271	7.443	-1.273
		(-0.20)	(-0.14)		
	10	7.391	-1.751	7.402	-1.754
		(-0.15)	(-0.21)		

Table 3.12 The results from combined SDM for single edge interface crack in finite plate

3.3.4 Interface Cracks in Four-Point Bend Specimen

The detailed reference solution is taken from Charalambides et al. (1989) as reported in Murakami (1987). The specimen in Figure 3.11 was modeled with various thickness ratios ($H_1/H_2 = 0.5$ and 1.0) and different modulus ratios ($E_2/E_1 =$ 1, 2.5, 5, 10 and 25). Their complex stress intensity factors were determined by the combined SDM. Taking advantage of symmetry, only the right half of the beam was

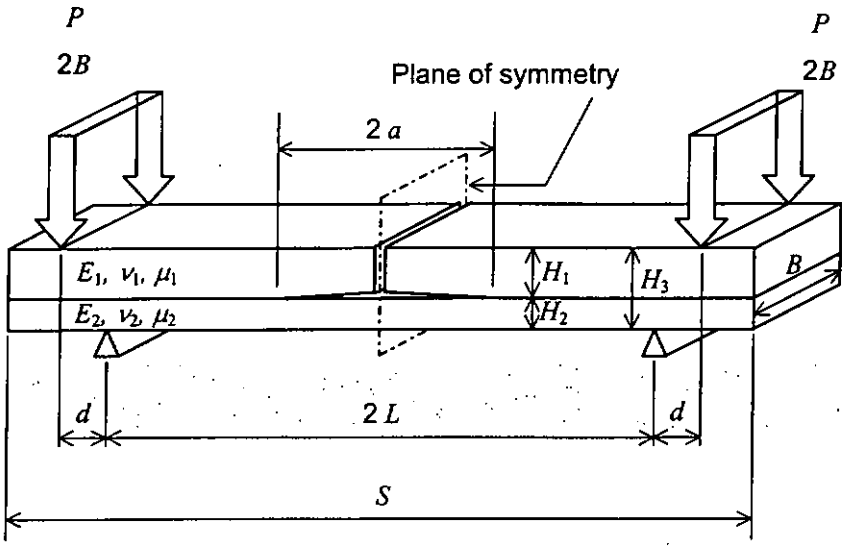

Figure 3.11 The Notched Bimaterial Specimen with Interface Crack under Symmetrical Four-point Bend Loading and its Dimensions

modeled. The material properties and geometrical parameters are : $E_1 = 3\times10^9$, $\nu_1 = \nu_2 = 0.3$, $P/2 = 1\times10^6$, $B = 1$, $H_1 = 10$ units, $S = 300$ units, $d = H_3$ units, $a = 45$ units, $L = S/2 - 2H_3$. Reference values are in graphical presentations of complex stress intensity factors given in the normalized formats:

$$K_{1norm} = \mathrm{Re}\left(\boldsymbol{K}H_3^{i\varepsilon}\right)\frac{BH_3^{3/2}}{Pd} \qquad \text{and}$$

$$K_{2norm} = \mathrm{Im}\left(\boldsymbol{K}H_3^{i\varepsilon}\right)\frac{BH_3^{3/2}}{Pd} \qquad \ldots(3.24)$$

where $\mathrm{Re}(z) = y$ and $\mathrm{Im}(z) = x$ denotes the real part and the imaginary part of the complex number $z = y + \mathrm{i}\,x$ respectively.

Since $\boldsymbol{K} = K_1 + \mathrm{i}\,K_2$, Equation ...(3.24) is therefore:

$$K_{1norm} = \frac{\left[K_1 \cos(\varepsilon \ln(H_3)) - K_2 \sin(\varepsilon \ln(H_3))\right] \cdot BH_3^{3/2}}{Pd}$$

$$K_{2norm} = \frac{\left[K_1 \sin(\varepsilon \ln(H_3)) + K_2 \cos(\varepsilon \ln(H_3))\right] \cdot BH_3^{3/2}}{Pd} \qquad \ldots(3.25)$$

Results calculated by the present approach are also converted to these forms for easy reference and are presented in Table 3.13 and Table 3.14. The maximum error is below 3.5%. It should be pointed out that the extraction of the normalized referenced values from the graphs in the reference makes it rather difficult to demonstrate extremely high accuracy. The corresponding values without normalization and the conversion from normalized reference values to complex stress intensity factors are given in Table III.3 and 4 of Appendix III.

$H_1/H_2 = 1$ (642 elements)	Combined SDM		Reference values (Charalambides et al. (1989))	
E_2/E_1	K_{1norm}	K_{2norm}	K_{1norm}	K_{2norm}
1	2.422	2.073	2.442	2.105
	(-0.83)	(-1.50)		
2.5	1.687	1.610	1.674	1.657
	(0.74)	(-2.85)		
5	1.167	1.201	1.169	1.209
	(-0.18)	(-0.66)		
10	0.776	0.806	0.761	0.807
	(1.90)	(-0.06)		
25	0.397	0.417	0.384	0.407
	(3.41)	(2.39)		

Table 3.13 Normalized K-values by the combined SDM for four point bend specimen with $H_1/H_2 = 1$

$H_1/H_2 = 0.5$ (652 elements)	Combined SDM		Reference values (Charalambides et al. (1989))	
E_2/E_1	K_{1norm}	K_{2norm}	K_{1norm}	K_{2norm}
1	1.360	1.301	1.387	1.293
	(-1.91)	(0.63)		
2.5	0.847	0.930	0.868	0.925
	(-2.44)	(0.46)		
5	0.526	0.634	0.534	0.638
	(-1.62)	(-0.63)		
10	0.304	0.386	0.314	0.384
	(-3.12)	(0.71)		
25	0.135	0.178	0.140	0.174
	(-3.37)	(2.34)		

Table 3.14 Normalized K-values by the combined SDM for four point bend specimen with $H_1/H_2 = 0.5$

The complex stress intensity factors, K_1 and K_2, of notched-beams under symmetrical four-point bend loading have been studied numerically by Klingbeil and Beuth (1997), and Charalambides et al. (1989, 1990). Numerical results of Charalambides' (1989) have been collected in the stress intensity manual by Murakami (1987). Analytical solutions by considering the dislocation theory have been given in Suo and Hutchinson (1990) for a more general case with the four-point bend specimen as one of the cases considered. One of the uncertainties in this solution is the value of ω, which is a function of the Dundurs' parameters α, β and the thickness ratio H_2/H_1. The value of ω is obtained from numerical results and is given in table form for interpolation. Another limitation of this solution is that $0 < H_2/H_1 \leq 1$. Therefore the analytical solution for this type of specimen is still not well developed.

3.4 CONCLUSION

From all the tested cases, the accuracy and stability of the combined SDM is proven. The relative virtual crack extension length is recommended as $\Delta a/e$ = 1/500 to 1/1000. The arbitrary ΔKs were taken as 1/100 times of the expected K-values. The mesh parameters will be taken as e/a = 1/100 and m = 1.5. From the results in closed form solution of infinite plate, the accuracy is within 1% with the recommended parameter values.

The accuracy of the CSD is only comparable to the combined SDM when the element size is small with mild geometric progression and with the mesh method as used in here (first three elements are of the same size).

Chapter 4 Design of a Four Point Bend Specimen for Subinterfacial Crack Studies

4.1 INTRODUCTION

Although the analysis of interfacial cracks problems in general is still a formidable task, there is a special class of interfacial crack problems which may be treated according to linearly elastic fracture mechanics (LEFM) concepts, namely, the "boundary layer fracture", or "subinterface crack" phenomenon, in which fracture is observed to be close to but not exactly at the interface. For example, cracks in solder joints are known to exhibit this phenomenon. A thin layer of solder being left behind at the interface while the crack develops inside the solder (Clough et al. (1995)). Such cases of interfacial fracture would favor a traditional LEFM analysis provided that the stress intensity factors K_I and K_{II} are determinable. So far studies on subinterface cracks as a separate class of problem from interfacial cracks in general are few. A summary of the works of Hutchinson et al. (1987), Lu and Lardner (1992), and Yang and Kim (1993) can be found in Venkatesha et al. (1998). Beom and Atluri (1995) analysed a subinterface crack between two dissimilar orthotropic solids and obtained analytical expressions for stress intensity factors of the subinterface crack in terms of the complex stress intensity factor of the corresponding interface crack. Fett and co-workers (1997a,1997b) derived weight functions for edge cracks and internal cracks in the vicinity of interfaces of dissimilar materials using reference values generated by finite element analysis. While all the above analytical work contribute to possible predictions of subinterface crack behaviour, experimental work is necessary to verify these predictions and lend further insight into this class of fracture problems.

In this Chapter, a four-point bend specimen (see Figure 4.1) is being developed for the study of cracks close to and parallel to the interface of two dissimilar materials, i.e. subinterface cracks. This specimen configuration is chosen since it can simulate the bending effects on thermomechanical loading applied on subinterface cracks in solder and its simplicity of its loading equipment which is the

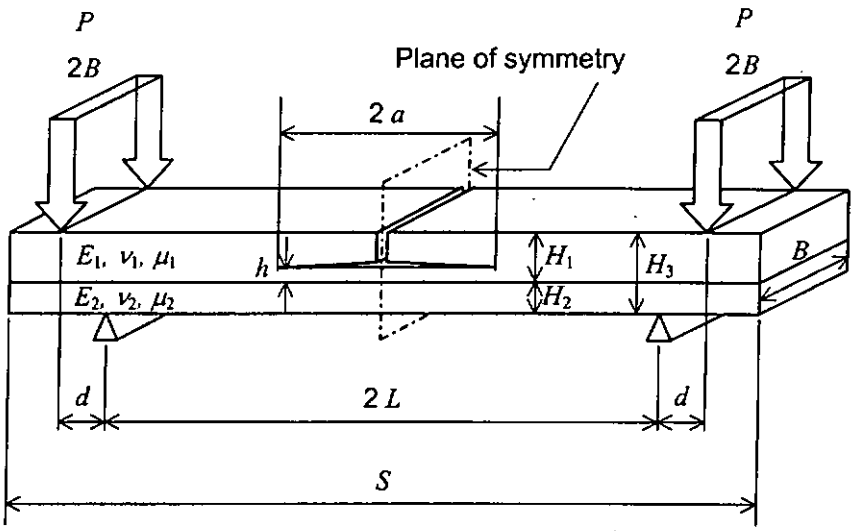

Figure 4.1 The Notched Bimaterial Specimen with Subinterface Crack under Symmetrical Four-point Bend Loading and its Dimensions

basic four point bend apparatus on loading machines. The stress intensity factors associated with this specimen are determined from crack surface displacements generated by finite element analysis. Basing on the strain energy release rates and stress intensity factor plots, recommendations for support spacing and specimen heights are made. The normalized values of the associated stress intensity factors are curve-fitted using a combination of power and polynomial terms in the distance between the crack and the interface. The use of these curves is demonstrated by an application to cracks near Ni/MgO, Si/Cu and solder/copper interface.

4.2 FOUR-POINT BENDING SPECIMEN FOR SUB-INTERFACIAL CRACK DETERMINATION

Our specimen design has arisen from the four-point bend specimen (Figure 3.11) for the study of interfacial cracks, developed by Matos (1989), and Charalambides et al. (1989, 1990 and 1996).

For the interface crack specimen, the crack propagates along the interface. Moreover, the strain energy release rate exhibits steady-state characteristics so that it is not necessary to monitor crack length accurately during testing. This strain energy release rate can be evaluated from consideration of the energies in the uncracked section and in a section of the lower beam beneath the crack. Thus the measurement of the critical load through experiment will lead to the critical strain energy release rate (G_c) of the interface concerned. Furthermore the deformation produced resembles that caused by thermal loading on bimaterial interfaces.

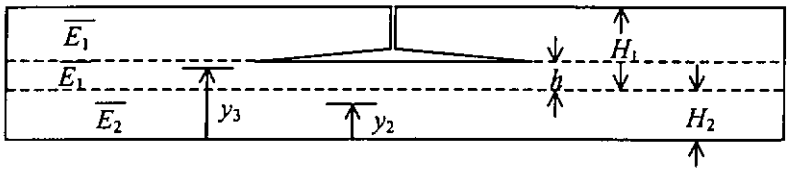

Figure 4.2 Subinterface crack specimen as a three layered specimen with the notations of neutral axis and material properties

Unlike the interface crack specimen, the crack in our specimen for subinterface cracks does not propagate along a parallel direction with the interface due to mixed mode effects. The G-value derived from the energies of the uncracked and cracked section at critical load does not represent G_c. Here in this Chapter, the

stress intensity factors will be determined as a function of the load and crack position for the study of subinterfacial cracks. The stress intensity factors obtained by FEA will be verified by the *G*-values derived from a three layered specimen model (Figure 4.2) by Klingbeil and Beuth (1997). The model was used to extend the interface crack specimen to a three-layer configuration for the study of interfacial fracture of deposited metal layers. In the present study we assign the same material properties to the layers at the top so that a crack parallel but close to the interface of two different materials is obtained. The strain energy release rate expression is then given by:

$$G_3 = \frac{M^2}{2B\overline{E_1}} \cdot \left(\frac{1}{I_2} - \frac{1}{I_3} \right) \qquad \ldots(4.1)$$

where I_2 and I_3 (given in Equation ...(4.2) and Equation ...(4.3)) are the moment of inertia of the section under the crack and the uncracked section of the beam respectively and $M = \frac{P}{2B} \times d$.

The subscript 3 in the strain energy release rate G_3 denotes the value obtained from the three-layered beam equation, i.e. Equation ...(4.1).

Taking the upper layer, where the crack is located, as the reference material:

$$I_2 = B\left[\frac{1}{12} \cdot \left(h^3 + n \cdot H_2^{\,3} \right) + h \cdot \left(y_2 - H_2 - \frac{h}{2} \right)^2 + n \cdot H_2 \cdot \left(y_2 - \frac{H_2}{2} \right)^2 \right] \ldots(4.2)$$

$$I_3 = B\left[\frac{1}{12} \cdot \left(H_1^{\,3} + n \cdot H_2^{\,3} \right) + H_1 \cdot \left(y_3 - H_2 - \frac{H_1}{2} \right)^2 + n \cdot H_2 \cdot \left(y_3 - \frac{H_2}{2} \right)^2 \right] \qquad \ldots(4.3)$$

where y_2 and y_3 are the distances of the neutral axes from the bottom, of the cracked and the uncracked section respectively:

$$y_2 = \frac{H_2}{2} \cdot \frac{n + (h/H_2)(h/H_2 + 2)}{(n + h/H_2)},$$

$$y_3 = \frac{H_2}{2} \cdot \frac{n + (H_1/H_2)(H_1/H_2 + 2)}{(n + H_1/H_2)}, \quad \text{and} \quad n = \frac{\overline{E_2}}{\overline{E_1}}. \qquad \ldots(4.4)$$

Note that the strain energy release rate in Equation ...(4.1) is independent of the crack length.

4.3 Determination of Stress Intensity Factors for Cracks Parallel to an Interface

Work associated with the determination of stress intensity factors for subinterface cracks have been mainly analytical. Hutchinson et al (1987) analyzed cracks parallel and close to an interface to establish a relationship between the traditional stress intensity factors and the complex stress intensity factor associated with the corresponding interface crack problem. The condition for cracks to propagate near and parallel to, but not along, an interface was also derived. The basic assumption is that at distance (r) from the tip which are large compared to the distance between crack and interface (h) and small compared with the crack length, the near-tip field of the corresponding interface crack problem applies. Lu and Lardner (1992) attempted to determine stress intensity factors for the cases of uniform pressure and concentrated force pair loadings through the use of dislocation density functions and found that the stress intensity factors and energy release rate approach to an asymptotic solution derived in Hutchinson et al (1987), when h/a is small. In these and other references (Yang and Kim (1993), Venkatesha et al.(1998), Beom and Atluri (1995) and Fett et al. (1997a and 1997b)), load cases reported usually involve infinite or semi-infinite systems and with purely remote mode I loading. In this Chapter, stress intensity factors for the four-point bend specimen will be determined, with a view to obtain suitable specimen geometries for the verification of their conclusions by actual experimentation using different combinations of materials for this specimen.

Since the crack is contained in a homogeneous medium, its crack-tip stress intensities can be characterized by the near crack-tip surface profile. The semi-infinite crack model in Chapter 2 is used to provide expressions for the calculation of K_I and K_{II}. Quarter-point elements and transition elements are employed at the crack tip to model stress singularity. Two-dimensional models of 900 configurations were built with dimensions H_1 = 10 units, S = 250 units, d = 30 units and $2L$ = 100 units and with various parameters :

1. crack length (see Figure 4.3) : a = (20, 25, 30, 40, 48) units;
2. modulus ratio : E_2/E_1 = (0.5, 1, 2.5, 5, 10), with E_1 fixed at 3×10^9 ; and $\nu_1 = \nu_2 = 0.3$
3. thickness ratio (see Figure 4.4) : H_1/H_2 = (0.5,1,1.5, 2); and
4. penetration ratio : h/H_1 = (1/1000, 2/1000, 5/1000, 1/100, 2/100, 5/100, 1/10, 2/10 and 5/10).

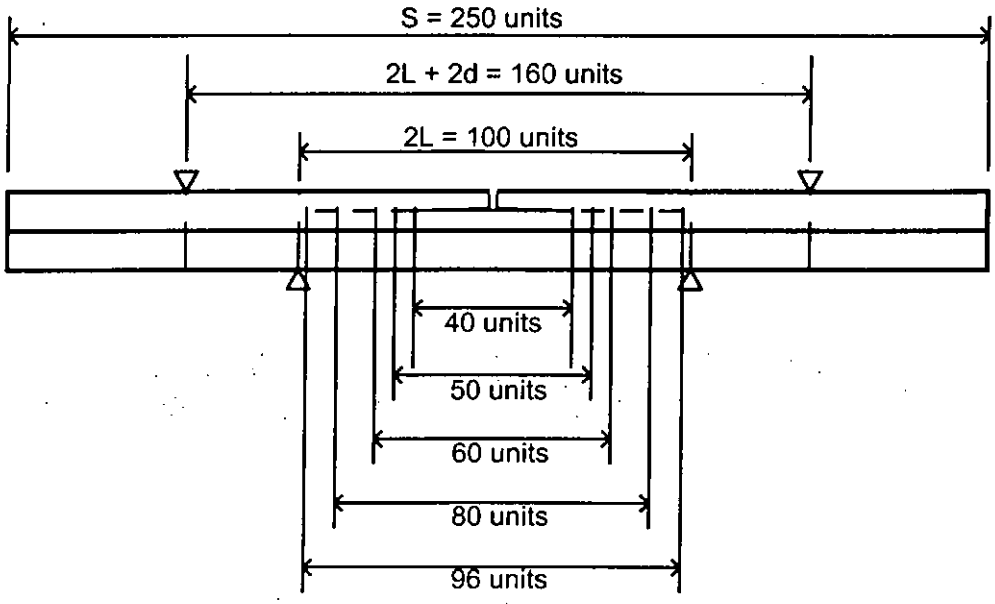

Figure 4.3 Drawn-to-scale beam with length quantities and different crack lengths $2a$

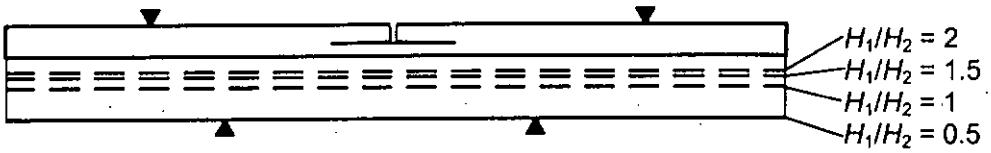

Figure 4.4 Drawn-to-scale beam with various thickness ratios H_1/H_2

All the cases have $\nu_1 = \nu_2 = 0.3$. The right half-beam model was used taking advantage of symmetry. Plane strain conditions applied with the load ($P/2 = 10^6$ units) on the upper load point and $u_y = 0$ at lower load point. The element mesh has twelve quarter-point elements and twelve transition elements forming a circular ring surrounding the crack-tip as shown in Figure 3.2. Geometric progressing eight-noded rectangular quadratic elements filled the remaining area. The crack-tip is at least five elements apart from the interface. Approximately 8000 elements were applied in each analysis, the exact number depending on the various dimensions of the specimens.

4.3.I The Normalization Procedure

For results to be applicable to geometrically similar systems, a normalization procedure should be employed. To cope with possible variations in H_1/H_2 and n values the solution of Suo (1990), originally derived for delamination specimens with orthotropic materials, is employed.

Suo (1990) had solved the stress intensity factors in homogeneous beams with the loading shown in Figure 4.5. The stress intensity factors for $0 \le \eta \le 1$ and for isotropic material 1 are given as :

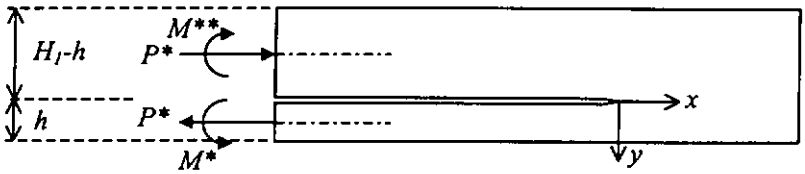

Figure 4.5 Suo's homogeneous beam with solution for stress intensity factors

$$K_{I0} = \pm\left\{\frac{P^*}{\sqrt{2hA}}\cos\omega + \frac{M^*}{\sqrt{2h^3 I}}\sin(\omega+\gamma)\right\} \qquad \ldots(4.5)$$

$$K_{II0} = \pm\left\{\frac{P^*}{\sqrt{2hA}}\sin\omega - \frac{M^*}{\sqrt{2h^3 I}}\cos(\omega+\gamma)\right\} \qquad \ldots(4.6)$$

where $\frac{1}{A} = 1 + 4\eta + 6\eta^2 + 3\eta^3, \quad \frac{1}{I} = 12(1+\eta^3),$ $\ldots(4.7)$

$$\frac{\sin\gamma}{\sqrt{AI}} = 6\eta^2(1+\eta), \quad \eta = \frac{h}{H_1 - h} \quad \text{and} \qquad \ldots(4.8)$$

ω can be estimated as $\omega = 52.1\text{-}3\eta$, with ω and η in degrees ...(4.9)

The last subscript, '0', for the stress intensity factors K are used to designate them as the eventual denominator quantities for the normalization procedure.

The stress intensity factors for a homogeneous half-beam specimen/loading system as shown in Figure 4.5 are the same as those for the system in Figure 4.6. By the superposition operation in Appendix IV and V, any homogenous beam with the general form in Figure 4.6 can be expressed as that in Figure 4.5. P* and M* are related to P_o and M_o by:

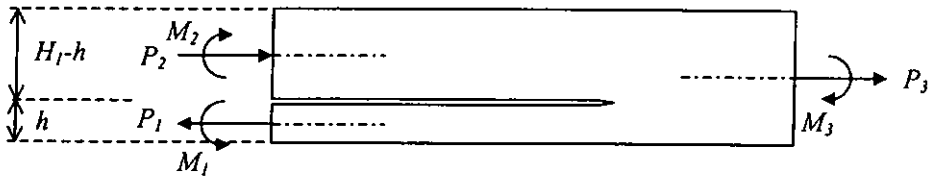

Figure 4.6 Homogeneous beam with loading in general form

$$P^* = (1 - C_1)P_o + \frac{C_2 M_o}{h},$$

$$M^* = M_1 - C_3 M_o = \left[M_o + \frac{P_o}{2}(H_1 - h) \right] - C_3 M_o \qquad \ldots(4.10)$$

where $C_1 = \dfrac{1}{(1/\eta)+1}$, $C_2 = \dfrac{6/\eta}{[(1/\eta)+1]^3}$ and $C_3 = \dfrac{1}{[(1/\eta)+1]^3}$.

In our application, P_o and M_o are obtained as the resultants of stresses acting on the material 1 area of the full cross-section in front of the crack tip using elementary beam bending theory as follows:

First the nominal flexural (x-direction) stresses in material 1 at the top layer (free surface) and on the bottom layer (interface), σ_{xt} and σ_{xb} respectively (see Figure 4.7), are calculated from the constant bending moment M generated by the four

Figure 4.7 The flexural stresses in our specimen taken for normalization

point bending load:

$$\sigma_{xt} = \frac{M}{I_3}(H_1 + H_2 - y_3), \qquad \sigma_{xb} = \frac{M}{I_3}(H_2 - y_3) \qquad \ldots(4.11)$$

where y_3 and I_3 are defined in equations ...(4.3) and ...(4.4).

The loads P_o and M_o are then obtained by considering superposition (see Figure 4.8) of the corresponding stresses should result in σ_{xt} and σ_{xb} :

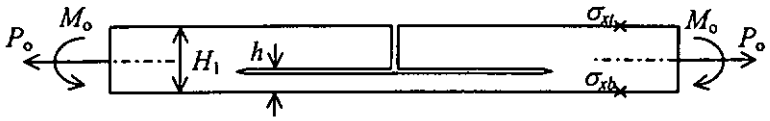

Figure 4.8 The homogeneous beam used to model our beam for normalization

$$P_o = \left(\frac{\sigma_{xt} + \sigma_{xb}}{2}\right)BH_1, \qquad M_o = \frac{BH_1^3}{12}\frac{(\sigma_{xt} - \sigma_{xb})/2}{H_1/2} \qquad \ldots(4.12)$$

From these values K_{I0} (Equation ...(4.5)) and K_{II0} (Equation ...(4.6)) are given by:

$$K_{I0} = \left| \left\{ \begin{array}{l} \left[\frac{-(1+\eta)^2 P_o h - 6\eta^2 M_o}{(1+\eta)^3 h\sqrt{2h}}\right]\sqrt{1+4\eta+6\eta^2+3\eta^3}\cos\omega \\ +\left[\frac{2M_o(1+3\eta+3\eta^2)+P_o(H_1-h)(1+\eta)^3}{2(1+\eta)^3 h\sqrt{2h}}\right]\sqrt{12(1+\eta^3)}\sin(\omega+\gamma) \end{array} \right\} \right|$$

$$K_{II0} = \left| \left\{ \begin{array}{l} \left[\frac{-(1+\eta)^2 P_o h - 6\eta^2 M_o}{(1+\eta)^3 h\sqrt{2h}}\right]\sqrt{1+4\eta+6\eta^2+3\eta^3}\sin\omega \\ -\left[\frac{2M_o(1+3\eta+3\eta^2)+P_o(H_1-h)(1+\eta)^3}{2(1+\eta)^3 h\sqrt{2h}}\right]\sqrt{12(1+\eta^3)}\cos(\omega+\gamma) \end{array} \right\} \right| \qquad \ldots(4.13)$$

The resulting K_{I0} and K_{II0} are then used to normalize actual K_I and K_{II} values derived from the bimaterial configuration with the corresponding H_1, H_2, h and n values. Comparing with the configuration for generating K_{I0} and K_{II0}, the normalized values, K_I/K_{I0} and K_{II}/K_{II0} should, reflect the influence of the interface and also that of the proximity to the beam support.

4.3.2 Verification of the Preliminary Results

The obtained stress intensity factors are verified in 3 ways. Firstly, they are compared with the other two displacement methods : QPDT and DCT (see Chapter 2 for details). The maximum deviations of our K-values from those obtained from DCT are 2.6% and 4.5% for K_I and K_{II} respectively. While for QPDT, the maximum deviations are 1.3% and 2.2% for K_I and K_{II} respectively. Therefore the obtained K-values are reliable. Secondly, the K-values with $E_2/E_1 = 1$ are verified with those obtained by Suo's expression in Equation ...(4.5) and Equation ...(4.6) by taking $P_o = 0$ and with the same dimensions of the beam. The maximum deviation is 1.2%. Thirdly, the strain energy release rate G, obtained from the mixed mode K's, using Equation ...(1. 10), are compared with the strain energy release rate G_3, calculated from the three layered configuration by Equation ...(4.1). The deviation, however, is related to the crack length or, specifically, whether the crack-tip is located in the *steady state region*, which is discussed in the following section.

4.3.3 The Relation of Steady State to the Crack Length

In the case of interfacial cracks, the four-point bend specimen exhibits steady-state strain energy release rate characteristics. Such characteristics are now investigated into for the proposed specimen. Shown in Figure 4.9a is a typical

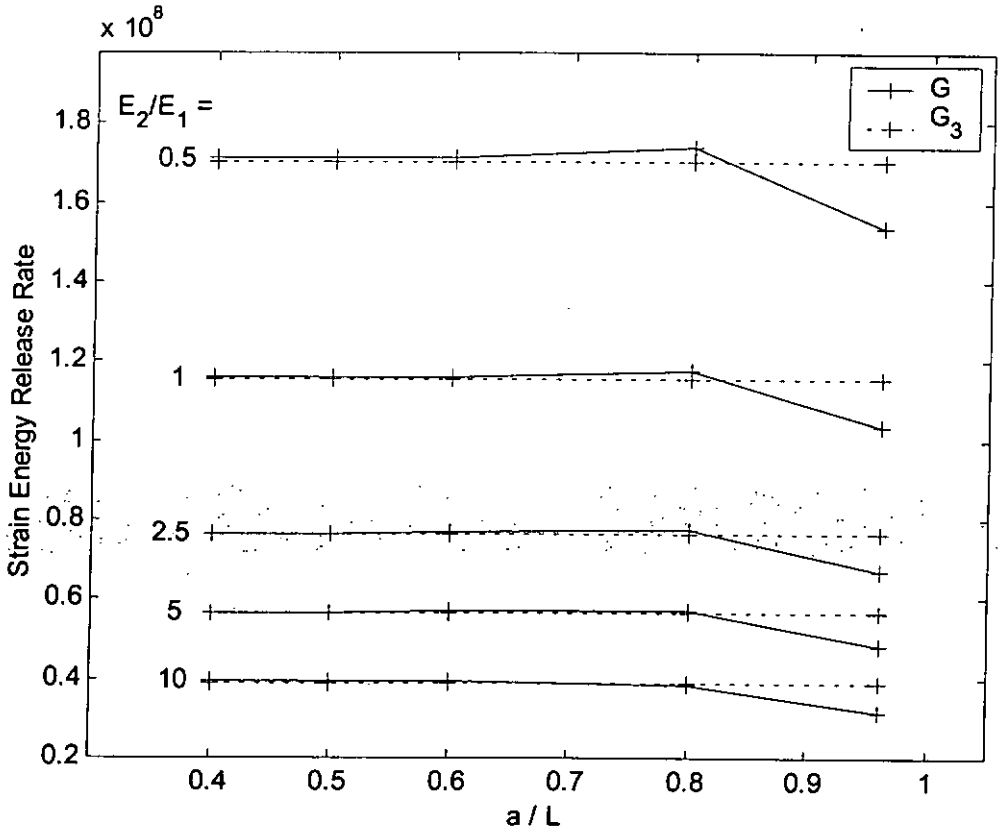

Figure 4.9a Strain Energy Release Rate against the Normalized Crack Length a/L for different E_2/E_1 with $h/H_1 = 5/10$, $H_1/H_2 = 2$ ($H_3 = 15$).

example (for the case: $h/H_1 = 5/10$ and $H_1/H_2 = 2$) of G against the relative crack length a/L for different modulus ratios E_2/E_1 . When $a = 30$ units (with $L = 50$) or below, the maximum deviation of G values (obtained from Equation ...(1.10) from our resulting K-values) from G_3 is 2.5% with a mean deviation of 0.4% only. When a increases towards the lower load point, i.e. a tends to L, the maximum and mean deviation also increases greatly. At $a = 40$, the maximum and mean deviation is 16%

and 4.0% respectively. While at a = 48, the maximum and mean deviation is 44% and 22% respectively. So it can be concluded that the strain energy release rate is influenced by the crack length through the position of the crack-tip. There are some values of crack length where the strain energy release rate are constant and can be estimated by the three-layered beam G_3, i.e. Equation ...(4.1). So it is possible to find some crack lengths which will lead to *steady state strain energy release rate* G_{ss}. This situation is called *steady state cracking*. At those particular values of crack length, not only the strain energy release rate are constant, the stress intensity factors are almost constant as well. The stress intensity factor plots against relative crack length are all collected in Appendix VI.

This observation is in line with the arguments of Charalambides et al. (1989) and of Klingbeil and Beuth (1997) for interfacial fracture specimens. They concluded that as the crack extends along the interface, the stress is relieved from the debonded portion of the specimen so that once the cracks becomes sufficiently long, the near tip stresses simply translate with the crack front and the strain energy release rate G is equal to the difference of the strain energy between the cracked and the uncracked portion of the beam, i.e. by Equation ...(4.1) for our case. This is referred to as the steady-state strain energy release rate G_{ss}. The applicability of Equation ...(4.1) obviously depends on the validity of the elementary beam bending formula at the beam sections concerned. The 'sufficiently long' condition ensures that the local effect of the free surfaces at the central notched section is not present. Likewise the crack tip should not be too close to the support and loading points. Hence the specimen should have a suitable combination of horizontal, vertical and crack-length dimensions.

In our specimen, by observing the same plots with different thickness ratios H_1/H_2, it can be seen that the steady state region depends on the thickness of the beam H_3 as well. Shown in Figure 4.9b-d are the strain energy release rate plots against the relative crack length a/L with the same h/H_1 = 5/10 as Figure 4.9a but with different thickness ratios. The region of steady state diminishes as the thickness H_3 increases. Comparing Figure 4.9a and Figure 4.9d, the region of steady state is smaller when the thickness H_3 is greater in Figure 4.9d. Similar behaviour can be observed from the other plots with different h/H_1, which are collected in Figure VI.1 to Figure VI.9 in Appendix VI.

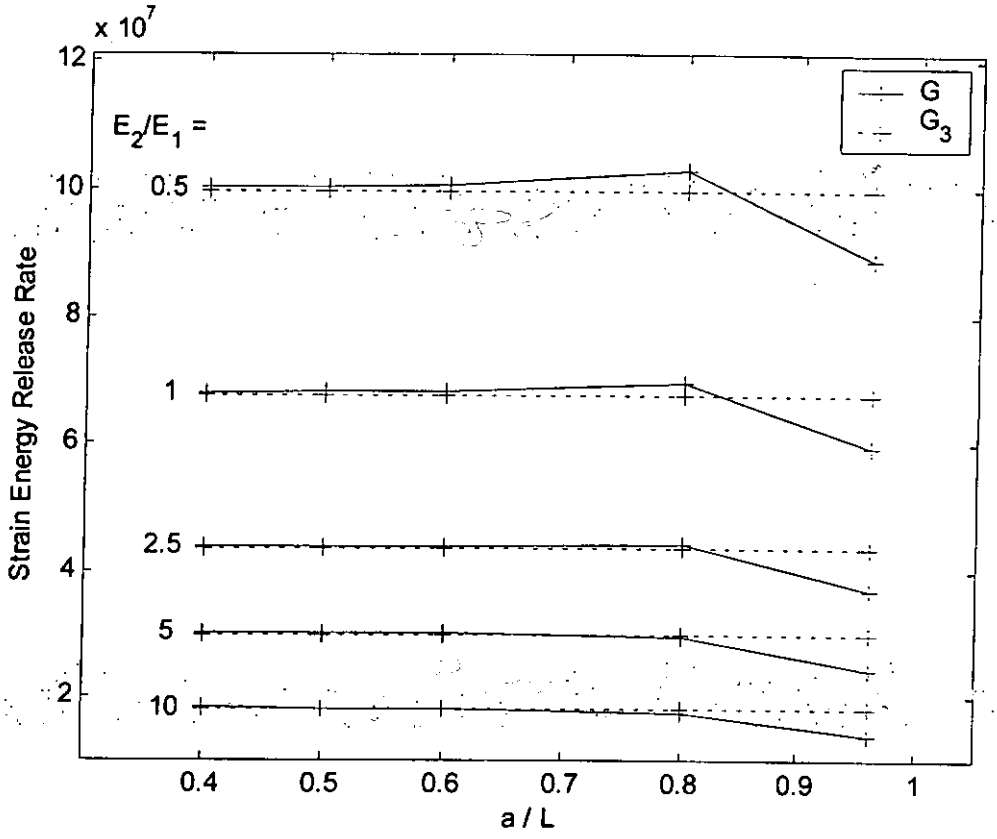

Figure 4.9b Strain Energy Release Rate against the Relative Crack Length a/L for different E_2/E_1 with h/H_1 = 5/10, H_1/H_2 = 1.5 (H_3 = 16.7).

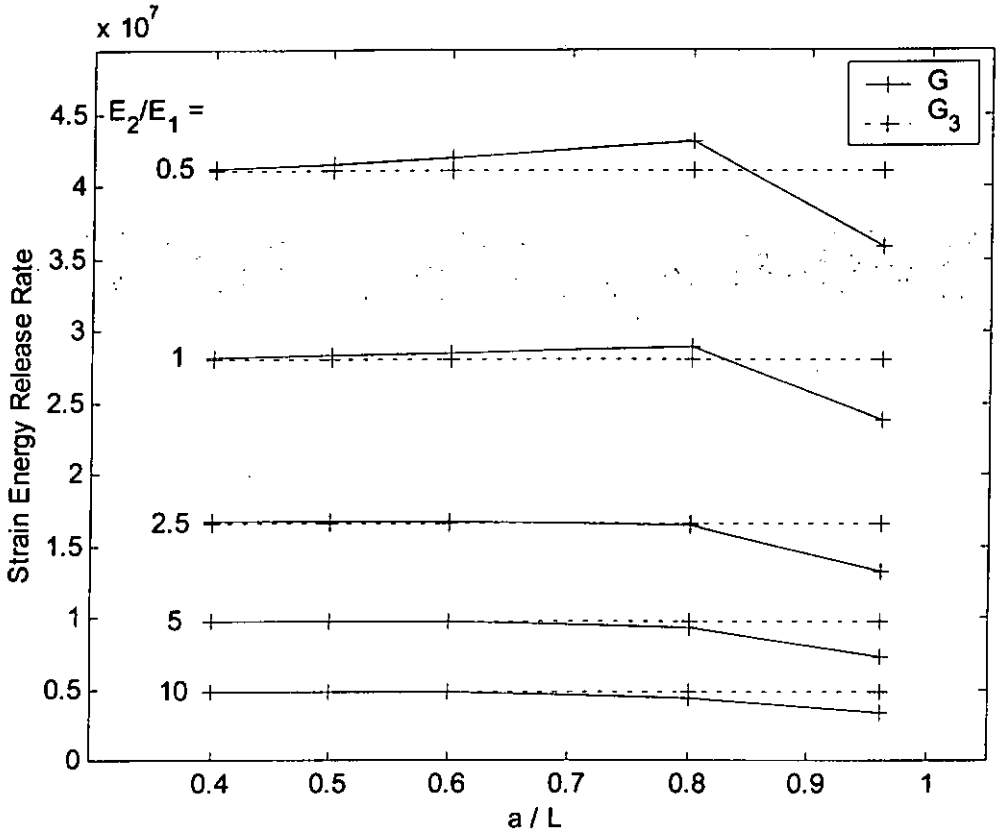

Figure 4.9c Strain Energy Release Rate against the Relative Crack Length a/L for different E_2/E_1 with $h/H_1 = 5/10$, $H_1/H_2 = 1.0$ ($H_3 = 20$).

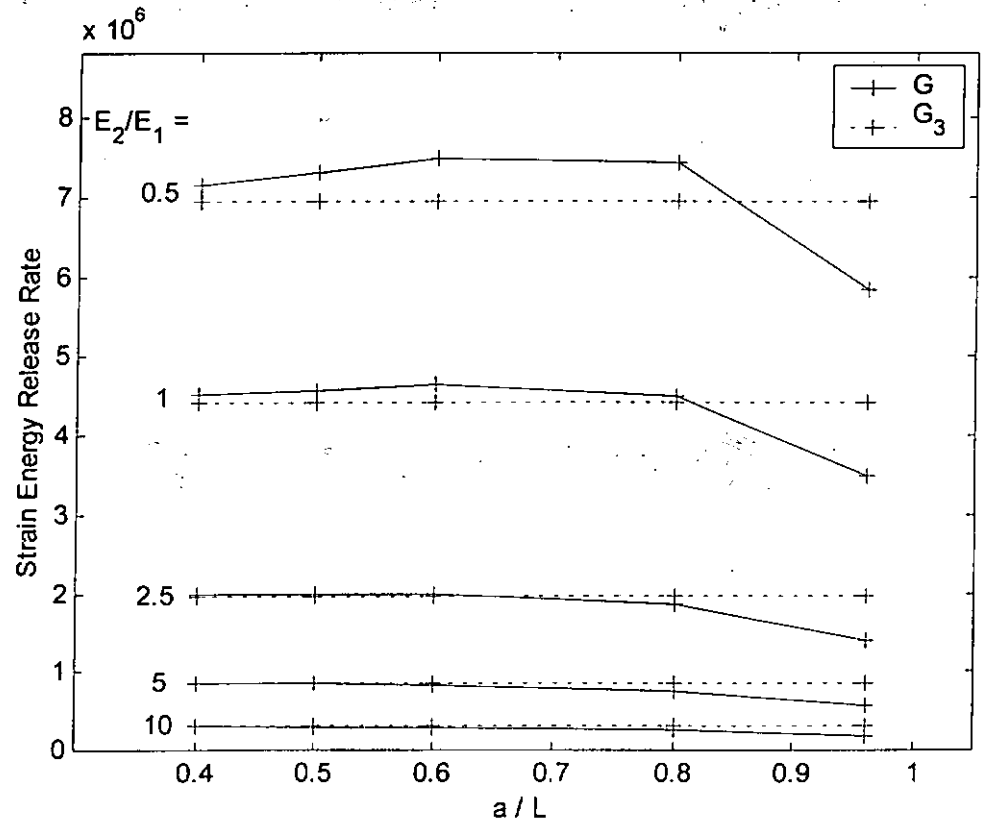

Figure 4.9d Strain Energy Release Rate against the Relative Crack Length a/L for different E_2/E_1 with $h/H_1 = 5/10$, $H_1/H_2 = 0.5$ ($H_3 = 30$).

In particular, 8 types of cases were recalculated with finer divisions of a/L to investigate the relation of beam thickness and relative crack length (a/L) to the steady state region. The 8 types are the combination of extreme values of our chosen modulus ratios ($E_2/E_1 = 0.5$ and $E_2/E_1 = 10$), thickness ratios ($H_1/H_2 = 0.5$ and $H_1/H_2 = 2$) and penetration ratios ($h/H_1 = 1/1000$ and $h/H_1 = 5/10$). The additional crack lengths a are: $a = 1, 2, 3, 5, 7.5, 10, 15, 35$ and 45, added to the original $a = 20, 25, 30, 40, 48$. $2L$ is kept as 100 as before. Two typical plots of Ks and Gs-values against relative crack length a/L are shown in Figure 4.10a and 4.10b to demonstrate the relation of the beam thicknesses and crack length to the size of steady state region. The other six plots are kept in Appendix VII.

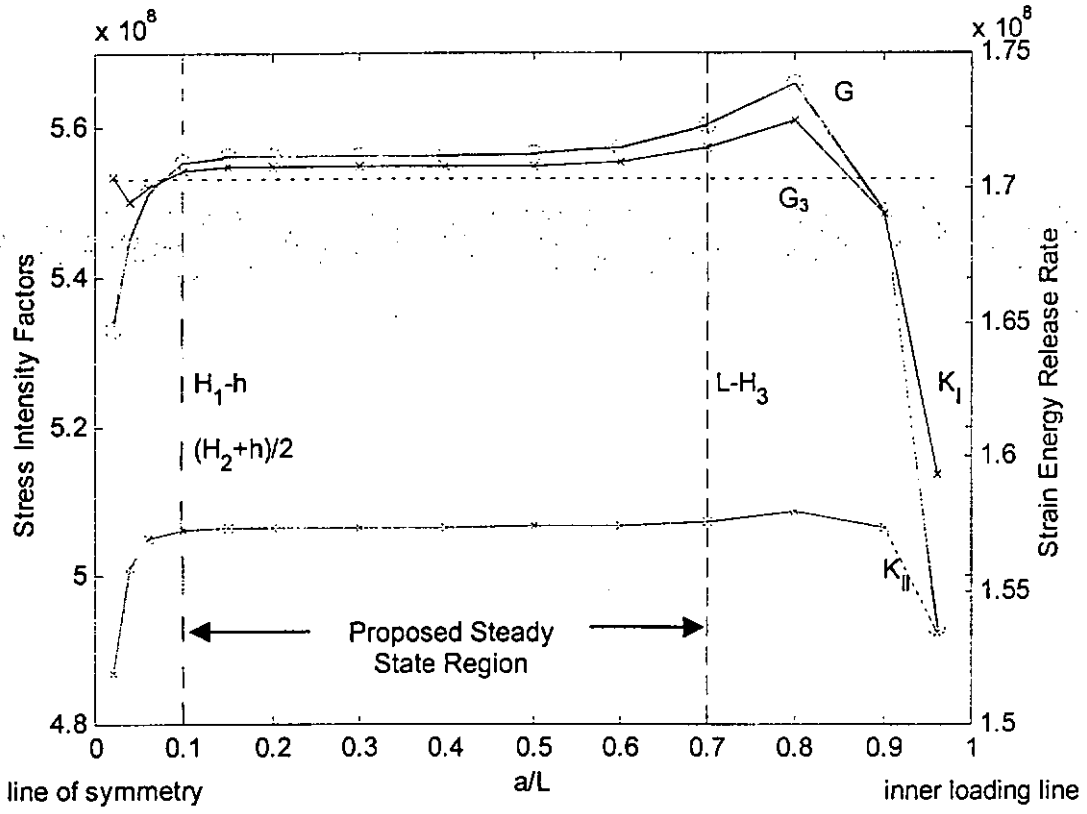

Figure 4.10a Steady State Region (Long) for $E_2/E_1 = 0.5$, $H_1/H_2 = 2$, $h/H_1 = 5/10$

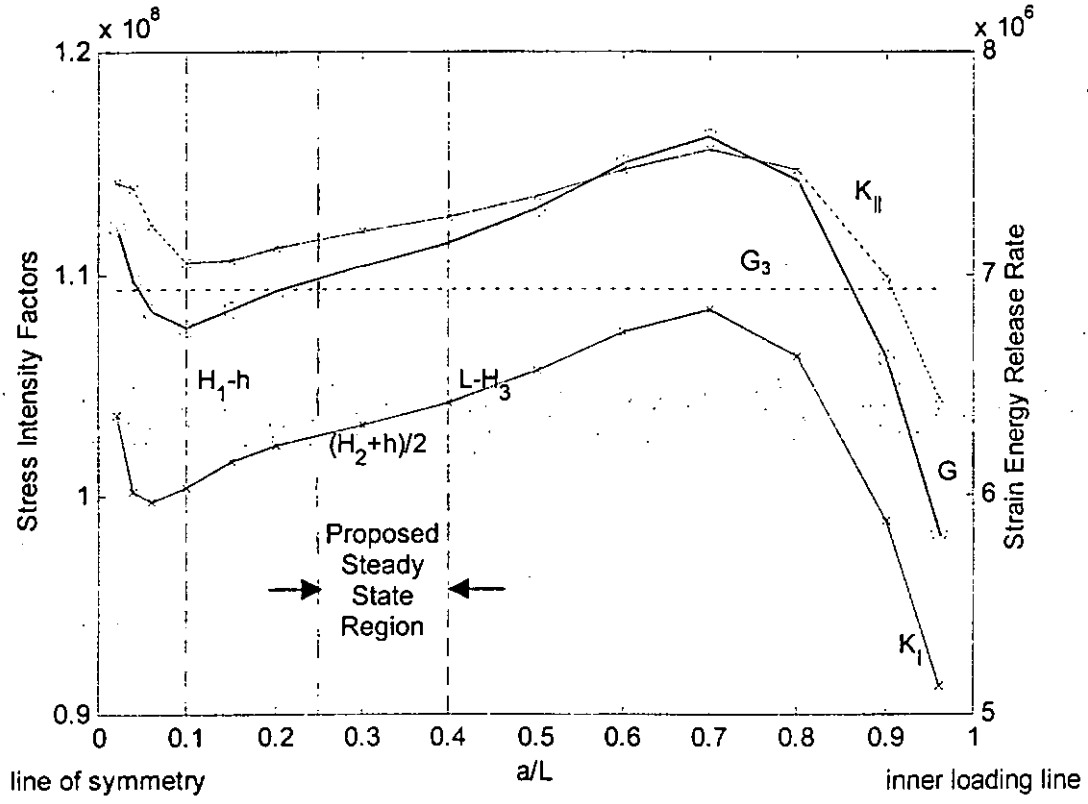

Figure 4.10b Steady State Region (Short) for $E_2/E_1 = 0.5$, $H_1/H_2 = 0.5$, $h/H_1 = 5/10$

An initial estimate of the size of steady state region is : it is bounded between the dashed lines which starts at [$a = (H_2 + h)/2$] or [$a = H_1 - h$], whichever is maximum; and ends at [$a = L - H_3$]. This proposition is shown in the side view of a beam in Figure 4.11. When the crack-tip is inside the squares (shown in dashed dotted lines, with sides same as the thickness of that section), the stresses are still

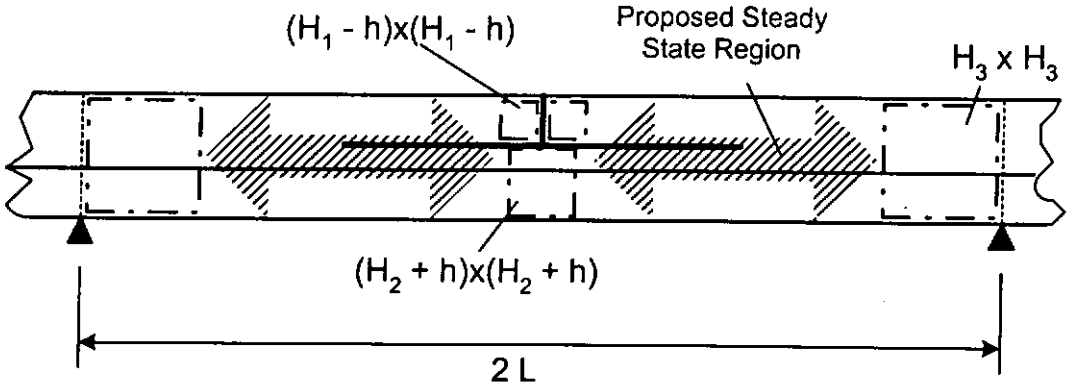

Figure 4.11 Proposed Steady State Region bounded by squares with sides same as the thickness of the section.

influenced by the central notch, or the line of symmetry or the inner load point. Steady state is observed when the crack-tip is in the steady state region, boundary marked by hatched arrows. Figure 4.10a shows the plot of a beam (with configuration $E_2/E_1 = 0.5$, $H_1/H_2 = 2$, $h/H_1 = 0.5$, i.e. giving $H_3 = 15$, $H_1 - h = 5$, $H_2 + h = 10$, $L = 50$) with the steady state region in such boundaries. Within the steady state region, G- (represented by circled lines) and K-values (represented by crossed lines) are almost constant, with Gs very close to the G_3 (represented by dotted lines) values. Outside this region, K_I, K_{II} and G are not constant.

However, by considering the case in Figure 4.10b (with configuration E_2/E_1 = 0.5, H_1/H_2 = 0.5, h/H_1 = 0.5, i.e. giving H_3 = 30, H_1 - h = 5, H_2 + h = 25, L = 50), there are no constant values of Ks and Gs despite having crack-tip inside the proposed steady state region. The proposed method seems not sufficient to locate the boundary of steady state region. Another implication is that the beam is not long enough, or more accurately, the inner load points are not far enough to provide a steady state region for the beam. So this case is redesigned using same thicknesses but different lengths: specimen length S = 300 and inner load point $2L$ = 180. And the boundaries of the steady state region (see Figure 4.12) are limited by rectangles with 1.5 times the thicknesses, instead of squares. The result of the improved beam is shown in Figure 4.13. Steady state region exists and can be located by the proposed method.

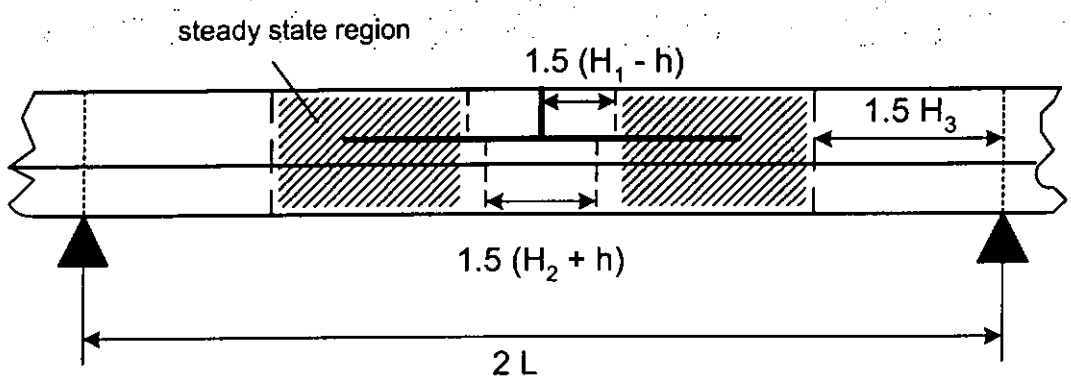

Figure 4.12 Improved method in drawing the boundaries of Steady State Region

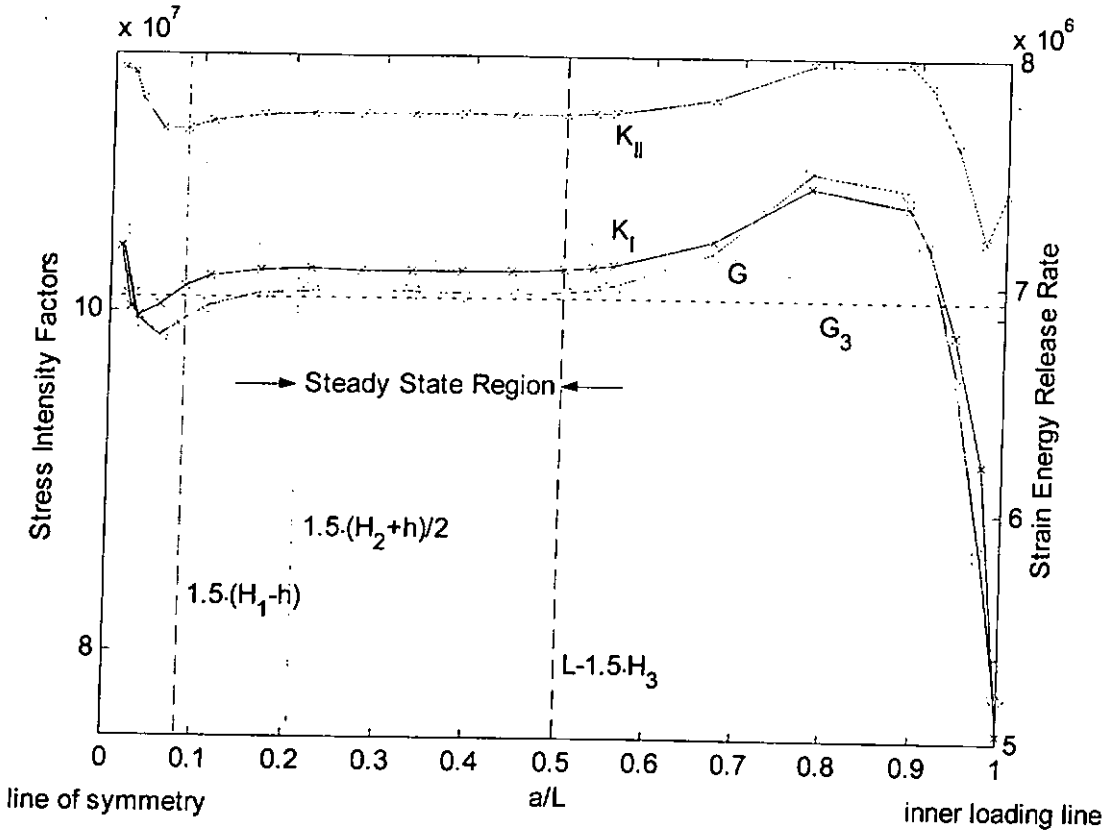

Figure 4.13 Enlonged beam in Figure 4.10b with steady state region bounded with the new method

To ensure the steady state region exists, it is therefore recommended that L >3 H_3. While the crack-tip should be inside the boundary drawn by : (a) 1.5×H_3 horizontally away from the inner load point; and (b) 1.5×(H_1 – h) from the upper free plane and 1.5×(H_2 + h)/2 from the plane of symmetry. Thus the criteria for the inner load point and the crack length is:

$$L > 3H_3 \text{ and } \max\left[1.5\cdot(H_1-h), 1.5\cdot\left(\frac{H_2+h}{2}\right)\right] \le a \le (L-1.5\cdot H_3) \quad \ldots(4.14)$$

where $\max(x,y) = \begin{cases} x & if \quad x \ge y \\ y & if \quad y > x \end{cases}$

Since some of our results are not under steady state cracking, FEA were redone with beams redesigned with crack-tip inside the steady state region.

4.3.4 Curvefitting for Normalization of K_I and K_{II}

FEA were redone for various penetration ratios (h/H_1 = 1/1000, 2/1000, 5/1000, 1/100, 2/100, 5/100, 1/10, 2/10, 5/10) under steady state cracking with two sets of configurations :

a) with same Poisson's ratio ($\nu_1 = \nu_2 = 0.3$) and with parameters : $E_1 = 3\times10^9$; $E_2/E_1 = 0.5, 1, 1.75, 2.5, 3.4375, 5, 7, 8.5, 10$; $\nu_1 = \nu_2 = 0.3$; $P/2 = 1\times10^6$; $B = 1$; $H_1 = 10$ units; $H_1/H_2 = 2, 1.5, 1, 0.5$; $S = 300$ units; $d = H_3$; $a = 45$ units and $L = 150 - 2H_3$.

b) with different Poisson's ratio and with parameters : $E_1 = 3\times10^9$ and other material parameters shown in Table 4.1; $P/2 = 1\times10^6$; $B = 1$; $H_1 = 10$ units; $H_1/H_2 = 2, 1.5, 1, 0.5$; $S = 300$ units; $d = 15$ units; $a = 60$ units and $L = 120$ units.

E_2/E_1 :	ν_1	ν_2	n
0.5	0.2	0.4	0.5714
0.8	0.2	0.4	0.9143
1	0.17	0.42	1.1791
1.5	0.4	0.35	1.4359
2	0.2	0.35	2.188
2.8	0.4	0.3	2.5846
3	0.4	0.2	2.625
3.2	0.2	0.25	3.2768
4	0.35	0.3	3.8571
6	0.3	0.2	5.6875
7	0.4	0.3	6.4615
9	0.4	0.2	7.875

Table 4.1 material properties of the specimens modeled with different Poisson's ratio

The numerical values of the obtained stress intensity factors are given in Appendix VIII. The plots of stress intensity factors against h/H_1 (for E_2/E_1 = 0.5, 1, 2.5, 5, 10 only) are given in Appendix IX.

Since the stress intensity factors depend on a large number of parameters, geometric and material, it is not practical to include all parameters in one single equation or graph. The choice of K_{I0} and K_{II0} described in the previous section makes it possible to group data logically either for graphical presentation or curve-fitting purposes. In what follows we try to establish a procedure for recording and using available data for the determination of K_I and K_{II} for a particular test.

Firstly, the values of K_I and K_{II} in the constant K region (i.e. steady state region) of a/L are collected. For each combination of H_1/H_2 and E_2/E_1, values of K_I/K_{I0} and K_{II}/K_{II0} are plotted against h/H_1. One typical plot is shown in figure 4.14. It is found that all data points fall onto smooth curves. This confirms that the choice of K_{I0} and K_{II0} is appropriate. Each set of data is then curve-fitted using a combination of power and polynomial terms. It is found that the following equation provides for a high accuracy for all data sets examined:

$$\frac{K_i}{K_{i0}} = Y_{Ki} = A_n \cdot \left(\frac{h}{H_1}\right)^{B_n} + C_n \cdot \left(\frac{h}{H_1}\right)^3 + D_n \cdot \left(\frac{h}{H_1}\right)^2 + E_n \cdot \left(\frac{h}{H_1}\right) + F_n \quad \ldots(4.15)$$

where i represents I or II.

The constants A_n through F_n for the cases examined are given in Table 4.2. and Table 4.3. The ranges of geometric and material parameters are chosen to demonstrate the general applicability of the expression. The maximum error observed is 0.7%. In actual applications, more data may be required and further

curvefitting of data generated from these expressions may have to be done. An illustration of such a procedure is presented here for applications to Ni/MgO, Si/Cu and solder/copper interfaces.

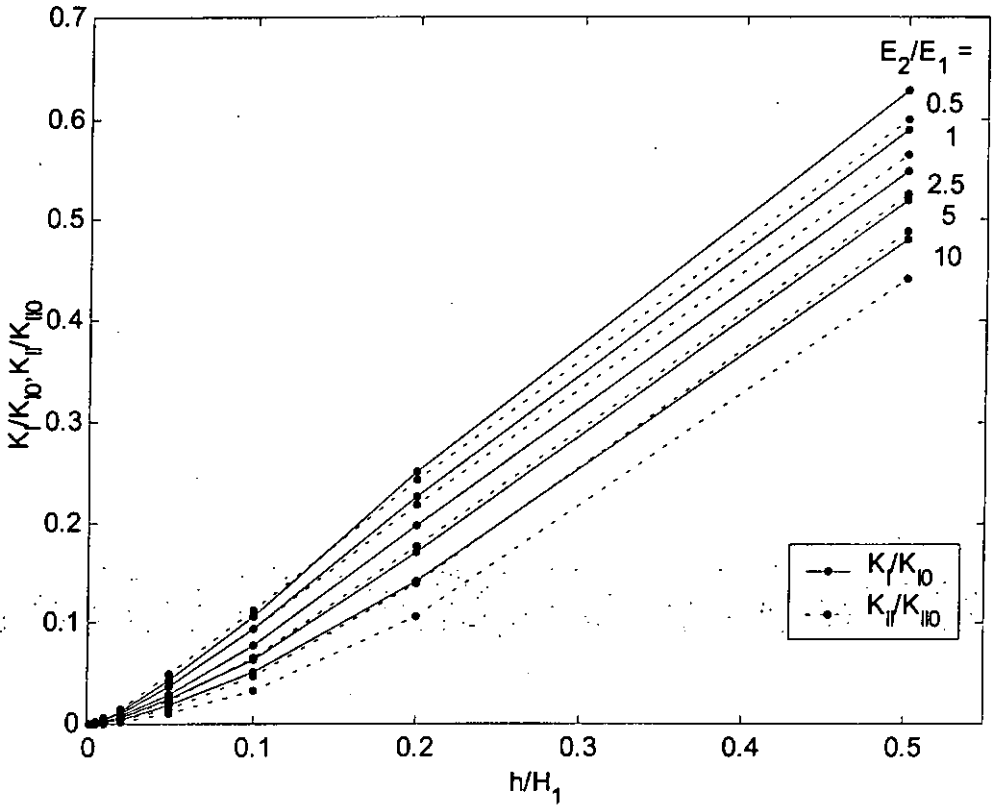

Figure 4.14 A typical plot of normalized stress intensity factors against the penetration ratio h/H_1 $(H_1/H_2 = 2)$

Y_{KI}	A_n	B_n	C_n	D_n	E_n	F_n
$H_1/H_2 = 2.0$						
n = 0.5	6.4586	1.5621	1.8937	-7.1766	-3.292E-03	4.247E-06
n = 1	6.1983	1.5921	1.6329	-6.7357	2.428E-02	-4.417E-06
n = 1.75	5.0753	1.5904	0.6258	-4.8582	2.869E-02	-6.015E-06
n = 2.5	4.0224	1.5705	-0.1325	-3.2023	2.354E-02	-5.124E-06
n = 3.4375	3.1194	1.5432	-0.6941	-1.8233	1.588E-02	-3.591E-06
n = 5	2.2735	1.5062	-1.0972	-0.5894	5.804E-03	-1.571E-06
n = 7	1.7377	1.4747	-1.2104	0.1151	-2.205E-03	-3.059E-08
n = 8.5	1.5094	1.4592	-1.1885	0.3728	-5.847E-03	6.429E-07
n = 10	1.3545	1.4481	-1.1339	0.5218	-8.237E-03	1.074E-06
n = 0.5714	5.0554	1.5119	1.2706	-5.2511	-2.492E-03	4.474E-06
n = 0.9143	5.1600	1.5430	1.3532	-5.4324	1.810E-02	-2.817E-06
n = 1.1791	4.8550	1.5444	1.1071	-4.9424	2.194E-02	-4.065E-06
n = 1.4359	6.0167	1.6124	1.1354	-6.2084	2.911E-02	-6.041E-06
n = 2.188	4.1045	1.5578	0.1495	-3.4852	2.328E-02	-5.109E-06
n = 2.5846	4.2488	1.5900	-0.2026	-3.3966	2.375E-02	-5.188E-06
n = 2.625	4.3035	1.5951	-0.2307	-3.4344	2.333E-02	-5.133E-06
n = 3.2768	3.1556	1.5364	-0.5692	-1.9486	1.510E-02	-3.567E-06
n = 3.8571	2.8850	1.5398	-0.8881	-1.4275	1.385E-02	-3.101E-06
n = 5.6875	2.0466	1.4951	-1.1810	-0.2690	2.918E-03	-9.751E-07
n = 6.4615	1.8594	1.4927	-1.3003	0.0309	1.770E-03	-5.740E-07
n = 7.875	1.5850	1.4745	-1.3064	0.3602	-2.115E-03	1.835E-07

Table 4.2a Constants for the Y_{KI} expression (for $H_1/H_2 = 2$)

Y_{KI}	A_n	B_n	C_n	D_n	E_n	F_n
H_1/H_2 = 1.5						
n = 0.5	4.7102	1.5710	0.8332	-4.4933	1.441E-03	1.984E-06
n = 1	3.9612	1.5724	0.3469	-3.3901	1.509E-02	-2.840E-06
n = 1.75	2.8826	1.5431	-0.3576	-1.7498	1.273E-02	-2.596E-06
n = 2.5	2.2292	1.5136	-0.7026	-0.7907	6.963E-03	-1.529E-06
n = 3.4375	1.7651	1.4858	-0.8639	-0.1534	1.031E-03	-4.416E-07
n = 5	1.3702	1.4570	-0.8799	0.3158	-5.016E-03	6.234E-07
n = 7	1.1267	1.4379	-0.7793	0.5301	-8.619E-03	1.230E-06
n = 8.5	1.0215	1.4301	-0.6932	0.5906	-9.836E-03	1.429E-06
n = 10	0.9486	1.4253	-0.6137	0.6160	-1.043E-02	1.525E-06
n = 0.5714	3.6506	1.5158	0.4350	-3.0940	1.286E-03	2.446E-06
n = 0.9143	3.4671	1.5305	0.3005	-2.8251	1.172E-02	-1.983E-06
n = 1.1791	3.1219	1.5210	0.0818	-2.3076	1.151E-02	-2.219E-06
n = 1.4359	3.4770	1.5724	-0.0910	-2.5751	1.498E-02	-3.039E-06
n = 2.188	2.3549	1.5075	-0.5398	-1.0435	6.988E-03	-1.645E-06
n = 2.5846	2.2861	1.5295	-0.7701	-0.8050	7.566E-03	-1.582E-06
n = 2.625	2.2980	1.5338	-0.7902	-0.8026	7.392E-03	-1.550E-06
n = 3.2768	1.8089	1.4812	-0.7987	-0.2478	1.720E-04	-4.064E-07
n = 3.8571	1.6393	1.4825	-0.9201	0.0303	-2.182E-05	-1.807E-07
n = 5.6875	1.2647	1.4500	-0.8610	0.4260	-6.298E-03	8.643E-07
n = 6.4615	1.1684	1.4509	-0.8738	0.5463	-5.947E-03	9.388E-07
n = 7.875	1.0443	1.4412	-0.7923	0.6332	-7.328E-03	1.180E-06

Table 4.2b Constants for the Y_{KI} expression (for $H_1/H_2 = 1.5$)

Y_{KI}	A_n	B_n	C_n	D_n	E_n	F_n
$H_1/H_2 = 1.0$						
n = 0.5	3.0108	1.5723	0.1653	-2.1718	2.166E-03	8.350E-07
n = 1	2.1412	1.5335	-0.2728	-0.9620	5.056E-03	-9.169E-07
n = 1.75	1.4994	1.4872	-0.5183	-0.0937	3.265E-04	-1.060E-07
n = 2.5	1.2095	1.4602	-0.5411	0.2454	-3.522E-03	5.239E-07
n = 3.4375	1.0228	1.4417	-0.4878	0.4163	-6.278E-03	9.501E-07
n = 5	0.8679	1.4275	-0.3743	0.5032	-8.182E-03	1.226E-06
n = 7	0.7703	1.4209	-0.2582	0.5166	-8.771E-03	1.301E-06
n = 8.5	0.7267	1.4192	-0.1938	0.5089	-8.770E-03	1.294E-06
n = 10	0.6958	1.4186	-0.1437	0.4974	-8.646E-03	1.270E-06
n = 0.5714	2.3194	1.5108	-0.0433	-1.2967	1.367E-03	1.364E-06
n = 0.9143	1.9936	1.5008	-0.2272	-0.8335	3.448E-03	-5.881E-07
n = 1.1791	1.7425	1.4813	-0.3303	-0.4912	9.789E-04	-2.792E-07
n = 1.4359	1.7711	1.5180	-0.4682	-0.4266	2.845E-03	-5.345E-07
n = 2.188	1.2840	1.4554	-0.4997	0.1332	-4.116E-03	5.211E-07
n = 2.5846	1.2192	1.4745	-0.5745	0.2587	-2.512E-03	4.343E-07
n = 2.625	1.2217	1.4786	-0.5812	0.2617	-2.429E-03	4.323E-07
n = 3.2768	1.0490	1.4371	-0.4684	0.3741	-7.341E-03	1.037E-06
n = 3.8571	0.9691	1.4419	-0.4761	0.4670	-6.168E-03	9.789E-07
n = 5.6875	0.8248	1.4254	-0.3353	0.5196	-8.250E-03	1.245E-06
n = 6.4615	0.7813	1.4312	-0.3194	0.5516	-7.025E-03	1.143E-06
n = 7.875	0.7301	1.4288	-0.2524	0.5514	-7.018E-03	1.140E-06

Table 4.2c Constants for the Y_{KI} expression (for $H_1/H_2 = 1$)

Y_{KI}	A_n	B_n	C_n	D_n	E_n	F_n
$H_1/H_2 = 0.5$						
n = 0.5	1.4541	1.5524	-0.0929	-0.3480	-1.842E-04	6.242E-07
n = 1	0.9642	1.4802	-0.1764	0.2215	-2.225E-03	4.208E-07
n = 1.75	0.7566	1.4423	-0.1095	0.3860	-4.745E-03	7.895E-07
n = 2.5	0.6768	1.4288	-0.0407	0.4103	-5.767E-03	9.106E-07
n = 3.4375	0.6270	1.4223	0.0209	0.4053	-6.227E-03	9.505E-07
n = 5	0.5854	1.4191	0.0843	0.3850	-6.378E-03	9.456E-07
n = 7	0.5589	1.4186	0.1299	0.3631	-6.315E-03	9.182E-07
n = 8.5	0.5470	1.4189	0.1513	0.3508	-6.239E-03	8.990E-07
n = 10	0.5384	1.4194	0.1667	0.3412	-6.167E-03	8.826E-07
n = 0.5714	1.1352	1.4835	-0.1401	0.0195	-1.490E-03	1.087E-06
n = 0.9143	0.9336	1.4528	-0.1565	0.2401	-3.388E-03	5.549E-07
n = 1.1791	0.8405	1.4322	-0.1295	0.3177	-5.572E-03	8.331E-07
n = 1.4359	0.8367	1.4667	-0.1490	0.3318	-3.381E-03	6.185E-07
n = 2.188	0.6989	1.4193	-0.0456	0.3946	-7.034E-03	1.033E-06
n = 2.5846	0.6823	1.4447	-0.0500	0.4093	-4.642E-03	8.016E-07
n = 2.625	0.6853	1.4497	-0.0505	0.4063	-4.435E-03	7.810E-07
n = 3.2768	0.6364	1.4155	0.0261	0.3936	-7.291E-03	1.054E-06
n = 3.8571	0.6120	1.4270	0.0332	0.4066	-5.614E-03	8.873E-07
n = 5.6875	0.5732	1.4201	0.1004	0.3801	-6.152E-03	9.153E-07
n = 6.4615	0.5596	1.4305	0.1029	0.3857	-4.919E-03	7.924E-07
n = 7.875	0.5445	1.4312	0.1250	0.3759	-4.733E-03	7.618E-07

Table 4.2d Constants for the Y_{KI} expression (for $H_1/H_2 = 0.5$)

Y_{KII}	A_n	B_n	C_n	D_n	E_n	F_n
$H_1/H_2 = 2.0$						
n = 0.5	4.3717	1.3797	3.5818	-5.8351	-1.378E-01	2.867E-05
n = 1	6.7097	1.5961	2.9383	-8.1393	2.403E-02	-3.955E-06
n = 1.75	6.9004	1.6843	0.9267	-6.9386	2.376E-02	-6.041E-06
n = 2.5	5.4671	1.6986	-0.4181	-4.4561	1.316E-02	-4.056E-06
n = 3.4375	3.8088	1.6882	-1.2896	-2.0530	3.713E-03	-1.917E-06
n = 5	2.2706	1.6615	-1.7508	-0.0315	-4.628E-03	1.437E-07
n = 7	1.4477	1.6394	-1.7162	0.8872	-9.003E-03	1.342E-06
n = 8.5	1.1772	1.6361	-1.5608	1.1020	-1.011E-02	1.660E-06
n = 10	1.0333	1.6410	-1.3858	1.1578	-1.042E-02	1.765E-06
n = 0.5714	5.9546	1.4893	4.3344	-8.1812	-4.571E-02	1.397E-05
n = 0.9143	8.7908	1.6399	3.9445	-11.0089	1.700E-02	-2.717E-06
n = 1.1791	11.3721	1.7192	3.4418	-13.3352	1.802E-02	-4.774E-06
n = 1.4359	6.0639	1.6286	1.4255	-6.4286	3.027E-02	-6.774E-06
n = 2.188	9.4907	1.7708	0.5546	-9.2927	9.459E-03	-3.927E-06
n = 2.5846	3.5462	1.6172	-0.8763	-2.1336	1.665E-02	-4.202E-06
n = 2.625	3.1501	1.5937	-0.9999	-1.6279	1.658E-02	-4.070E-06
n = 3.2768	5.8709	1.7567	-0.9389	-4.4292	-1.189E-04	-1.550E-06
n = 3.8571	2.5681	1.6301	-1.6149	-0.5073	3.190E-03	-1.467E-06
n = 5.6875	1.7430	1.6327	-1.8019	0.5874	-5.978E-03	5.843E-07
n = 6.4615	0.9398	1.5021	-1.8365	1.4892	-6.643E-03	9.001E-07
n = 7.875	0.6976	1.4657	-1.6857	1.6827	-9.396E-03	1.445E-06

Table 4.3a Constants for the Y_{KII} expression (for $H_1/H_2 = 2$)

Y_{KII}	A_n	B_n	C_n	D_n	E_n	F_n
$H_1/H_2 = 1.5$						
n = 0.5	3.9995	1.4430	2.9279	-5.0809	-4.476E-02	1.194E-05
n = 1	4.6929	1.5893	1.5480	-4.9910	1.813E-02	-3.263E-06
n = 1.75	3.6500	1.6280	-0.0241	-2.7713	1.135E-02	-2.759E-06
n = 2.5	2.6794	1.6281	-0.6913	-1.2352	3.828E-03	-1.320E-06
n = 3.4375	1.9497	1.6217	-0.9628	-0.2250	-1.656E-03	-1.747E-07
n = 5	1.3713	1.6187	-0.9545	0.4345	-5.657E-03	7.211E-07
n = 7	1.0725	1.6279	-0.7649	0.6505	-7.338E-03	1.185E-06
n = 8.5	0.9804	1.6418	-0.6164	0.6537	-7.639E-03	1.287E-06
n = 10	0.9469	1.6598	-0.4823	0.5985	-7.607E-03	1.288E-06
n = 0.5714	5.2467	1.5355	3.1923	-6.6585	-7.862E-03	4.487E-06
n = 0.9143	6.2638	1.6395	2.2077	-7.0947	1.473E-02	-2.878E-06
n = 1.1791	6.8560	1.6931	1.5492	-7.2381	1.107E-02	-3.019E-06
n = 1.4359	3.6091	1.5891	0.3723	-3.0235	1.647E-02	-3.560E-06
n = 2.188	4.2789	1.7011	-0.2826	-3.2016	2.185E-03	-1.426E-06
n = 2.5846	1.9151	1.5522	-0.8527	-0.3135	4.577E-03	-1.152E-06
n = 2.625	1.7483	1.5308	-0.8918	-0.1057	3.953E-03	-9.901E-07
n = 3.2768	2.7208	1.6857	-0.8433	-1.1156	-3.787E-03	-2.107E-08
n = 3.8571	1.4450	1.5725	-1.0355	0.3735	-2.123E-03	8.962E-08
n = 5.6875	1.1511	1.6025	-0.9069	0.6471	-6.070E-03	8.764E-07
n = 6.4615	0.7207	1.4946	-0.8598	1.0785	-6.102E-03	9.785E-07
n = 7.875	0.5964	1.4800	-0.7152	1.1202	-6.618E-03	1.078E-06

Table 4.3b Constants for the Y_{KII} expression (for $H_1/H_2 = 1.5$)

Y_{KII}	A_n	B_n	C_n	D_n	E_n	F_n
$H_1/H_2 = 1.0$						
n = 0.5	3.4647	1.5022	2.1135	-4.0266	-2.301E-03	2.394E-06
n = 1	2.9057	1.5699	0.6728	-2.4599	1.068E-02	-1.964E-06
n = 1.75	1.9629	1.5784	-0.1306	-0.8612	3.386E-03	-7.799E-07
n = 2.5	1.5098	1.5835	-0.3022	-0.2306	-3.991E-04	-1.145E-07
n = 3.4375	1.2351	1.5945	-0.2922	0.0733	-2.586E-03	2.734E-07
n = 5	1.0458	1.6187	-0.1730	0.1988	-3.970E-03	5.179E-07
n = 7	0.9666	1.6492	-0.0332	0.1780	-4.649E-03	6.972E-07
n = 8.5	0.9560	1.6703	0.0476	0.1241	-4.865E-03	7.625E-07
n = 10	0.9691	1.6902	0.1130	0.0554	-4.958E-03	7.899E-07
n = 0.5714	4.1693	1.5712	2.0322	-4.7381	7.576E-03	-2.850E-07
n = 0.9143	3.8272	1.6222	1.0011	-3.6594	9.490E-03	-1.983E-06
n = 1.1791	3.6318	1.6527	0.5370	-3.1081	4.741E-03	-1.339E-06
n = 1.4359	2.0579	1.5490	0.0476	-1.1041	6.492E-03	-1.335E-06
n = 2.188	2.1604	1.6467	-0.1904	-0.9972	-1.384E-03	-1.585E-07
n = 2.5846	1.1745	1.5175	-0.3431	0.1531	-4.033E-04	3.465E-08
n = 2.625	1.0990	1.4997	-0.3485	0.2386	-8.927E-04	1.320E-07
n = 3.2768	1.5970	1.6503	-0.2558	-0.3285	-4.022E-03	3.921E-07
n = 3.8571	0.9985	1.5578	-0.2861	0.3204	-2.465E-03	3.339E-07
n = 5.6875	0.9445	1.6132	-0.1294	0.2724	-3.925E-03	5.402E-07
n = 6.4615	0.6489	1.5243	-0.1083	0.5602	-2.995E-03	4.714E-07
n = 7.875	0.5816	1.5225	-0.0313	0.5674	-2.895E-03	4.515E-07

Table 4.3c Constants for the Y_{KII} expression (for $H_1/H_2 = 1$)

Y_{KII}	A_n	B_n	C_n	D_n	E_n	F_n
H_1/H_2 = 0.5						
n = 0.5	2.4599	1.5362	1.1068	-2.3404	8.221E-03	-9.646E-07
n = 1	1.6075	1.5428	0.3607	-0.8911	4.481E-03	-8.074E-07
n = 1.75	1.1693	1.5547	0.1900	-0.2931	8.567E-04	-1.825E-07
n = 2.5	1.0292	1.5763	0.2035	-0.1558	-2.811E-04	-4.133E-08
n = 3.4375	0.9666	1.6024	0.2456	-0.1269	-1.026E-03	4.289E-08
n = 5	0.9475	1.6374	0.3028	-0.1608	-1.754E-03	1.292E-07
n = 7	0.9729	1.6704	0.3520	-0.2358	-2.292E-03	2.084E-07
n = 8.5	0.9981	1.6882	0.3763	-0.2871	-2.590E-03	2.755E-07
n = 10	1.0256	1.7026	0.3948	-0.3349	-2.810E-03	3.265E-07
n = 0.5714	2.6060	1.5772	0.9508	-2.3814	8.194E-03	-1.295E-06
n = 0.9143	1.9933	1.5883	0.4540	-1.3643	4.117E-03	-8.666E-07
n = 1.1791	1.8206	1.6095	0.3239	-1.0764	1.056E-03	-3.531E-07
n = 1.4359	1.2015	1.5248	0.2097	-0.3457	2.050E-03	-4.027E-07
n = 2.188	1.3174	1.6239	0.2319	-0.4720	-1.281E-03	2.970E-08
n = 2.5846	0.8496	1.5221	0.1842	0.0428	7.471E-05	-1.890E-08
n = 2.625	0.8091	1.5080	0.1828	0.0859	-4.358E-05	8.467E-09
n = 3.2768	1.1779	1.6479	0.2699	-0.3591	-2.202E-03	1.699E-07
n = 3.8571	0.8376	1.5763	0.2440	0.0027	-6.033E-04	1.164E-08
n = 5.6875	0.9013	1.6362	0.3139	-0.1268	-1.663E-03	1.172E-07
n = 6.4615	0.6667	1.5643	0.2946	0.1206	-4.318E-04	-9.811E-09
n = 7.875	0.6327	1.5656	0.3130	0.1332	-3.930E-04	-2.103E-08

Table 4.3d Constants for the Y_{KII} expression (for $H_1/H_2 = 0.5$)

4.3.5 Applications of the Tables 4.2 and 4.3

Three material pairs are used here as an illustration on how to use the correction factor tables in Table 4.2 and Table 4.3:

Material 1	Material 2	E_1 (GPa)	E_2 (GPa)	ν_1	ν_2	n (plane strain)
Si	Cu	167	129	0.22	0.345	0.8274
Ni	MgO	212	302	0.314	0.175	1.3203
Solder	Copper	32	129	0.38	0.345	3.9025

Table 4.4 Material properties of the 3 material pairs used for illustration

Suppose there is a specimen made of the above materials pairs with the crack located inside material 1 at $h/H_1 = 0.05$. The correction factors Y_{KI} and Y_{KII} for all n, listed in Table 4.2 and Table 4.3, of $h/H_1 = 0.05$ are calculated using Equation ...(4.15). After curvefitting these values (represented by dots), they are plotted in smooth curves against n in Figure 4.15a and Figure 4.15b respectively. Here the curves were fitted by Equation ...(4.16) and Equation ...(4.17). In practice, the user has to decide the choice of curve for curvefitting.

The equations for curvefitting are :

For Y_{KI} :

$$\begin{aligned}
Y_{KI}(H_1H_2 = 2) &= 0.1005 \cdot n^{1.0688} + 0.0000 \cdot n^3 - 0.0010n^2 - 0.1134n + 0.0512 \\
Y_{KI}(H_1H_2 = 1.5) &= 0.0813 \cdot n^{1.0641} + 0.0000 \cdot n^3 - 0.0007n^2 - 0.0911n + 0.0387 \\
Y_{KI}(H_1H_2 = 1) &= 0.1048 \cdot n^{1.0367} + 0.0000 \cdot n^3 - 0.0005n^2 - 0.1118n + 0.0271 \\
Y_{KI}(H_1H_2 = 0.5) &= 0.1350 \cdot n^{1.0172} + 0.0000 \cdot n^3 - 0.0003n^2 - 0.1387n + 0.0161
\end{aligned} \qquad \ldots(4.16)$$

and for Y_{KII} :

$$\begin{aligned}
Y_{KII}(H_1H_2 = 2) &= 0.2906 \cdot n^{1.0618} + 0.0001 \cdot n^3 - 0.0028n^2 - 0.3194n + 0.0692 \\
Y_{KII}(H_1H_2 = 1.5) &= 0.2346 \cdot n^{1.0642} + 0.0001 \cdot n^3 - 0.0024n^2 - 0.2581n + 0.0547 \\
Y_{KII}(H_1H_2 = 1) &= 0.1922 \cdot n^{1.0632} + 0.0000 \cdot n^3 - 0.0020n^2 - 0.2103n + 0.0409 \\
Y_{KII}(H_1H_2 = 0.5) &= 0.1471 \cdot n^{1.0606} + 0.0000 \cdot n^3 - 0.0016n^2 - 0.1594n + 0.0278
\end{aligned} \qquad \ldots(4.17)$$

The values of the estimated correction factors Y_{KI} and Y_{KII}, for different thickness ratios of the material pairs are marked by crosses (×) in Figure 4.15a and Figure 4.15b. Then these values are plotted against H_1/H_2 in Figure 4.16a-c. This is then the graph of correction factors for the specimens with $h/H_1 = 0.05$ at different thickness ratios. Independent finite element analysis runs are performed for these specimens. Results obtained are also plotted in Figure 4.16a-c, represented by squares. Good agreements are obtained.

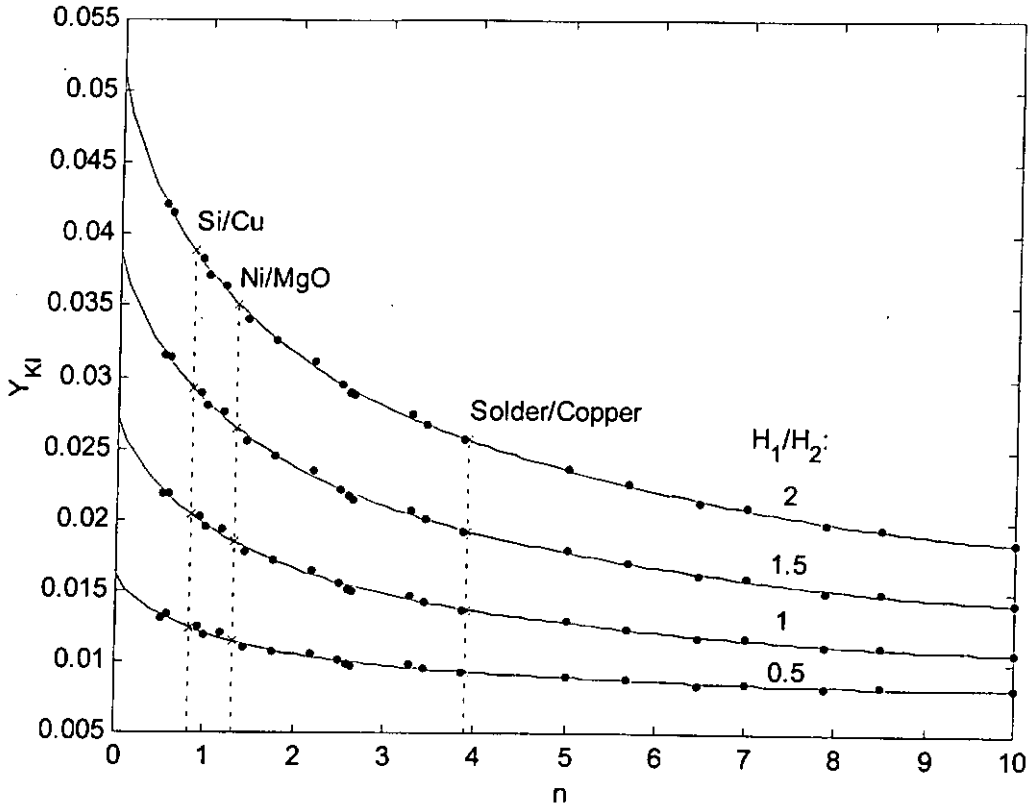

Figure 4.15a Curvefitted Y_{KI} against n, for different thickness ratio with $h/H_1 = 0.05$

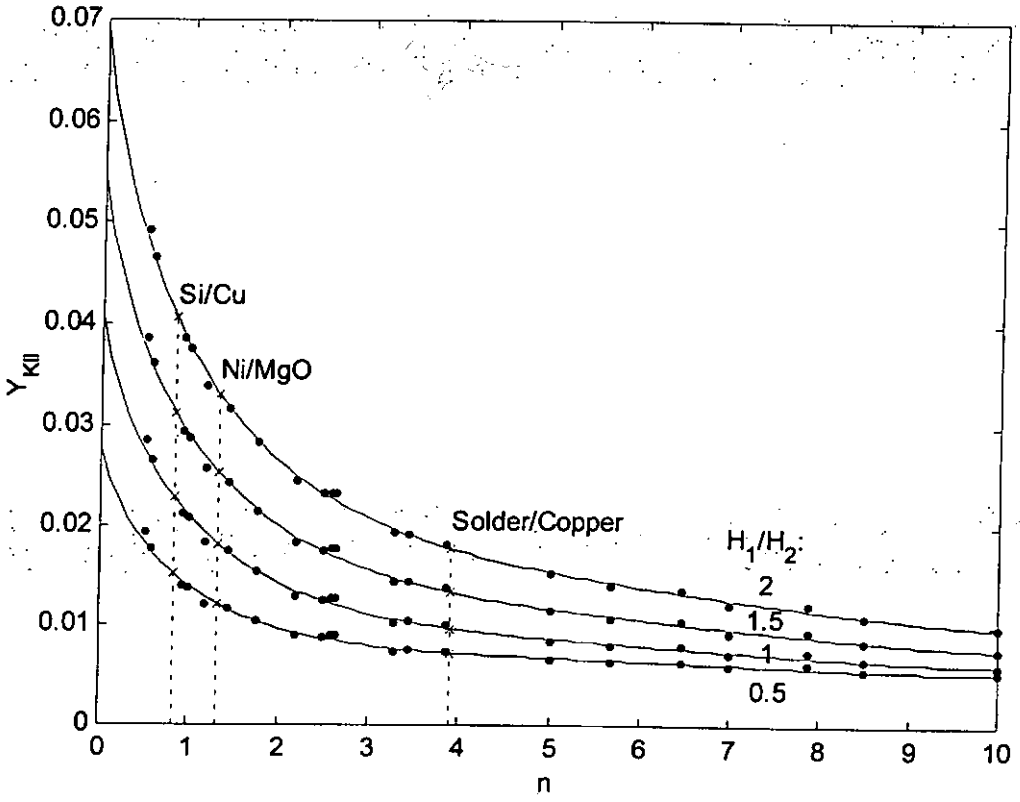

Figure 4.15b Curvefitted Y_{KII} against n, for different thickness ratio with $h/H_1 = 0.05$

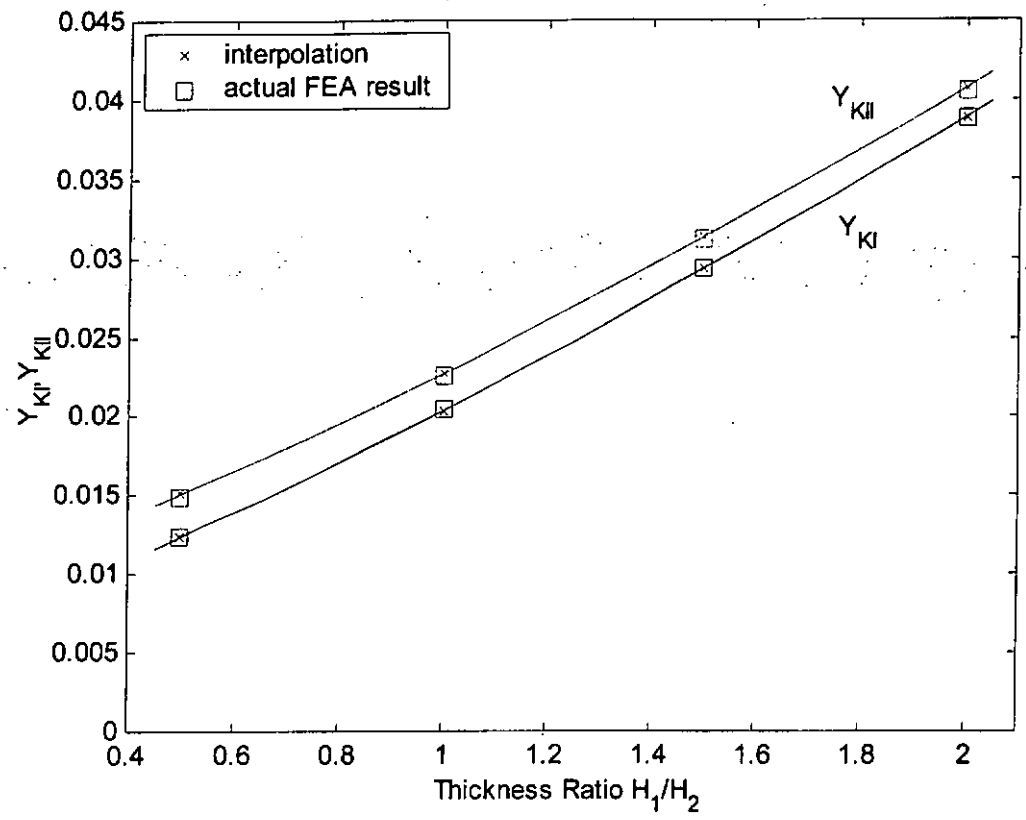

Figure 4.16a The Correction Factors at different Thickness Ratios for the Si/Cu specimen with $h/H_1 = 0.05$

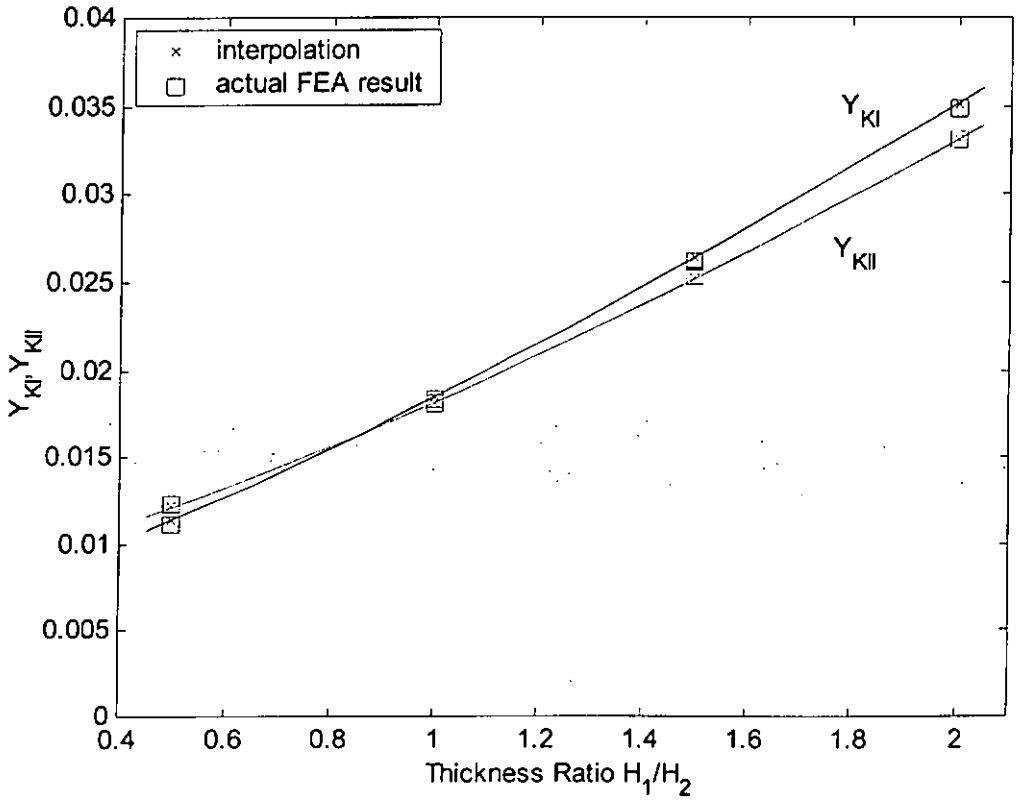

Figure 4.16b The Correction Factors at different Thickness Ratios for the Ni/MgO specimen with $h/H_1 = 0.05$

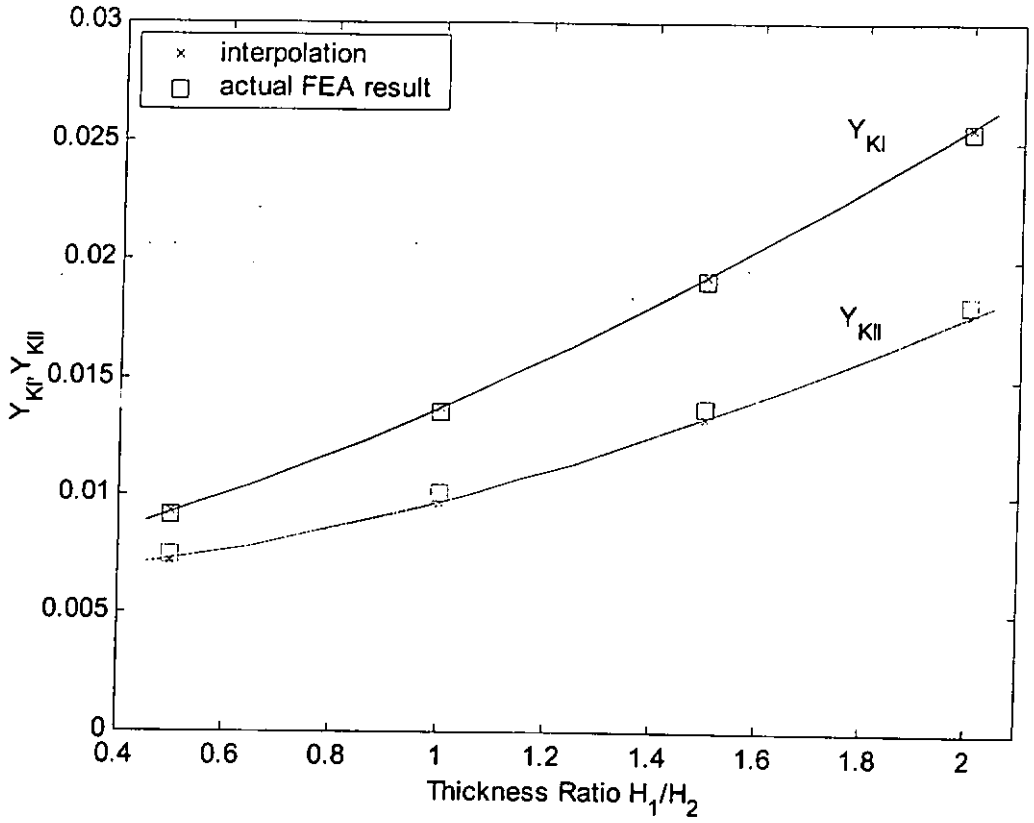

Figure 4.16c The Correction Factors at different Thickness Ratios for the Solder/Copper specimen with $h/H_1 = 0.05$

4.4 RELATION OF SUBINTERFACIAL CRACKS TO INTERFACIAL CRACKS

From Hutchinson et al. (1987), when h is small comparing to the other dimensions, the stress intensity factors of subinterfacial cracks can be determined by the distance of the crack from the interface h, and the complex stress intensity factors of the same specimen configuration but with the crack located on the interface $\boldsymbol{K}$. The equation relating the interface crack complex stress intensity factors and the subinterfacial crack stress intensity factors is :

$$K_I + iK_{II} = q_s e^{i\phi} \boldsymbol{K} \cdot h^{i\varepsilon} \qquad \ldots(4.18)$$

where ϕ is a material constant, dependent on α and β, the Dundurs parameters, and is obtained from interpolation of Table X.1 in Appendix X; and

$$q_s = \left(\frac{1-\beta^2}{1+\alpha}\right)^{0.5} \qquad \ldots(4.19)$$

However, the notation in the above reference is different from the one used in this study :

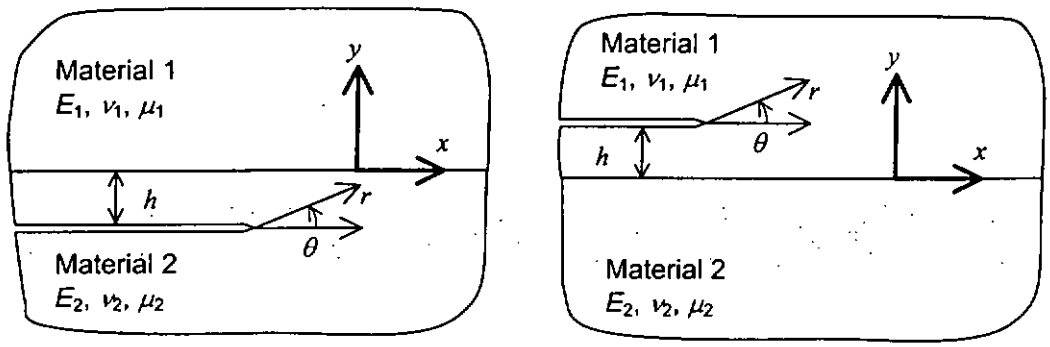

a) reference's notation b) notation in this study

Figure 4.17 Difference in notations from this study and the referrence

In the reference, the crack is located in the negative y, which is in Material 2. Following their notation, therefore, the specimen in this study is inverted up-side-

down to observe the effect. Six cases are studied with initial (before beam inversion) combinations of H_1/H_2 = 1 and 0.5, and E_2/E_1 = 1, 2.5 and 5. These cases are chosen because the complex stress intensity factors of such combinations are also reference cases taken from Charalambides et al. (1989) and were verified in Section 3.3.4. The cases with E_2/E_1 = 10 and 25 are not considered because α and β are outside the Table X.1 for interpolation of ϕ. The values of α, β and ϕ; and complex stress intensity factors (determined by the combined SDM in Chapter 3) of these inverted beam with interfacial crack are:

H_1/H_2	E_2/E_1	$K = K_1 + i K_2$ ($\times 10^6$)	α	β	ε	ϕ
1	1	342.5 - 293.2 i	0	0	0	0
1	2.5	201.0 - 261.4 i	0.4268	0.1224	-0.392	0.0731
1	5	119.8 - 204.2 i	0.6667	0.1905	-0.614	0.1123
0.5	1	157.1 - 150.3 i	0	0	0	0
0.5	2.5	82.1 - 119.7 i	0.4268	0.1224	-0.392	0.0731
0.5	5	43.7 - 84.5 i	0.6667	0.1905	-0.614	0.1123

Table 4.5 Complex stress intensity factors for determination of subinterfacial stress intensity factors

Negative K_2 values were the result of inverting the beam, giving opposite y-direction and thus opposite shear direction. Stress intensity factors of subinterfacial cracks (with $H_1 = 10\times10^{-3}$ units and $h/H_1 = 1\times10^{-3}$ to 0.5) are obtained with Equation ...(4.18) and are compared to our FEA results (with $H_1 = 10\times10^{-3}$ units and h/H_1 = 1/1000, 2/1000, 5/1000, 1/100, 2/100, 5/100, 1/10, 2/10, 5/10), represented by '×'. Two typical results are plotted in Figure 4.18a,b showing close values when h is small (h/H_1 < 1/100) and deviates gradually when h increases. This confirms our FEA results from subinterfacial cracks. Plots of other cases are kept in Appendix X.

The corresponding deviation of analytical values from FEA values are also kept in Appendix X, Table X.1 and 2.

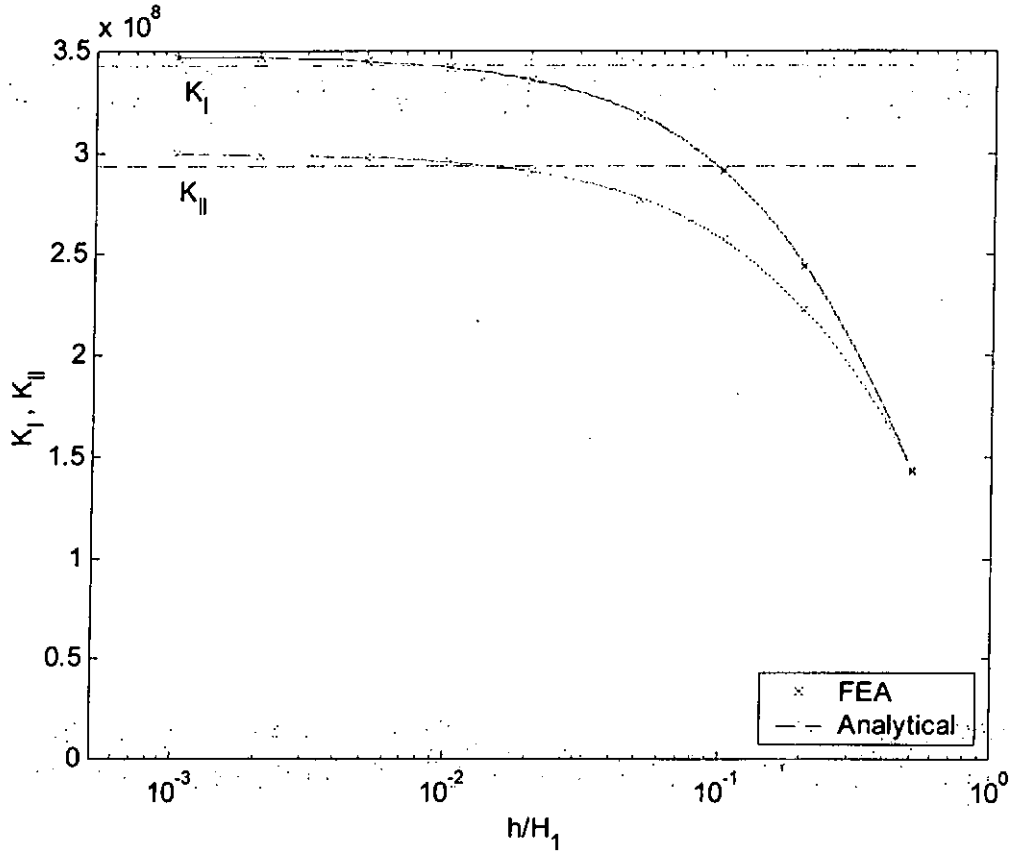

Figure 4.18a Comparison of analytical solution and FEA results against relative distance of crack from interface (for $E_2/E_1 = 1$, $H_1/H_2 = 1$)

The relationship in Equation ...(4.18) is based on cracks in infinite media without boundaries. So as the crack gets closer to the interface, i.e. smaller h/H_1, the system gets closer to an infinite media, and the results gets closer to the analytical solution. On the other hand, as the crack gets closer to the surface, i.e. larger h/H_1, the system no longer resembles an infinite media, and the results deviate from the analytical solution.

Figure 4.18a is the plot for $E_2/E_1 = 1$, i.e. homogenous beam. The K-values tends to constant as the crack gets closer to the imaginary "interface".

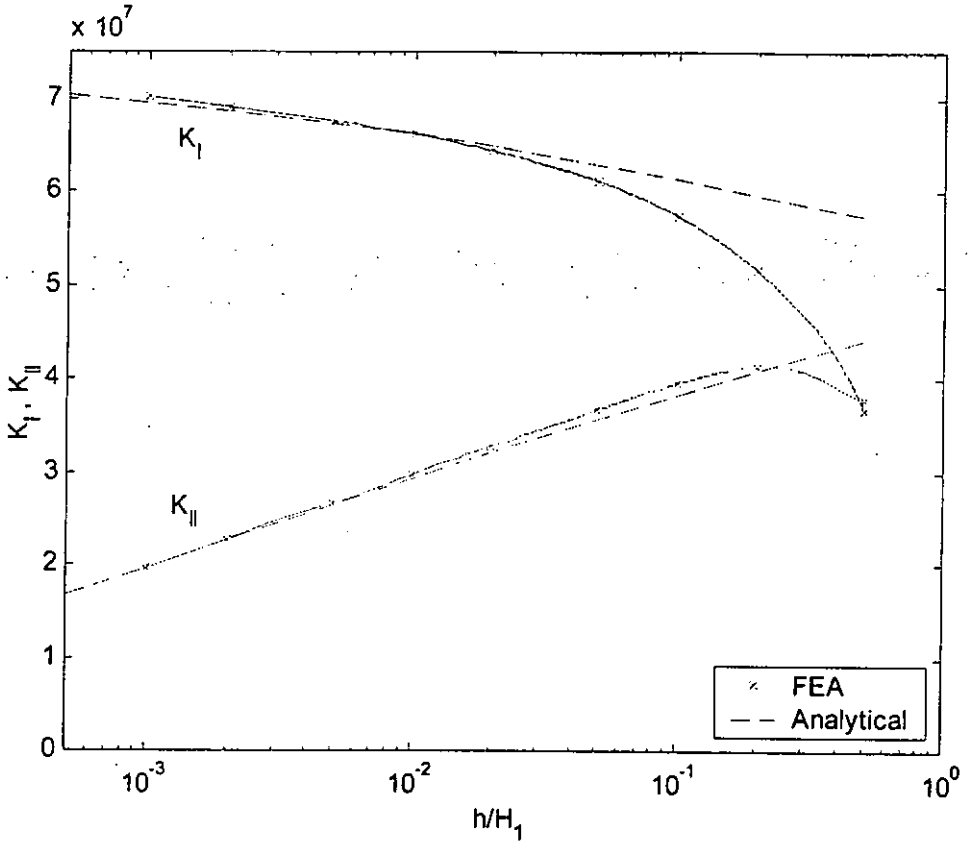

Figure 4.18b Comparison of analytical solution and FEA results against relative distance of crack from interface (for $E_2/E_1 = 5$, $H_1/H_2 = 0.5$)

From the graphs, it can be observed that the relation in Equation ...(4.18) can give close estimates of the subinterfacial stress intensity factors for cracks within the range $1/1000 \leq h/H_1 \leq 1/100$ and $H_1/H_2 = 0.5$ and 1. The percentage deviation is within 1.5% and 4% for K_I and K_{II} respectively. In general, K_{II} values give more deviation than that of K_I.

4.5 CONCLUSION

A four-point bend specimen has been proposed for the study of crack close to and parallel to the interface of dissimilar materials and finite element analysis was carried out to determine its characteristics. The associated stress intensity factors are presented in normalized format for application to geometrically similar specimens, which can be expressed in terms of the applied bending moment, basic elastic material properties and the dimensions of the specimen. It is found that when suitable dimensions are used, the specimen exhibits the attainment of a steady-state energy release rate. The relation between the subinterfacial stress intensity factors and the complex stress intensity factors is established.

Since the resulting stress intensity factors shows that it is always in mixed-mode conditions and $K_{II} \neq 0$. Therefore G_3 cannot be used as fracture toughness but it can be used as a verification of the K-values obtained. The fracture criterion can be studied through the critical stress intensity factors with the critical load obtained during the experiment. Another consideration is that special procedures have to be used for initiating a crack parallel to the interface. Suggestions for crack initiation will be given in Chapter 5.

Chapter 5 Preliminary Experimentation and Suggestions for Further Studies

5.1 Specimen Without "Interfacial Properties"

The properties of an interface are unknown since the interface acts as an intermediate material with new properties, thus making it difficult to study fracture with interfacial influence. Analytical and numerical solutions to such problems have so far not included experimental data for such properties. Examples on analytical study of subinterfacial cracks are given in Hutchinson et al. (1987) and Suo and Hutchinson (1990). The testing of such models by experiments cannot be performed without disconcerting uncertainties. An approach is suggested here to overcome this difficulty to allow experimental verifications of such models to go ahead. An illustration using our designed four-point bending specimen with subinterfacial crack in Chapter 4 is presented.

Simulation of a bi-material environment is made by Epoxy/Woven Fiberglass Composite specimens, taking Epoxy as the matrix medium of the glass fiber composite and also as the upper material of the beam. The advantages of such a configuration are the introduction of a sharp change of material properties across the interface (having no adhesives to bond the two layers and with a modulus ratio ≈ 4.5) as well as being isotropic (polymer) in the Epoxy layer where the crack is present. This is also the configuration for which some analytical solutions are available and for which finite element analysis can be carried out. The crack is introduced to the specimen by inserting a thin film into the unset epoxy and removed after the epoxy has solidified. The specimens are finally cut in beam form for four point bending

tests (see Figure 5.1). Only crude experiments were performed, being limited by production techniques.

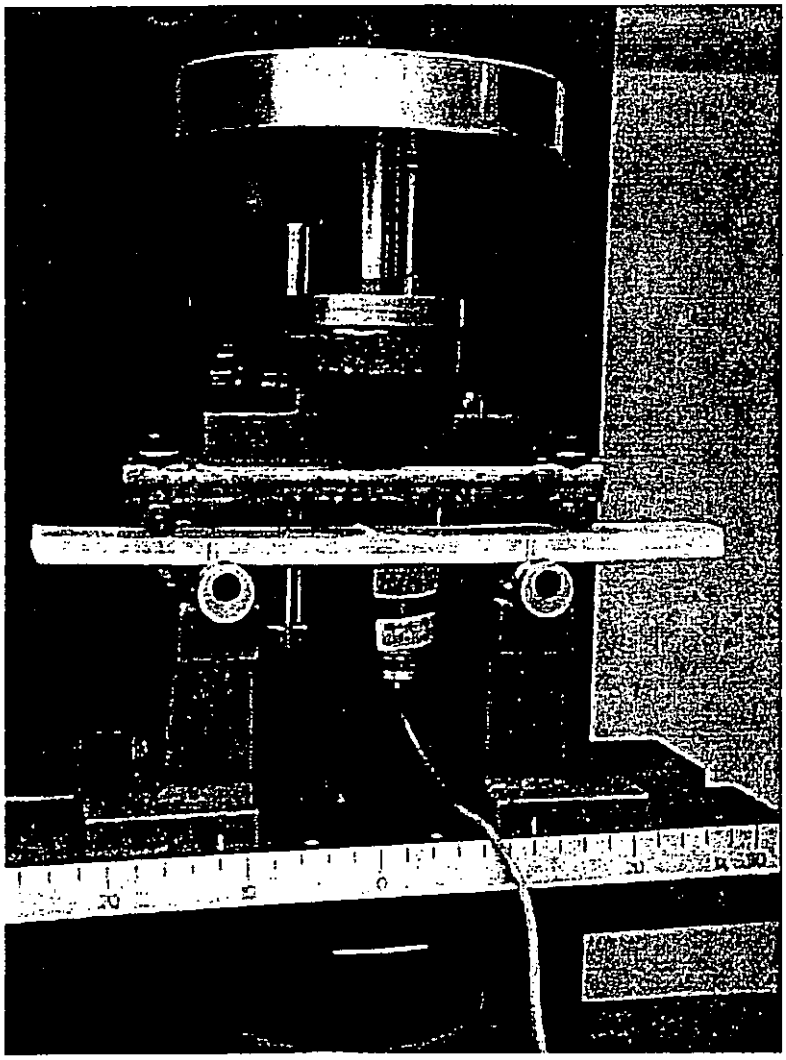

Figure 5.1 The specimen on the four point bend apparatus

Observations from the experiment includes the following :

1. The crack always propagates towards the interface (see Figure 5.2).
2. K_I and K_{II} (for the right-hand half) are always positive
3. There is no crack closure

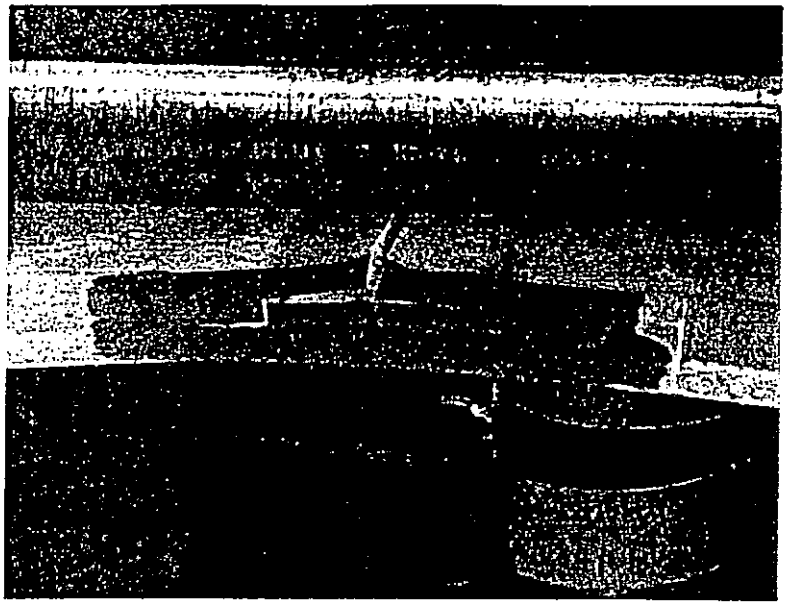

Figure 5.2 The crack propagated towards the interface and further run along the interface

5.2 Characteristics and Applications of the Specimen

Apart from being free of the influence of interfacial properties, the following aspects of the specimen are worth mentioning:

- By varying the fibre content of the composite layer, different material moduli ratios can be produced.
- The bending load can be used to simulate loading caused by differential expansions or contractions as a result of change of temperature.
- The choice of specimen design is not confined to beams and four point bending experiments. Other specimen shapes and loading configurations can be applied depending on the application.
- Since the existence of the bottom layer is mainly to provide the bi-material environment, it need not be made of the actual material involved in the material

pair under investigation, provided the same average constitutive properties are generated.

- The value of G_c obtained should be checked with the corresponding values of K_I and K_{II} for the validity of test results. The values of K_I and K_{II} can then be used to formulate failure criteria for sub-interfacial cracks.
- This approach is also suitable for the study of interfacial cracks, for which a greater number of analytical solutions are available.

It should be noted that there is a need to initiate a crack which is *sharp* enough and initially *runs parallel to the interface.* Some standard procedures on conducting fracture experiments including the fabrication of "initially sharp cracks" are contained in ASTM E399-90(1997) "Standard Test Method for Plane-Strain Fracture Toughness of Metallic Materials". Although the text is for metals, the procedures are well developed and well explained, and should be adopted in future experiments. Other relevant standards includes ASTM E1820 "Test Method for Measurement of Fracture Toughness" and ASTM E1290-99 "Standard Test Method for Crack-Tip Opening Displacement (CTOD) Fracture Toughness Measurement". The procedure suggested is by fatigue crack starter notch. However for our crude experiments conducted here in this study, it is not convenient to initate the crack with the standard procedure mentioned in the standards since the four point bend will lead to cracks going towards the interface. Here, in order to simulate the crack, a thin plastic film was inserted, parallel to the interface, prior to the curing of the epoxy layer and retrieved after the epoxy has solidified. The "crack", which was as "thick" as the plastic film plus the releasing agent painted onto it, still behaves as expected i.e. propagate towards the interface. But this method is limited to certain materials like

the Epoxy used here. With other materials, which do not allow insertions, other devices should be employed. Two procedures are suggested here :

1. It is recommended to follow the instructions on ASTM E1304-97(2002) "Standard Test Method for Plane-Strain (Chevron-Notch) Fracture Toughness of Metallic Materials". A chevron starter notch (Barker (1977)), originally designed for plane strain fracture toughness of brittle materials, is often adopted for crack initiation in mixed mode crack studies e.g. applied in experiments by Mahanty and Maiti (1990). The notch guides the crack path during fatigue pre-cracking. This procedure would usually call for a slightly wider transverse slot and a careful choice of cutting tools.
2. In the study of cracks under mixed-mode loading, it is common practice to grip the specimen first for fatigue pre-cracking under mode I loading, and then change to a different gripping configuration for the application of mixed-mode loading, e.g. in Mahanty and Maiti (1990). A similar procedure can be adopted here if the horizontal crack can be introduced first, by embedding insertions or by machining, preferably with a chevron starter notch, and pre-cracked in mode I before the vertical splitting notch is introduced. This procedure, however, would usually necessitate the drilling of holes in the mid-section of the beam. Since holes are also discontinuities, it should be noted that the criterion for deciding dimensions in attaining steady state should also include the presence of the holes.

In some cases, cracks are constrained to propagate in preferred paths, e.g. delamination in laminated uniaxial fiber-reinforced composites. The above special

procedures are then not necessary but Equation ...(4.5) and Equation ...(4.6) may have to be modified for orthotropic material properties as given in Suo (1990).

It should also be noted that, just as in other specimens for fracture testing, failure by general yielding should not occur before fracture. Hence the bending moment producing fracture should be checked to see whether it has exceeded the value for producing yield point stress at the central section of the specimen. Adjustments in specimen dimensions have to be made and testing performed again to give valid results.

Interface crack initiation verses Subinterface crack propagation

When preforming subinterfacial fracture experiments, the initiation of an interface crack should not occur prior to propagation of the subinterfacial crack. This can be prevented by the following steps :

1. Perform interface fracture experiments to obtain the interfacial toughness of the materials concerned.
2. Design the subinterfacial crack specimen and verify the dimensions and loading conditions with FEA that the expeiment will not favour interface fracture prior to subinterface crack propagation.

Issues concerning the plastic zones :

According to Rice (1988) the size of plastic zone of an interfacial crack is dependent on the phase angle, yield strength of the both solids, dimensionless properties of describing strain hardening and ratios of elastic constants and the size of plastic zone itself. In Shih and Asaro (1988) the largest plastic zones for arbitrary extreme cases

(extreme elastic ratios, yield strength ratios, phase angle ...) is about 2.5e-3 of the crack length.

Nevertheless, the issue of plastic zone is put aside until more studies on plastic zones of cracks in bimaterial non-infinite media arises. One suggestion towards the solution on plastic zones is through the studies on dislocation theory which allow us to study fracture in microscopic scales and down to the base of the problem. More and more solutions on fracture problems are based on the dislocation theory in addition to the classical fracture theories obtained from Muskhelishvilli representations and Williams's expansions. Such examples include the works by Hutchinson et. al. (1987) and Suo (1990).

Chapter 6 Conclusion

The study of cracks at or close to and parallel to an interface is carried out through improving and examining methods in determining the complex stress intensity factors of interface cracks and studying the stress intensity factors of a suggested specimen configuration with subinterfacial crack.

The new modified stiffness derivative method, which makes use of the strain energies of crack-tip elements before and after a virtual crack extension to determine the complex stress intensity factors of interfacial cracks is introduced. Verified with several reference cases : central cracks, edge cracks and the four point bending specimen configuration, this method is insensitive to mesh sizes and is accurate to within 1% with the recommended parameter values. The geometric progressing factor (after the first 3 elements from the crack-tip) should be m = 1.5. The relative virtual crack extension length is recommended as $\Delta a/e$ = 1/500 to 1/1000. The arbitrary ΔK should be taken as 1/100 times of the expected K-values. The crack surface displacement method is also studied. This method has accuracy comparable to the new combined stiffness derivative method only when crack-tip element sizes of $e/a \leq 50$ are employed.

A four-point bend specimen has been proposed for the study of crack close to and parallel to the interfacial of dissimilar materials and finite element analysis was carried out to determine its characteristics. To attain steady state cracking, which ensures the influences of the load point are not present and thus giving constant strain energy release rates, the half distance between the inner load points L and the half crack length a should be :

$$L > 3H_3 \text{ and } \max\left[1.5\cdot(H_1-h), 1.5\cdot\left(\frac{H_2+h}{2}\right)\right] \leq a \leq (L-1.5\cdot H_3).$$

A crack surface displacement method is employed to determine the stress intensity factors for beams of different thickness ratios and modulus ratios; different crack lengths, and for cracks at various distances from the interface. To be applied on geometrically similar specimens, the associated stress intensity factors are presented in normalized format in terms of the applied bending moment, basic elastic material properties and the dimensions of the specimen. These normalized values were curve-fitted using a combination of power and polynomial terms in the distance between the crack and the interface. Application of such curves is demonstrated by an application to cracks near solder/copper, Ni/MgO, and Si/Cu interfaces.

Finally the relationship between the conventional stress intensity factors for a crack close to and parallel to the interface and the complex stress intensity factors of a corresponding interfacial crack was studied. The relationship is applicable for $1/1000 \leq h/H_1 \leq 1/100$.

Reference List

1. Banks-Sills, L. and Sherman, D. "Comparison of methods for calculating stress intensity factors with quarter-point elements". *International Journal of Fracture*, Vol. 32, pp.127-140 (1986)
2. Barker, L.M. "A simplified method for measuring plane strain fracture toughness". *Engineering Fracture Mechanics*, Vol. 52, pp.777-790 (1977)
3. Barsoum, R.S. "On the use of isoparametric finite elements in linear fracture mechanics". *International Journal for Numerical Methods in Engineering*, Vol. 10, pp.25-37 (1976)
4. Beom, H.G. and Atluri, S.N. "Asymptotic analysis of a subinterface crack in dissimilar orthotropic media". *Engineering Fracture Mechanics*, Vol. 52, pp.777-790 (1995)
5. Chan, S.K. ; Tuba, I.S. and Wilson W.K. "On the finite element method in liner fracture mechanics". *Engineering Fracture Mechanics*, Vol. 2, pp.1-17 (1970)
6. Charalambides, P.G.; Cao, H.C.; Lund, J. and Evans, A.G. "Development of a test method for measuring the mixed mode fracture resistance of bimaterial interfaces". *Mechanics of Materials*, Vol. 8, pp.269-283 (1990)
7. Charalambides, P.G.; Lund, J.; Evans, A.G. and McMeeking, R.M. "A test specimen for determining the fracture resistance of bimaterial interfaces". *Journal of Applied Mechanics*, Vol. 56, pp.77-82 (1989)
8. Charalambides, P.G.and Zhang, W. "An energy method for calculating the stress intensities in orthotropic bimaterial fracture". *International Journal of Fracture*, Vol. 76, pp.97-120 (1996)

9. Chow, W.T. and Atluri, S.N. "Finite element calculation of stress intensity factors for interfacial crack using virtual crack closure integral". *Computational Mechanics*, Vol. 16, pp. 417-425 (1995)

10. Clough, R.B.; Shapiro, A.J.; Bayba, A.J. and Lucey, G.K. Jr. "Boundary layer fracture in composite solder joints". *Journal of Electronic Packaging*, Vol. 117, pp.270-274 (1995)

11. Comninou, M "An overview of interface cracks". *Engineering Fracture Mechanics,* Vol. 37 pp.197-208 (1990)

12. Erdogan, F. "Fracture mechanics of interfaces. In: Rossmanith H.P., ed., *Damage and Failure of Interfaces*. A.A. Balkema, Rotterdam, Brookfield p.3-36 (1997)

13. Fett, T; Munz, D. and Tilscher, M. "Weight functions for sub-interface cracks". *International Journal of Solid Structures*, Vol. 34, pp.393-400 (1997a)

14. Fett, T; Tilscher, M. and Munz, D. "Weight functions for cracks near the interface of a bimaterial joint, and application to thermal stress". *Engineering Fracture Mechanics*, Vol. 56, pp.87-100 (1997b)

15. Griffith, A.A. "The phenomena of rupture and flow in solids". *Philosophical Transactions of the Royal Society of London, series A*, Vol.221, pp.163-198 (1920)

16. Henshell, R.D. and Shaw, K.G. "Crack tip elements are unnecessary". *International Journal for Numerical Methods in Engineering*, Vol. 9, pp.495-507 (1975)

17. Hutchinson, J.W. and Suo, Z. "Mixed mode cracking in layered materials". Advances in Applied Mechanics, Volume 29, pp. 63-191 Academic Press, Inc. (1992)

18. Hutchinson, J.W.; Mear, M.E. and Rice, J.R. "Crack paralleling an interface between dissimilar materials". *Journal of Applied Mechanics*, Vol. 54, pp.828-832 (1987)

19. Irwin, G.R. "Analysis of stresses and strains near the end of a crack traversing a plate". *Journal of Applied Mechanics*, Vol. 24, pp.361-364 (1957)

20. Irwin, G.R. "Onset of Fast Crack Propagation in High Strength Steel and Aluminum Alloys". *Naval Research Laboratory Report No. 4763,* Naval Research Laboratory, USA (1936)

21. Klingbeil, N.W. and Beuth, J.L. "Interfacial fracture testing of deposited metal layers under four-point bending". *Engineering Fracture Mechanics*, Vol. 56, pp.113-126 (1997)

22. Lim, I.L.; Johnston, I.W. and Choi, S.K. "Application of singular quadratic distorted isoparametric elements in linear fracture mechanics". *International Journal for Numerical Methods in Engineering*, Vol. 36, pp.2473-2499 (1993)

23. Lim, I.L.; Johnston, I.W. and Choi, S.K. "Comparison between various displacement-based stress intensity factor computation techniques". *International Journal of Fracture*, Vol. 58, pp.193-210 (1992)

24. Lin, K.Y. and Mar, J.W. "Finite element analysis of stress intensity factors for cracks at bimaterial interface". *International Journal of Fracture*, Vol. 12, pp. 521-531 (1976)

25. Lu, H and Lardner, T.J. "Mechanics of subinterface cracks in layered material". *International Journal of Solid Structures*, Vol. 29, pp.669-688 (1992)

26. Lynn and Ingraffea "Transition elements to be used with quarter-point crack-tip elements". *International Journal for Numerical Methods in Engineering*, Vol. 15, pp.1427-1445 (1980)

27. Maiti, S.K. and Mahanty, D.K. "Experimental and Finite Element studies on mode I and mixed mode (I and II) stable crack growth - II. Finite element analysis". *Engineering Fracture Mechanics*, Vol. 37, pp.1251-1275 (1990)

28. Matos, P.P.L. ; McMeeking, R.M. ; Charalambides, P.G. and Drory, M.D. "A method for calculating stress intensities in bimaterial fracture". *International Journal of Fracture*, Vol. 40, pp.235-254 (1989)

29. Murakami, Y. *Stress Intensity Factors Handbook.* The Society of Materials Science, Kyoto (1987)

30. Naik, R.A. and Crews, J.H., Jr. "Calculation of stress intensity factors for interface cracks under mixed-mode loading". *ASTM STP*, Vol.1207, pp.778-792 (1994)

31. Ng, S.W. and Lau K.J. "A new way of implementing the stiffness derivative method for determining stress intensity factors". *International Journal of Fracture*, Vol. 102, pp.L29-L32 (2000)

32. Ng, S.W. and Lau K.J. "Determination of mixed-mode stress intensity factors using a semi-infinite crack model". *Engineering Fracture Mechanics*, Vol. 58, pp.43-59 (1997)

33. Orowan, E. "Fracture and Strength of Solids". *Report of Progress in Physics*, Vol.12, pp.185-232 (1949)

34. Parks, D..M. "A stiffness derivative finite element technique for determination of elastic crack tip stress intensity factors". *International Journal of Fracture*, Vol. 10, pp.478-502 (1974)

35. Rice, J.R. "A path independent integral and the approximate analysis of strain concentration by notches and cracks". *Journal Applied Mechanics*, Vol. 35, pp.379-386 (1968)

36. Rice, J.R. "Elastic fracture mechanics concepts for interfacial cracks". *Journal of Applied Mechanics*, Vol.55 pp.98-103 (1988)

37. Rice, J.R. "Some remarks on elastic crack-tip stress fields". *International Journal of Solids and Structures*, Vol. 8, pp.751-758 (1972)

38. Rice, J.R. and Sih, G.C. "Plane problems of cracks in dissimilar media". *Journal of Applied Mechanics*, Vol.32, pp.418-423 (1965)

39. Rice, J.R.; Suo, Z. and Wang, J-S. "Mechanics and thermodynamics of brittle interfacial failure in bimaterial systems" In : Ashby, A.G.; Rühle, M.; Evans, M.F. and Hirth, J.P. eds., *Metal-Ceramic Interfaces,* Pergamon Press, New York, pp.269-294 (1990)

40. Shih, C.F. and Asaro, R. "Elastic-plastic analysis of cracks on bimaterial interfaces: part I — small scale yielding". *Journal of Applied Mechanics*, Vol.55, pp.299-316 (1988)

41. Shih, C.F.; deLorenzi, H.G. and German, M.D. "Crack extension modelling with singular quadratic isoparameteric elements". *International Journal of Fracture*, Vol. 12, pp.647-651 (1976)

42. Sih, G.C. *Handbook of Stress Intensity Factors.* Institute of Fracture and Solid Mechanics, Lehigh University, Pennsylvania (1973)

43. Sneddon, I.N. "The distribution of stress in the neighbourhood of a crack in an elastic solid". *Proceedings of the Royal Society, London, series A*, Vol. 187, pp. 229-260 (1946)

44. Suo, Z. "Delamination specimens for orthotropic materials". *Journal of Applied*

Mechanics, Vol. 57, pp.627-634 (1990)

45. Suo, Z. and Hutchinson, J.W. "Interface crack between two elastic layers". *International Journal of Fracture*, Vol. 43, pp.1-18 (1990)

46. Tada, H.; Paris, P.C. and Irwin, G.R. *The stress analysis of cracks handbook 2nd Edition*. Paris Productions Incorporated (and Del Research Corporation), Missouri (1985)

47. Tracey, D.M. "Discussion of on use of isoparametric finite-elements in linear-fracture mechanics by Barsoum, RS". *International Journal of Numerical Methods in Engineering*, Vol. 11, pp.401-402 (1977)

48. Venkatesha, K.S.; Ramamurthy, T.S. and Dattaguru, B. "A study of the behavior of subinterface cracks in bimaterial plates". *Engineering Fracture Mechanics*, Vol. 59, pp.241-252 (1998)

49. Williams, M.L. "The stresses around a fault or crack in dissimilar media". *Bulletin of the Seismological Society of America*, Vol. 49, pp.199-204 (1959)

50. Wu, Y.L. "A new method for evaluation of stress intensities for interface cracks". *Engineering Fracture Mechanics*, Vol. 48, pp.755-761 (1994)

51. Yang, M and Kim, K. "The behavior of subinterface cracks with crack-face contact". *Engineering Fracture Mechanics*, Vol. 44, pp.155-165 (1993)

52. Yuuki, R. and Cho S.B. "Boundary element analysis of stress intensity facotrs for an interface crack in dissmilar materials". *Transactions of Japan Society of Mechanical Engineers*, Vol. 55 No.510, pp.340-347 (1989a)

53. Yuuki, R. and Cho S.B. "Efficient boundary element analysis of stress intensity facotrs for interface cracks in dissmilar materials". *Engineering Fracture Mechanics*, Vol. 34 No.1, pp.179-188 (1989b)

Appendix I Solving Algorithm of (p,b) and (τ,b)

The solution algorithm of (p,b) can be demonstrated by considering the plot of p against b (see Figure I.1).

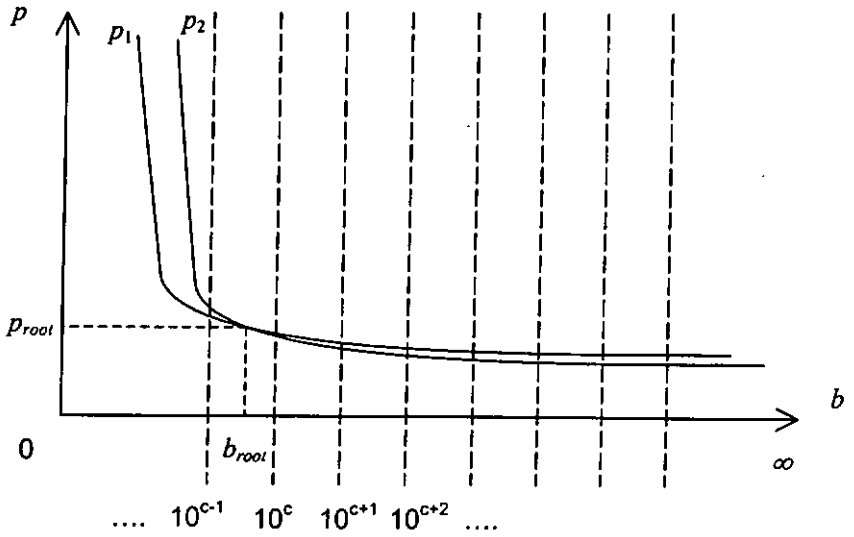

Figure I.1 Plot of p against b with solution at (b_{root},p_{root})

From Equation ...(2.6), p can be expressed as a function of b, at small values of b i.e. $x < -b$, by :

$$p(b) = \frac{(2\mu\pi)\cdot v_l}{(\kappa+1)\cdot b\cdot\left[\sqrt{\frac{|x|}{b}} + \left(1+\frac{x}{b}\right)\left(\coth^{-1}\left(\sqrt{\frac{|x|}{b}}\right)\right)\right]} \qquad \text{...(I.1)}$$

where x and v_l are the x-coordinate and the decoupled opening displacment in y-direction from ...(2.2) of the corresponding node respectively

It was shown by Ng and Lau (1997) that the nodes that gives the most accurate estimates are the 'midside' node and corner node of the quarter point element shown in Figure I.2.

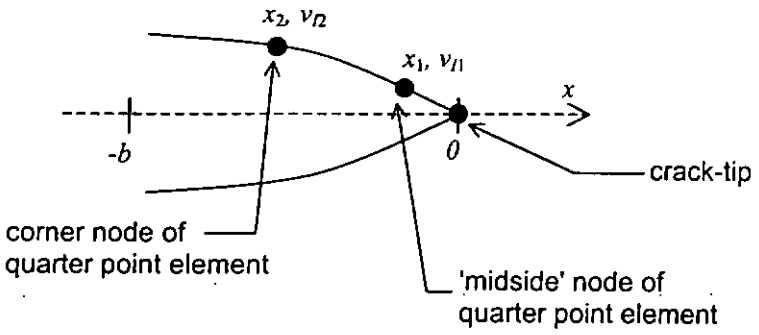

Figure I.2 The nodes taken for solving p and b

By substituting (x_1, v_{I1}) and (x_2, v_{I2}) into Equation ...(I.1), one gets $p_1(b)$ and $p_2(b)$. These lines are plotted in Figure I.1. For demonstration purpose, the case have solution and the root is located at (b_{root}, p_{root}), where the 2 lines cross each other. It is possible to check if the solution exists for any given (x_1, v_{I1}) and (x_2, v_{I2}). At $b \to 0$, it can be shown, in the following equations, that $p_2 - p_1 > 0$:

$$\lim_{b \to 0^+} (p_2 - p_1):$$

$$= \text{signum}\left[\frac{v_{I2} \cdot \sqrt{|x_2|} \cdot |x_1| + v_{I2} \cdot \sqrt{|x_2|} \cdot x_1 - v_{I1} \cdot \sqrt{|x_1|} \cdot |x_2| - v_{I1} \cdot \sqrt{|x_1|} \cdot x_2}{(|x_2| + x_2) \cdot (|x_1| + x_1)} \right] \cdot \infty$$

$$= \infty > 0 \qquad \ldots(I.2)$$

where signum(z) returns 1 if $z = 0$ and $\frac{z}{|z|}$ otherwise.

The root exist if at $b \to \infty$, $p_1 - p_2 > 0$. This condition can be checked by considering the limit of K by taking advantage of the $\sqrt{b}$ in K expression from Equation ...(2.4). Substituting Equation ...(2.5) into Equation ...(2.4) for b at large values i.e. $-b < x \le 0$, the limit of K when $b \to \infty$ is:

$$\lim_{b\to\infty} K = \lim_{b\to\infty} \frac{2\sqrt{2}}{\sqrt{\pi}} p\sqrt{b}$$

$$= \lim_{b\to\infty} \frac{2\sqrt{2}}{\sqrt{\pi}} \frac{(2\mu\pi)\cdot v_I \cdot \sqrt{b}}{(\kappa+1)\cdot b\cdot\left[\sqrt{\frac{|x|}{b}} + \left(1+\frac{x}{b}\right)\left(\tanh^{-1}\left(\sqrt{\frac{|x|}{b}}\right)\right)\right]}$$

$$= \frac{2\mu\pi}{(\kappa+1)} \cdot \frac{v_I}{\sqrt{|x|}} \cdot \sqrt{\frac{2}{\pi}} \qquad \ldots(I.3)$$

Therefore, to have solution, the condition of having at $b \to \infty$, p_1 - $p_2 > 0$ is equivalent to :

$$\lim_{b\to\infty}(p_1 - p_2) > 0$$

$$\Rightarrow \lim_{b\to\infty}\left(\frac{2\sqrt{2}}{\sqrt{\pi}} p_1\sqrt{b} - \frac{2\sqrt{2}}{\sqrt{\pi}} p_2\sqrt{b}\right) > 0$$

$$\Rightarrow \left(\frac{2\mu\pi}{(\kappa+1)} \cdot \frac{v_{I1}}{\sqrt{|x_1|}} \cdot \sqrt{\frac{2}{\pi}} - \frac{2\mu\pi}{(\kappa+1)} \cdot \frac{v_{I2}}{\sqrt{|x_2|}} \cdot \sqrt{\frac{2}{\pi}}\right) > 0$$

By taking out constant terms, the condition is simplied as :

$$\Rightarrow \left(\frac{v_{I1}}{v_{I2}}\right)^2 > \frac{x_1}{x_2} \qquad \ldots(I.4)$$

Similarly, the condition for τ and b to have solution is :

$$\Rightarrow \left(\frac{u_{II1}}{u_{II2}}\right)^2 > \frac{x_1}{x_2} \qquad \ldots(I.5)$$

The condition is checked by every interval of $b = 10^c$ with c = -10 to 15. If solution exists, it is bounded by 10^c and 10^{c-1}. After the solution is located, it is solved by the bisection method with accuracy up to 10^{-14}. When no solution exists, the value of v_{I1} or u_{II1} is increased till solution exists. The maximum deviation is 1.27% and 2.19% for K_I and K_{II} respectively.

Appendix II The Displacement Functions for Interface Cracks

From Matos et al. (1989), the functions f_{x1}, f_{y1}, f_{x2} and f_{y2} are defined as :

$$f_{x1} = D_j + 2\delta_j \sin\theta \sin\Psi \qquad f_{y1} = -C_j - 2\delta_j \sin\theta \cos\Psi$$

$$f_{x2} = -C_j + 2\delta_j \sin\theta \cos\Psi \qquad f_{y2} = -D_j + 2\delta_j \sin\theta \sin\Psi$$

where

$$\delta_1 = e^{-(\pi-\theta)\varepsilon}, \quad \text{and} \quad \delta_2 = e^{(\pi+\theta)\varepsilon},$$

$$\Psi = \varepsilon \ln r + \frac{\theta}{2},$$

$$D_j = \beta\gamma_j \cos\frac{\theta}{2} + \beta'\gamma'_j \sin\frac{\theta}{2}, \qquad C_j = \beta'\gamma_j \cos\frac{\theta}{2} - \beta\gamma'_j \sin\frac{\theta}{2},$$

$$\beta = \frac{0.5\cos(\varepsilon \ln r) + \varepsilon \sin(\varepsilon \ln r)}{0.25 + \varepsilon^2}, \quad \beta' = \frac{0.5\sin(\varepsilon \ln r) - \varepsilon \cos(\varepsilon \ln r)}{0.25 + \varepsilon^2},$$

$$\gamma_j = \kappa_j \delta_j - \frac{1}{\delta_j} \quad \text{and} \quad \gamma'_j = \kappa_j \delta_j + \frac{1}{\delta_j}$$

with (r, θ) the polar coordinates of the node,

ε, κ_j the material constants and j the material index.

Appendix III Tables of Results in Chapter 3

The numerical data of the graphs in Chapter 3 are given here.

1. For central interfacial crack in infinite plate with $E_1 = 1000$, $E_2 = 10$, $\nu_1 = 0.3$, $\nu_2 = 0.3$ and gives K_{1ref} and K_{2ref} as 1.79874 and -0.262529 respectively,

e/a	Combined SDM		CSD		No. of elements	No. of nodes
	K_{1SDM} (% deviation)	K_{2SDM} (% deviation)	K_{1CSD} (% deviation)	K_{2CSD} (% deviation)		
1/4	1.80427 (0.307)	-0.263877 (0.514)	1.73194 (-3.714)	-0.254308 (-3.132)	292	937
1/5	1.80424 (0.306)	-0.263808 (0.487)	1.73791 (-3.382)	-0.270329 (2.971)	364	1163
1/6	1.80421 (0.304)	-0.263761 (0.469)	1.74180 (-3.165)	-0.268818 (2.395)	364	1163
1/7	1.80421 (0.304)	-0.263728 (0.457)	1.74452 (-3.014)	-0.267739 (1.984)	444	1413
1/8	1.80420 (0.303)	-0.263700 (0.446)	1.74651 (-2.904)	-0.266909 (1.668)	444	1413
1/9	1.80419 (0.303)	-0.263676 (0.437)	1.74936 (-2.745)	-0.266258 (1.420)	444	1413
1/10	1.80419 (0.303)	-0.263659 (0.430)	1.75493 (-2.436)	-0.265749 (1.226)	532	1687
1/50	1.80423 (0.305)	-0.263416 (0.338)	1.79628 (-0.137)	-0.262028 (-0.191)	964	3023
1/100	1.80428 (0.308)	-0.263336 (0.308)	1.80098 (0.125)	-0.263300 (0.294)	1128	3529
1/1000	1.80453 (0.322)	-0.263172 (0.245)	1.80485 (0.340)	-0.262501 (-0.011)	2028	6285
1/10000	1.80484 (0.339)	-0.263171 (0.245)	1.80590 (0.398)	-0.262727 (0.076)	3252	10017

Table III.1 The complex stress intensity factors obtained by the combined SDM and the CSD with their corresponding percentage deviation from the reference values with respect to the change in quarter point element size.

$\Delta a/e$	K_{1SDM} (% deviation)	K_{2SDM} (% deviation)
1/10	1.64606 (-8.488)	-0.214949 (-18.124)
1/50	1.77391 (-1.380)	-0.254479 (-3.066)
1/100	1.79071 (-0.447)	-0.259402 (-1.191)
1/500	1.80428 (0.308)	-0.263336 (0.308)
1/1000	1.80598 (0.403)	-0.263828 (0.495)
1/5000	1.80735 (0.479)	-0.264221 (0.645)
1/10000	1.80752 (0.488)	-0.264270 (0.663)

Table III.2 Effect on the accuracy due to the relative length of virtual crack extension $\Delta a/e$

The K-values derived from the reference normalized values are :

$$K_{1der} = \frac{\left[K_{1norm}\cos(\varepsilon \ln(H_3)) + K_{2norm}\sin(\varepsilon \ln(H_3))\right]\cdot Pd}{BH_3^{3/2}}$$

$$K_{2der} = \frac{\left[K_{2norm}\cos(\varepsilon \ln(H_3)) - K_{1norm}\sin(\varepsilon \ln(H_3))\right]\cdot Pd}{BH_3^{3/2}} \qquad \ldots(\text{III.1})$$

$H_1/H_2 = 1$ (642 elements)	Combined SDM $\times 10^6$		Reference values (Charalambides et al. (1989)) $\times 10^6$	
E_2/E_1	K_1	K_2	K_{1der}	K_{2der}
1	342.5	293.2	345	298
	(-0.83)	(-1.50)		
2.5	201.0	261.4	198	268
	(1.38)	(-2.37)		
5	119.8	204.2	120	205
	(-0.01)	(-0.57)		
10	71.6	141.1	70	141
	(2.84)	(0.38)		
25	33.5	74.1	32	72
	(4.02)	(2.64)		

Table III.3 K-values by the combined SDM for four point bend specimen with $H_1/H_2 = 1$

$H_1/H_2 = 0.5$ (652 elements)	Combined SDM $\times 10^6$		Reference values (Charalambides et al. (1989)) $\times 10^6$	
E_2/E_1	K_1	K_2	K_{1der}	K_{2der}
1	157.1	150.3	160	149
	(-1.91)	(0.63)		
2.5	82.1	119.7	85	120
	(-2.95)	(0.12)		
5	43.7	84.5	45	85
	(-1.98)	(-0.78)		
10	22.2	52.3	23	52
	(-5.02)	(0.01)		
25	8.7	24.3	9	24
	(-6.99)	(1.20)		

Table III.4 K-values by the combined SDM for four point bend specimen with $H_1/H_2 = 0.5$

Appendix IV Superposition for Beams

Suppose a thin beam, with thickness T, simulates a portion A'B'CD (with the same thickness T) of the beam ABCD, shown in Figure IV.1, by having the same stress distribution, as it is part of the original beam.

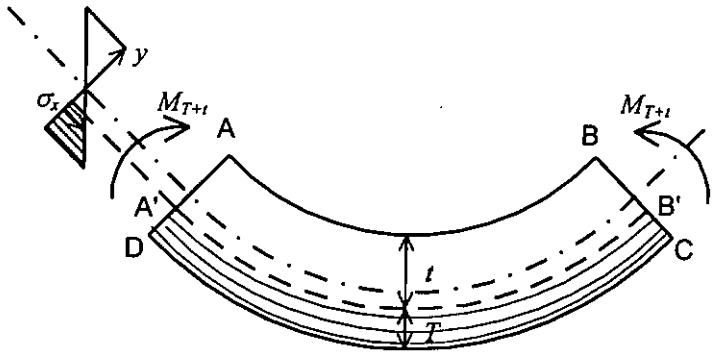

Figure IV.1 The stress distribution of a thinner portion of a beam

M_{T+t} is the bending moment applied on the original beam ABCD. (T+t) is the total thickness of the original beam. Then the equivalent tensile load F_T and the moment M_T superposed together on the thinner beam A'B'CD (shown in Figure IV.2) to give the same stress distribution can be determined by :

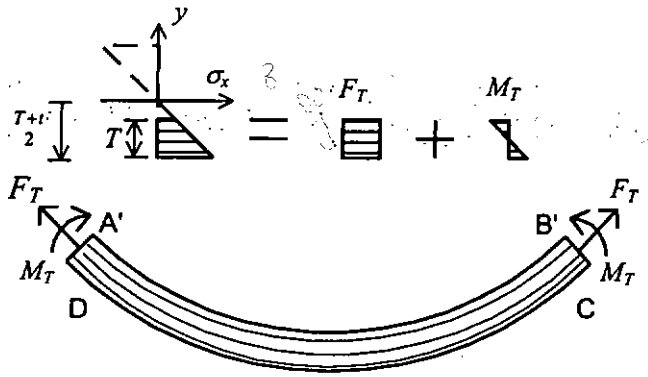

Figure IV.2 Superposition of the two loads F_T and M_T on the thinner beam A'B'CD

F_T can be found by the average tensile stress on the beam :

$$F_T = \int_{\frac{T+t}{2}-T}^{\frac{T+t}{2}} \sigma_x dA$$

$$= \int_{\frac{T+t}{2}-T}^{\frac{T+t}{2}} \frac{M_{(T+t)}}{I_{(T+t)}} yBdy$$

$$= \frac{M_{(T+t)}}{\left[\frac{B(T+t)^3}{12}\right]} \cdot \frac{y^2}{2}\Bigg|_{\frac{T+t}{2}-T}^{\frac{T+t}{2}}$$

$$\therefore F_T = \frac{6M_{(T+t)}Tt}{(T+t)^3} \qquad \ldots(\text{IV.1})$$

where B is the width of the beam and $I_{(T+t)}$ is the moment of inertia of the whole beam ABCD.

M_T, i.e. the equivalent bending moment, can be found by considering the gradient of σ_x against y :

$$\text{i.e. } \frac{M_{(T+t)}}{I_{(T+t)}} = \frac{\sigma_x}{y} = \frac{M_T}{I_T} = \text{constant}$$

$$\therefore M_T = M_{(T+t)} \cdot \frac{\left[\frac{BT^3}{12}\right]}{\left[\frac{B(T+t)^3}{12}\right]}$$

$$\therefore M_T = M_{(T+t)} \cdot \left(\frac{T}{T+t}\right)^3 \qquad \ldots(\text{IV.2})$$

So the thinner beam A'B'CD can represent the portion in the original beam if it is loaded with the tensile load $F_T = \frac{6M_{(T+t)}Tt}{(T+t)^3}$ and the bending moment M_T $= M_{(T+t)} \cdot \left(\frac{T}{T+t}\right)^3$.

Appendix V Equilibrium in Beams

This superposition scheme is adapted from Suo (1990) with the forces in the opposite direction as in the original source. In Figure V.1, all the forces P_1, P_2, P_3 and bending moments M_1, M_2 and M_3 are loaded on the neutral axis of that section.

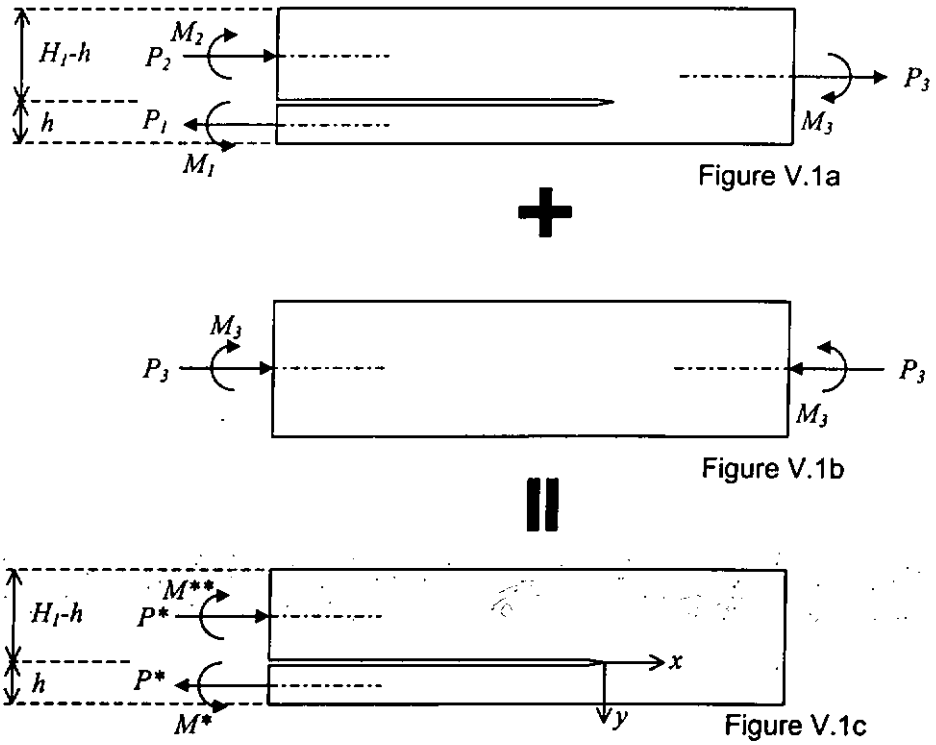

Figure V.1 Convention for Superposition

Considering equilibrium in the beam in Figure V.1a gives :

$$\sum F_x = 0 \Rightarrow$$

$$-P_1 + P_2 + P_3 = 0 \qquad \ldots(V.1)$$

Taking moment about the neutral axis of the upper cracked beam with thickness H_1-h and taking the anticlowise direction positive :

$$\sum M = 0 \Rightarrow$$

$$M_1 - M_2 - M_3 - P_1\left(\frac{H_1 - h}{2} + \frac{h}{2}\right) + P_3\left(\frac{H_1}{2} - \frac{H_1 - h}{2}\right) = 0 \qquad \ldots(V.2)$$

Among the six loads, only 4 (say P_1, P_3, M_1 and M_3) are independent after considering equilibrium. P_1 and M_1 can be represented by the other 4 loads :

$$P_1 = P_2 + P_3 \qquad \ldots(V.3)$$

$$M_1 = M_2 + M_3 + P_1\left(\frac{H_1}{2}\right) - P_3\left(\frac{h}{2}\right) \qquad \ldots(V.4)$$

Superposition of the two beams in Figure V.1a and Figure V.1b gives the resultant Figure V.1c. On the right hand side of Figure V.1c., P_3 and M_3 canceled out each other. Focusing on Figure V.1c, the resultant on the lower portion on the left hand side of the beam P^* and M^* are :

$$P^* = P_1 - P_3\left(\frac{h}{H_1}\right) + \underbrace{M_3\left(\frac{6h(H_1 - h)}{H_1^{\,3}}\right)}_{\text{superposition}} \qquad \ldots(V.5)$$

$$M^* = M_1 - \underbrace{M_3\left(\frac{h}{H_1}\right)^3}_{\text{superposition}} \qquad \ldots(V.6)$$

(The two terms at the back are derived from Equation...(IV.1) and Equation...(IV.2) of the superposition scheme of beams in Appendix IV.)

and M^{**} is the reaction of M^* :

$$M^{**} = M^* + P^*\left(\frac{H_1}{2}\right) \qquad \ldots(V.7)$$

For a specimen with applied load P_o and M_o. Then $P_2 = M_2 = 0$. Denote $P_3 = P_o$ and $M_3 = M_o$. Then the resultant M^* and P^* are :

$$P^* = P_o - P_o\left(\frac{h}{H_1}\right) + M_o\,\frac{6h(H_1 - h)}{H_1^{\,3}} \qquad \ldots(V.8)$$

$$M^* = M_o + P_o\left(\frac{H_1 - h}{2}\right) - M_o\left(\frac{h}{H_1}\right)^3 \qquad \ldots(V.9)$$

Expressing Equation ...(V.8) and Equation ...(V.9) in terms of the thickness ratio $\eta = \frac{h}{H_1 - h}$, defined by Suo (1990) :

$$\frac{h}{H_1} = \frac{h}{H_1 - h + h}$$

$$= \frac{1}{\frac{H_1 - h}{h} + \frac{h}{h}}$$

$$= \frac{1}{\frac{1}{\eta} + 1} = C_1 \qquad \text{...(V.10)}$$

$$\frac{6h(H_1 - h)}{H_1^3} = \frac{\frac{6h(H_1 - h)}{h^3}}{\left(\frac{H_1}{h}\right)^3}$$

$$= \frac{\frac{6(H_1 - h)}{h}}{\left(\frac{H_1 - h}{h} + \frac{h}{h}\right)^3} \cdot \frac{1}{h}$$

$$= \frac{\frac{6}{\eta}}{\left(\frac{1}{\eta} + 1\right)^3} \cdot \frac{1}{h} = \frac{C_2}{h} \qquad \text{...(V.11)}$$

$$\left(\frac{h}{H_1}\right)^3 = \left(\frac{h}{H_1 - h + h}\right)^3$$

$$= \left(\frac{1}{\frac{H_1 - h}{h} + \frac{h}{h}}\right)^3$$

$$= \frac{1}{\left(\frac{1}{\eta} + 1\right)^3} = C_3 \qquad \text{...(V.12)}$$

Therefore Equation ...(V.8) and Equation ...(V.9) become :

$$P^* = (1 - C_1)P_o + \frac{C_2 M_o}{h}, \qquad \ldots(V.13)$$

$$M^* = \left[M_o + \frac{P_o}{2}(H_1 - h) \right] - C_3 M_o \qquad \ldots(V.14)$$

where $C_1 = \frac{1}{(1/\eta)+1}$, $C_2 = \frac{6/\eta}{[(1/\eta)+1]^3}$ and $C_3 = \frac{1}{[(1/\eta)+1]^3}$.

in Equation ...(4.10).

Appendix VI Plots of Stress Intensity Factors Against Crack Length for Specimens with Subinterfacial Cracks

These are the plots of stress intensity factors against the crack length for different modulus ratios. Steady state can be observed at crack lengths with crack-tip far away from the load point. K_I is marked with solid line and K_{II} with dotted lines. The corresponding modulus ratio is labeled on the left and right side of the line for K_I and K_{II} respectively. Compare between Figure (a) and (d) for each set. The steady state region diminishes as the beam thickness increases.

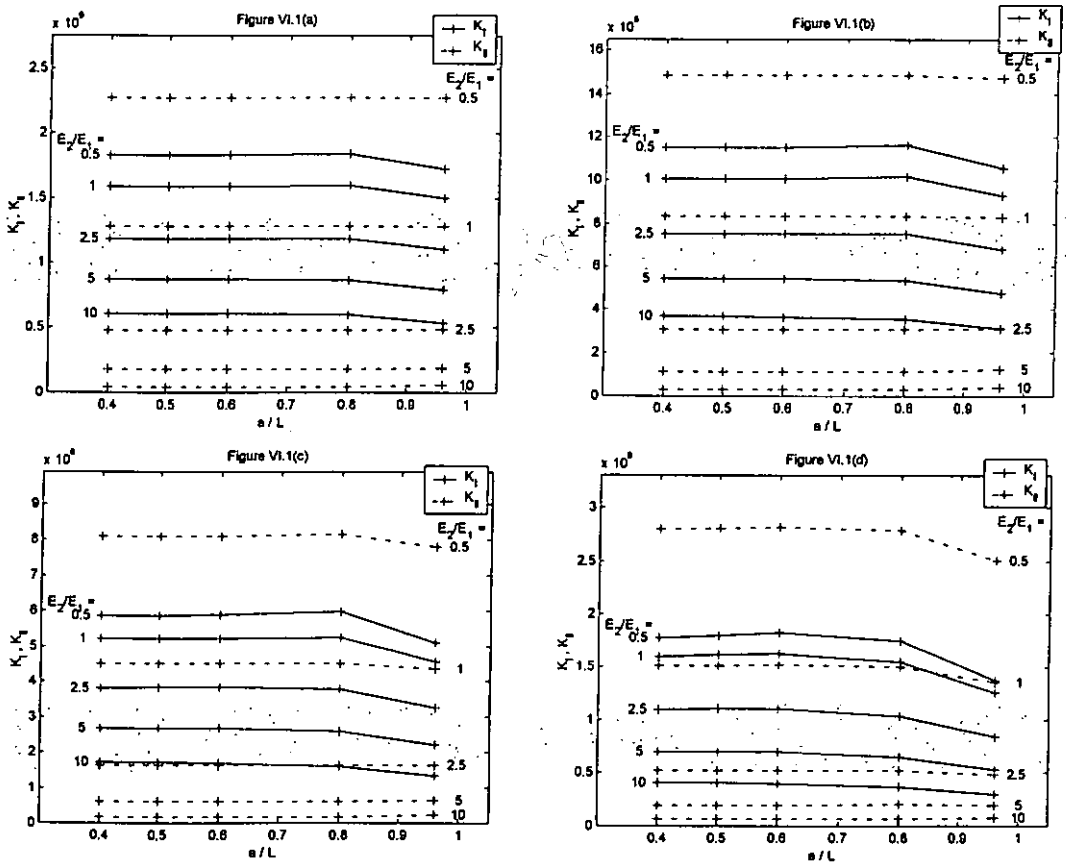

Figure VI.1 K-values against crack length (a/L) for $h/H_1 = 1/1000$:
(a) $H_1/H_2 = 2$, (b) $H_1/H_2 = 1.5$, (c) $H_1/H_2 = 1$, (d) $H_1/H_2 = 0.5$

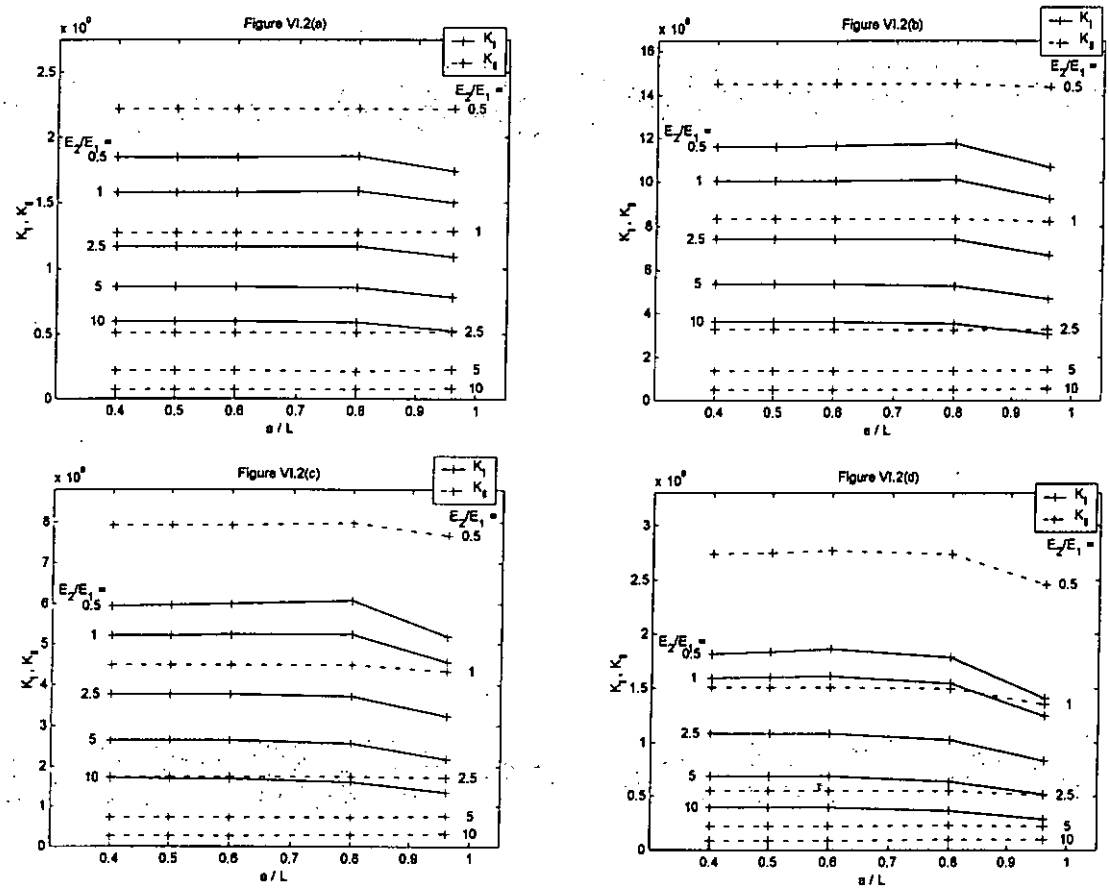

Figure VI.2 K-values against crack length (a/L) for $h/H_1 = 2/1000$:
(a) $H_1/H_2 = 2$, (b) $H_1/H_2 = 1.5$, (c) $H_1/H_2 = 1$, (d) $H_1/H_2 = 0.5$

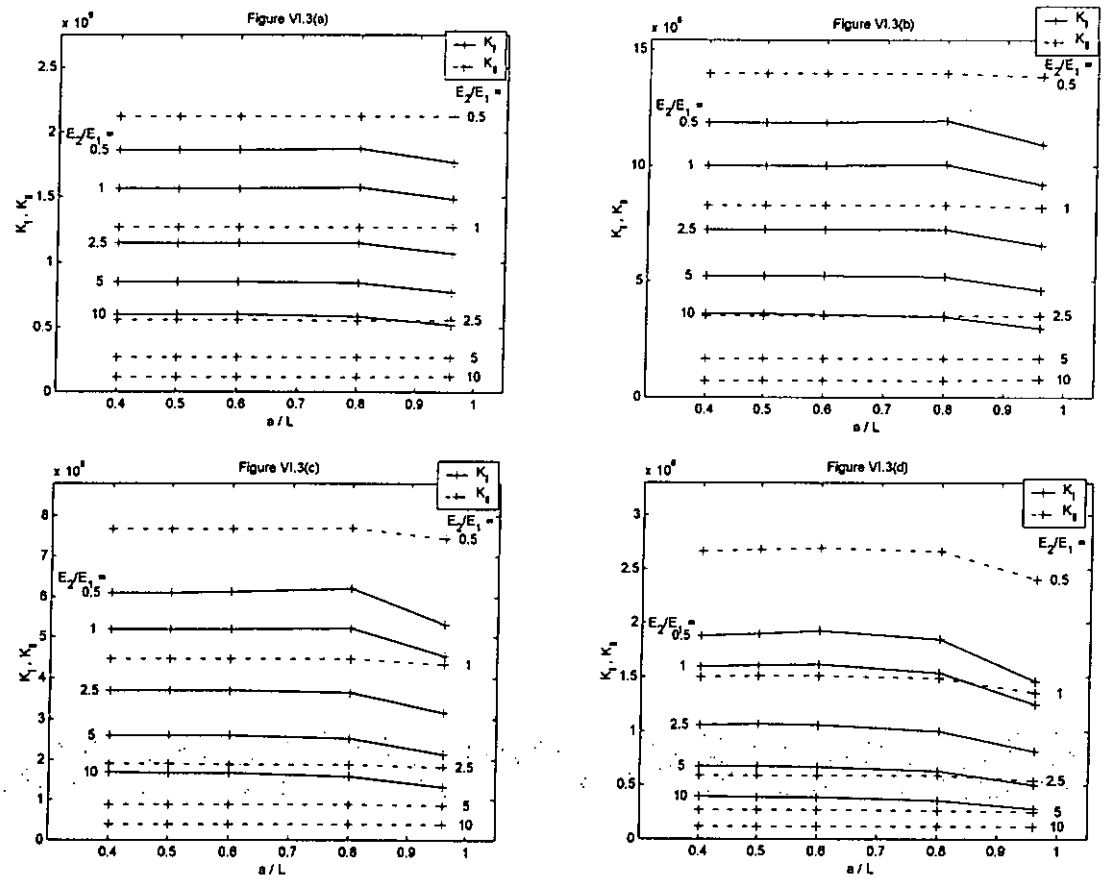

Figure VI.3 K-values against crack length (a/L) for $h/H_1 = 5/1000$:
(a) $H_1/H_2 = 2$, (b) $H_1/H_2 = 1.5$, (c) $H_1/H_2 = 1$, (d) $H_1/H_2 = 0.5$

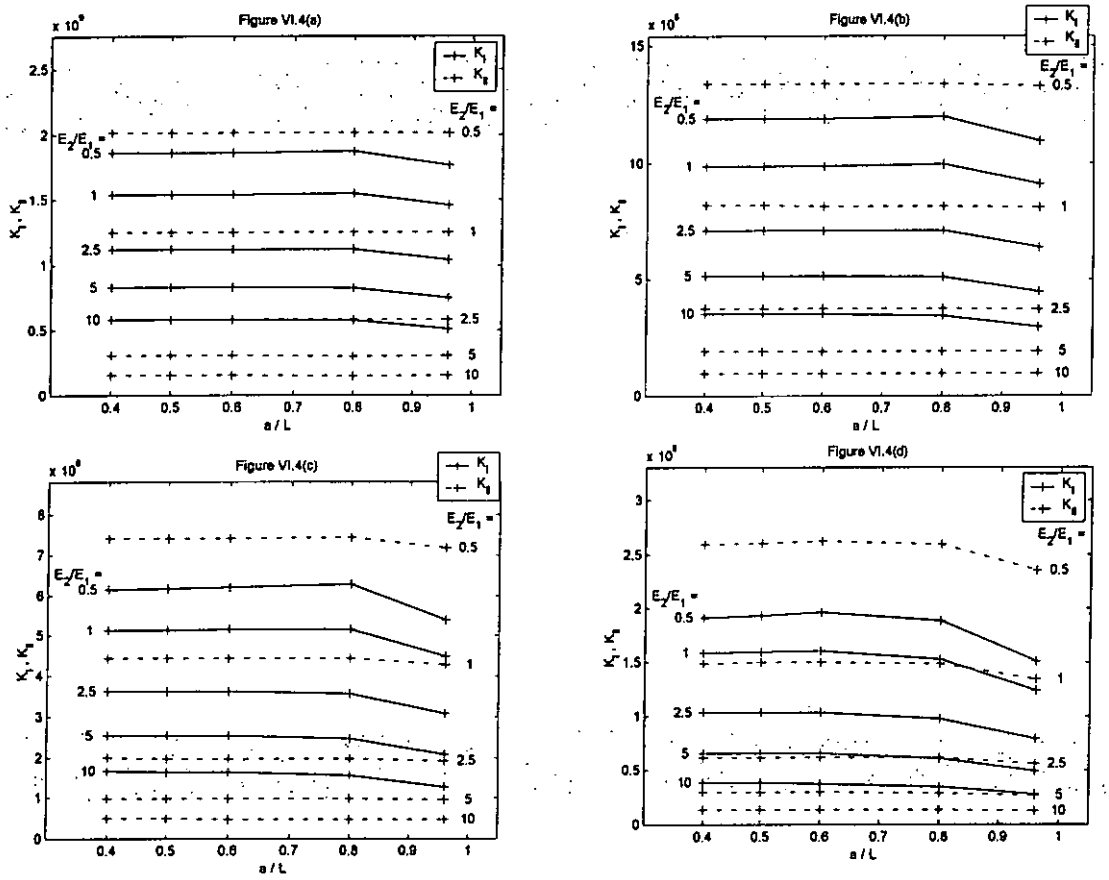

Figure VI.4 K-values against crack length (a/L) for $h/H_1 = 1/100$:
(a) $H_1/H_2 = 2$, (b) $H_1/H_2 = 1.5$, (c) $H_1/H_2 = 1$, (d) $H_1/H_2 = 0.5$

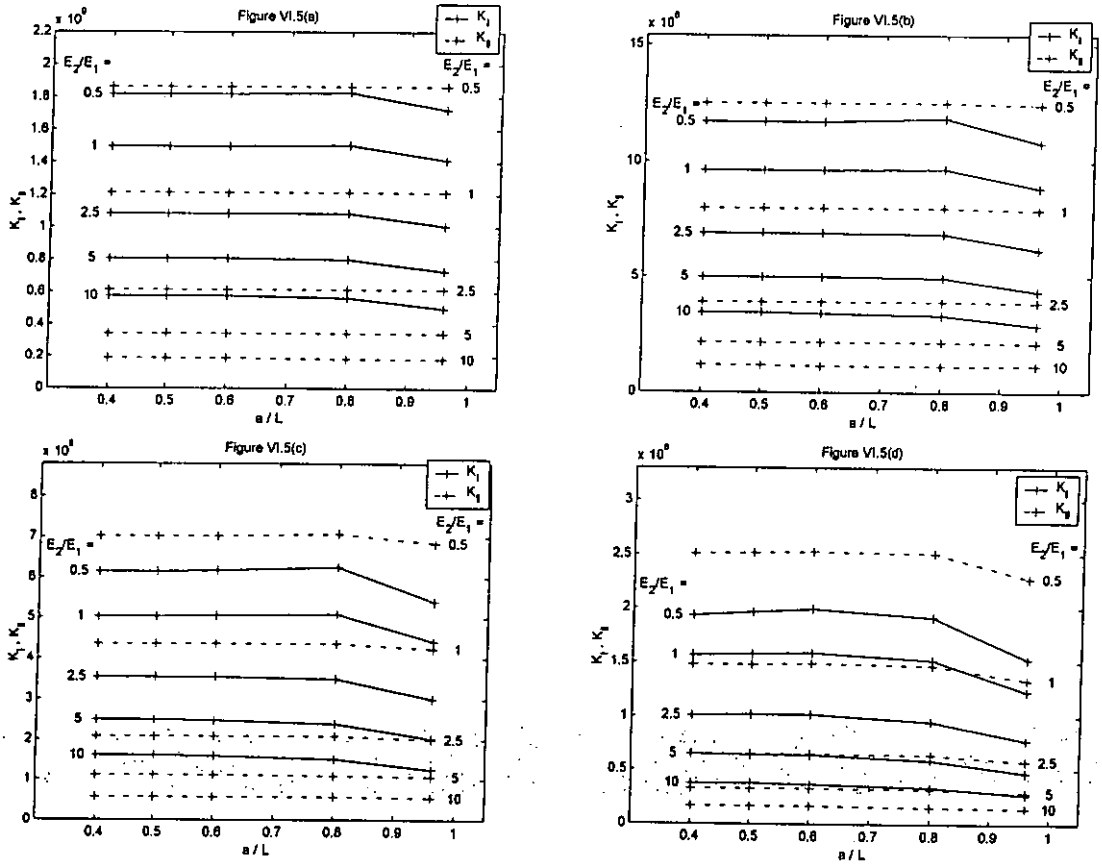

Figure VI.5 K-values against crack length (a/L) for $h/H_1 = 2/100$:
(a) $H_1/H_2 = 2$, (b) $H_1/H_2 = 1.5$, (c) $H_1/H_2 = 1$, (d) $H_1/H_2 = 0.5$

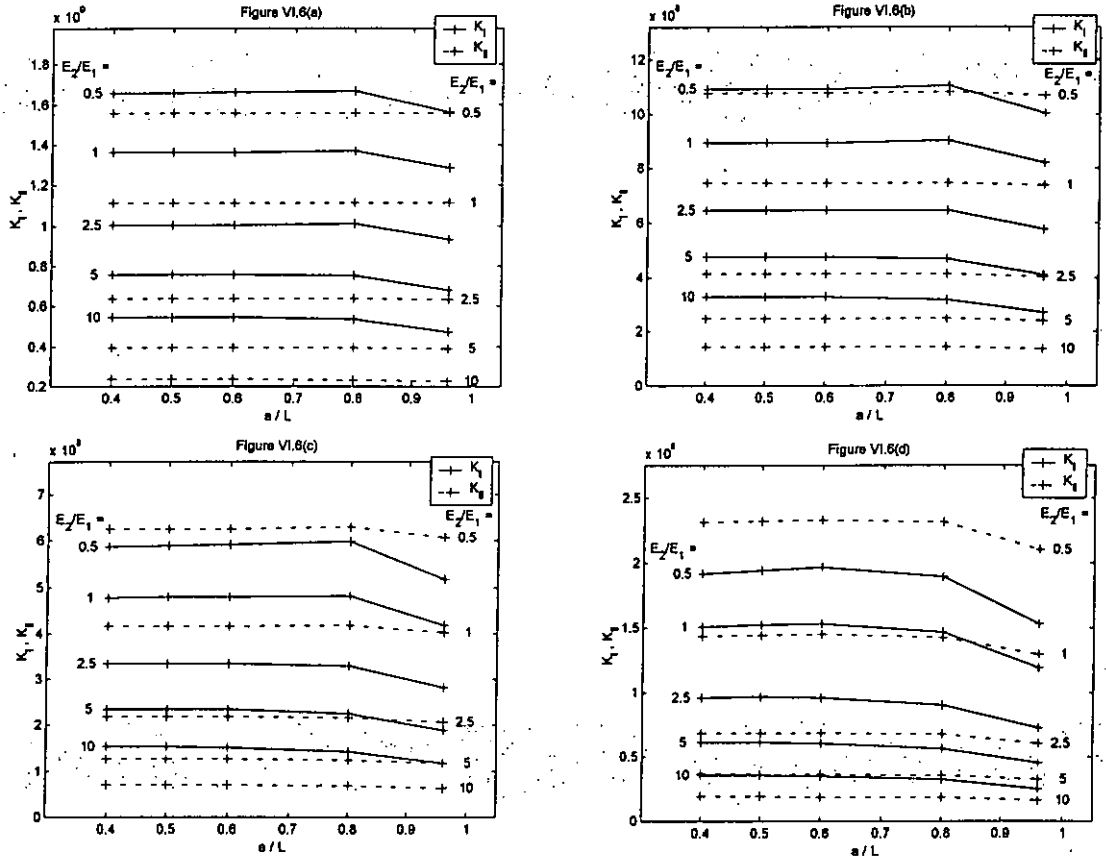

Figure VI.6 *K*-values against crack length (a/L) for $h/H_1 = 5/100$:
(a) $H_1/H_2 = 2$, (b) $H_1/H_2 = 1.5$, (c) $H_1/H_2 = 1$, (d) $H_1/H_2 = 0.5$

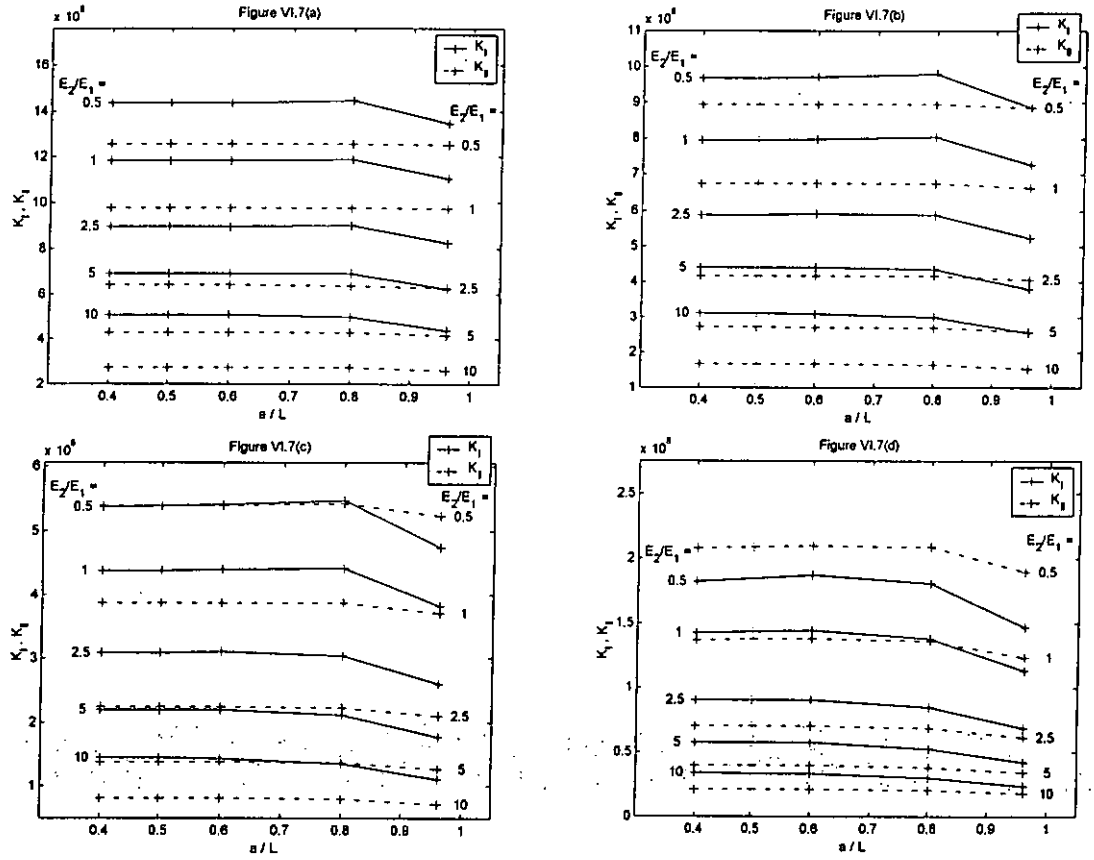

Figure VI.7 K-values against crack length (a/L) for $h/H_1 = 1/10$:
(a) $H_1/H_2 = 2$, (b) $H_1/H_2 = 1.5$, (c) $H_1/H_2 = 1$, (d) $H_1/H_2 = 0.5$

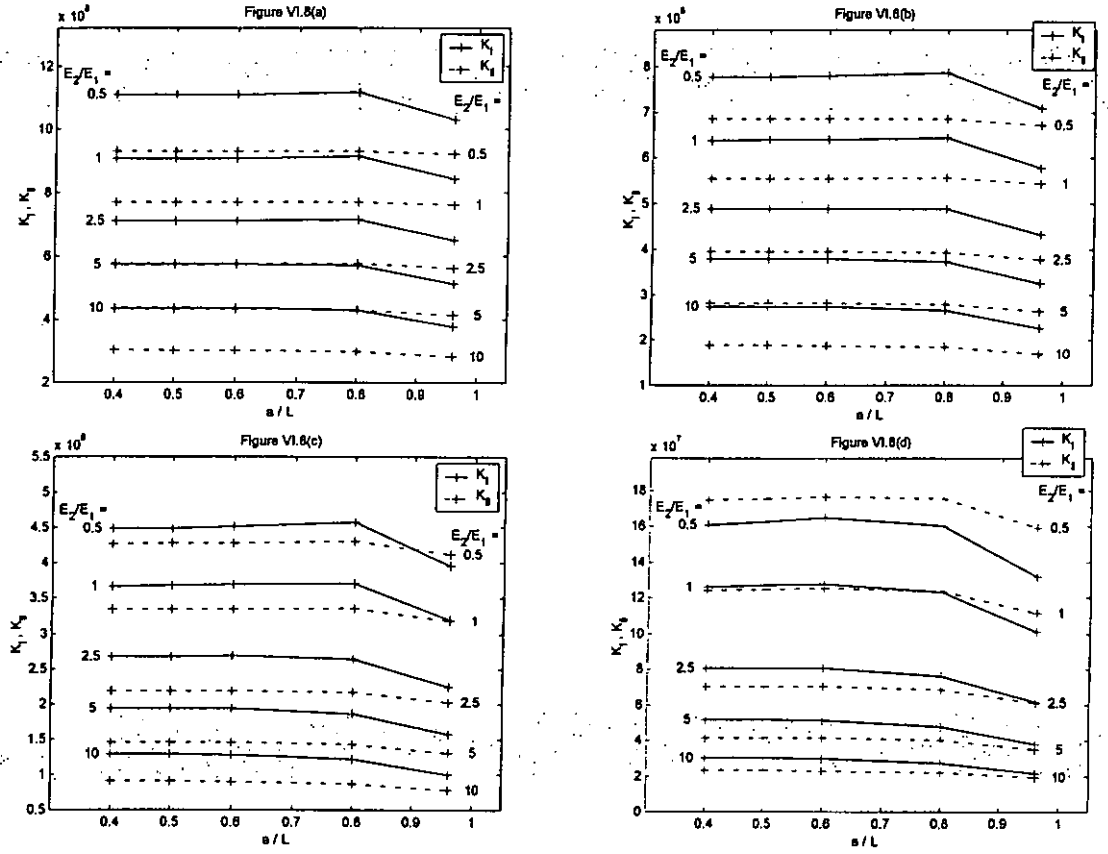

Figure VI.8 *K*-values against crack length (a/L) for $h/H_1 = 2/10$:
(a) $H_1/H_2 = 2$, (b) $H_1/H_2 = 1.5$, (c) $H_1/H_2 = 1$, (d) $H_1/H_2 = 0.5$

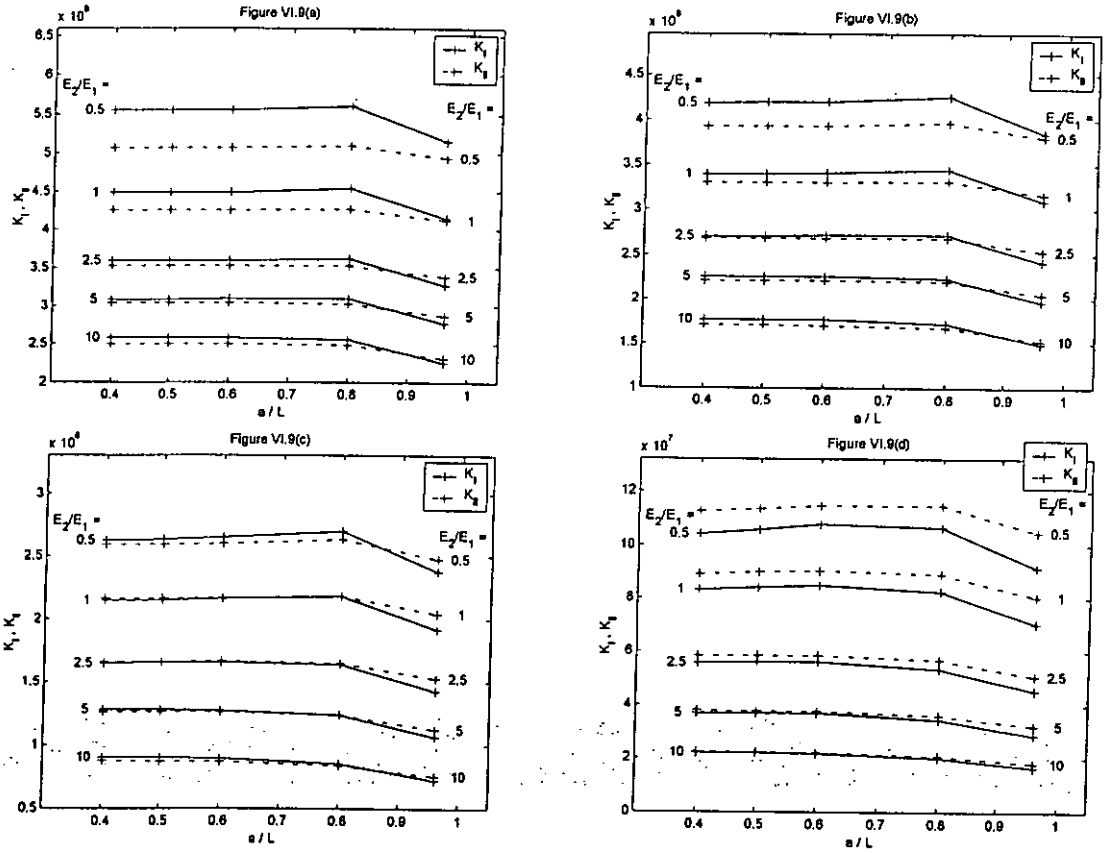

Figure VI.9 K-values against crack length (a/L) for $h/H_1 = 5/10$:
(a) $H_1/H_2 = 2$, (b) $H_1/H_2 = 1.5$, (c) $H_1/H_2 = 1$, (d) $H_1/H_2 = 0.5$

Appendix VII Steady State Regions of Extreme Cases

It can be seen that the steady state region is longer for thinner beams i.e. $H_1/H_2 = 2$ and thus $H_3 = 15$, and shorter for thicker beams i.e. $H_1/H_2 = 0.5$ and thus $H_3 = 30$.

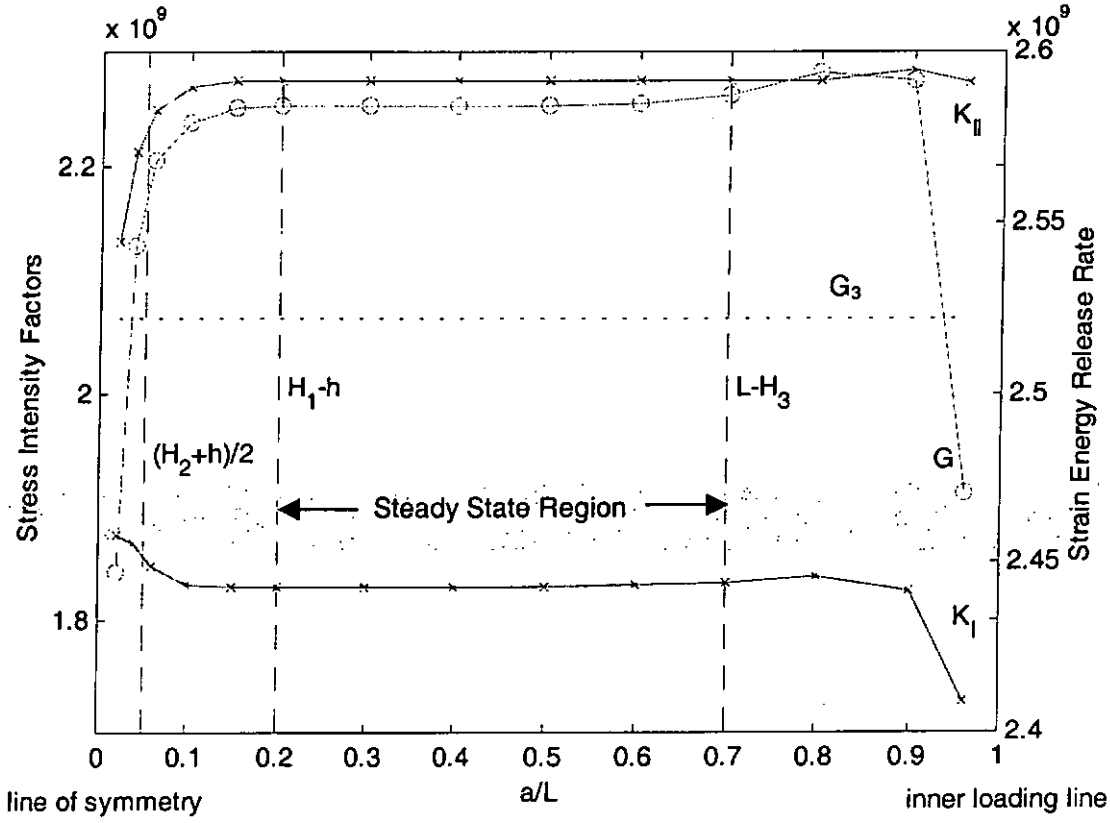

Figure VII.1a Steady State Region (Long) for $E_2/E_1 = 0.5$, $H_1/H_2 = 2$, $h/H_1 = 1/100$

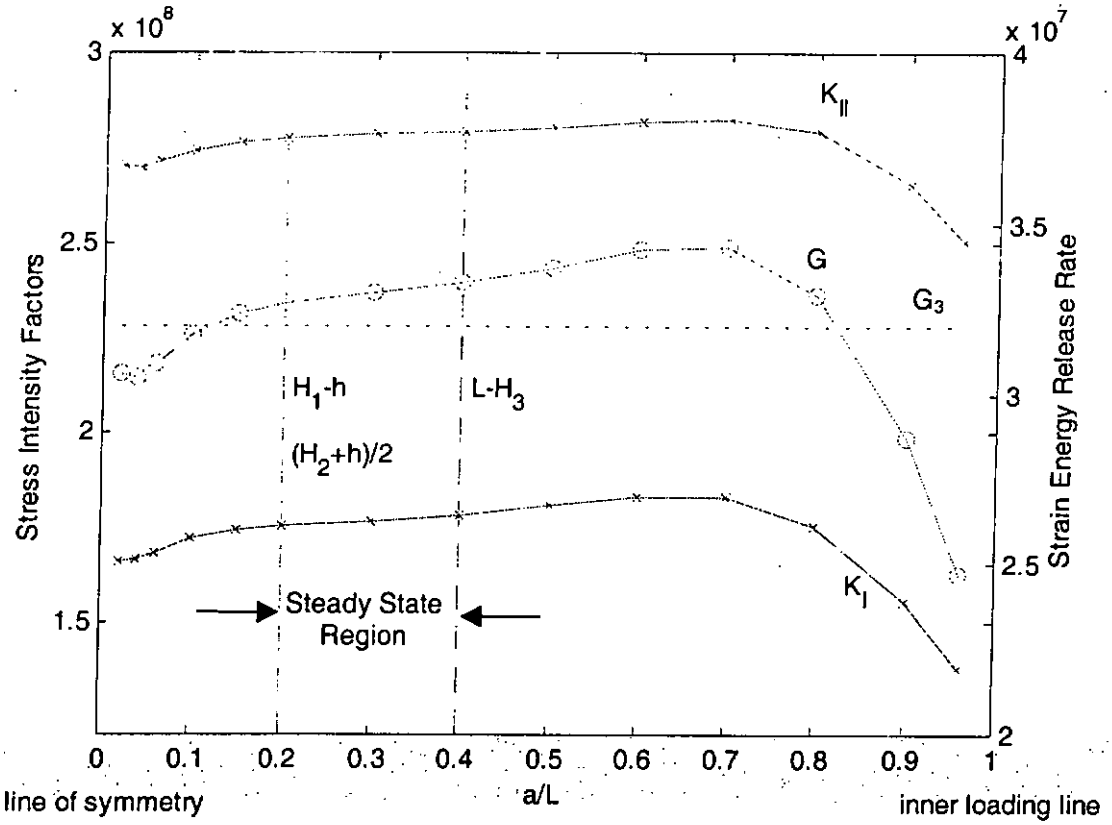

Figure VII.1b Steady State Region (Short) for $E_2/E_1 = 0.5$, $H_1/H_2 = 0.5$, $h/H_1 = 1/1000$

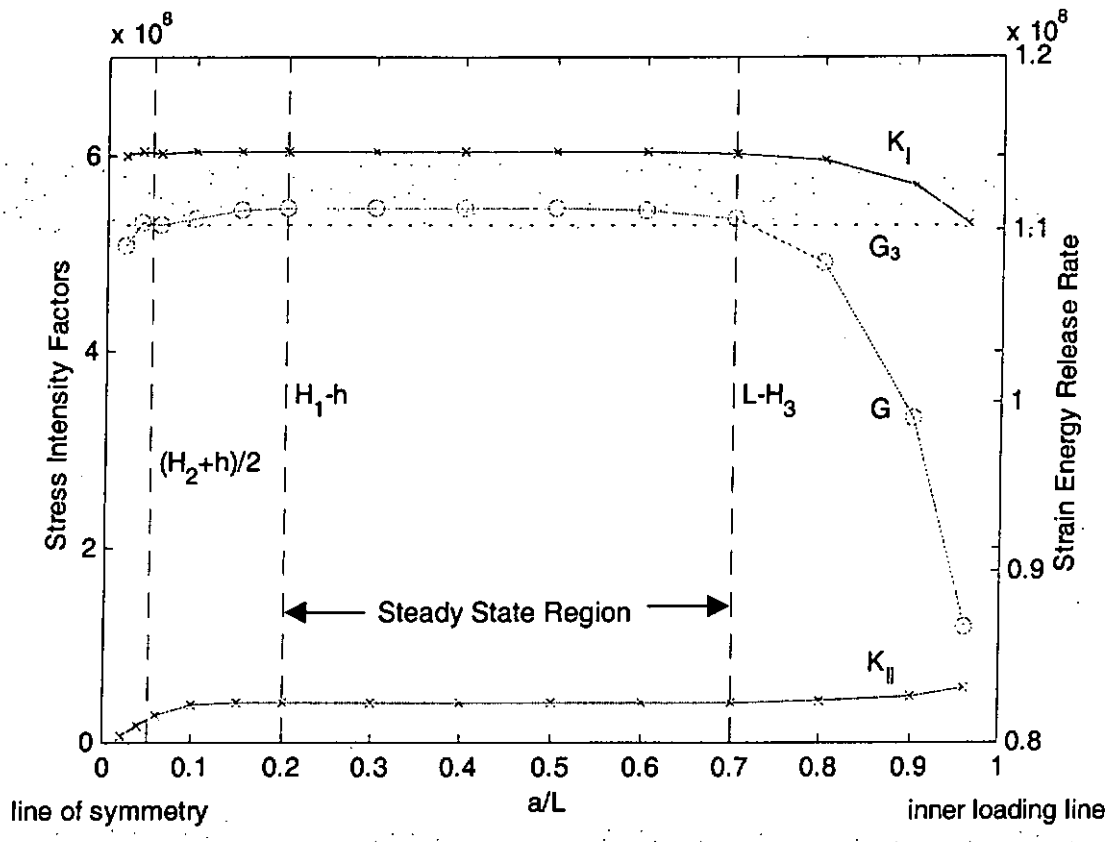

Figure VII.2a Steady State Region (Long) for $E_2/E_1 = 10$, $H_1/H_2 = 2$, $h/H_1 = 1/1000$

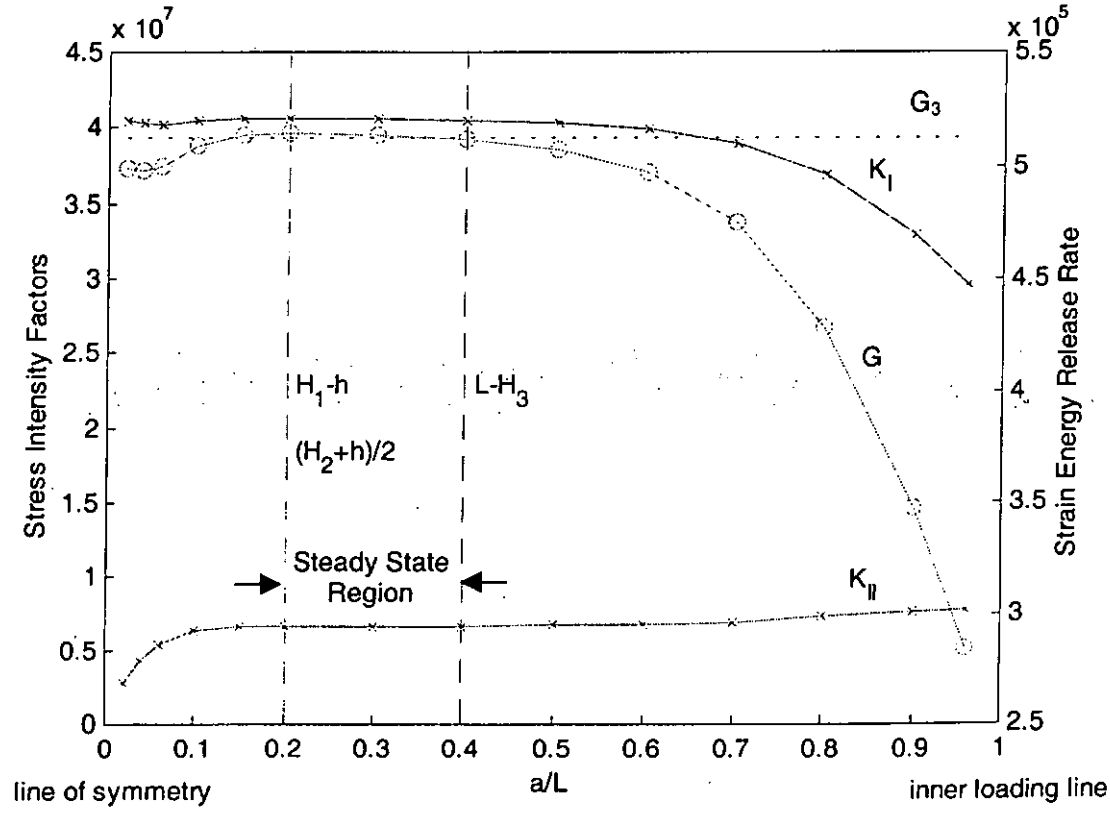

Figure VII.2b Steady State Region (Short) for $E_2/E_1 = 10$, $H_1/H_2 = 0.5$, $h/H_1 = 1/1000$

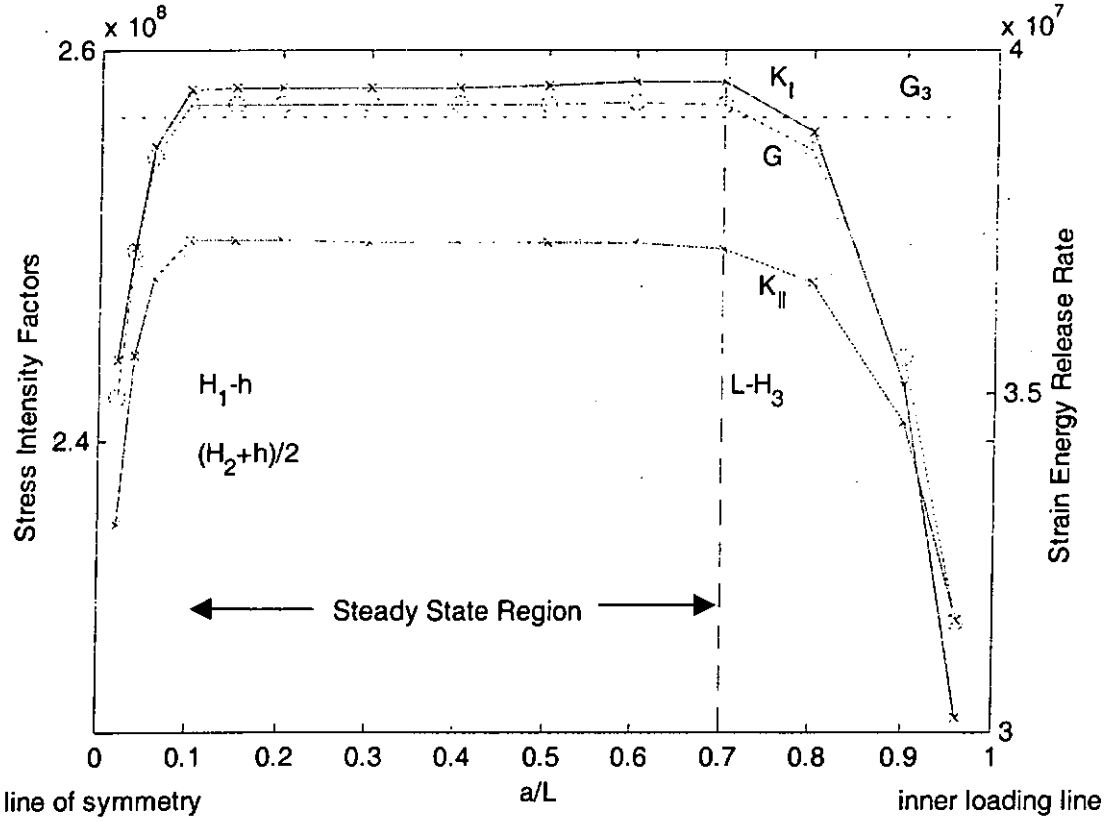

Figure VII.3a Steady State Region (Long) for $E_2/E_1 = 10$, $H_1/H_2 = 2$, $h/H_1 = 5/10$

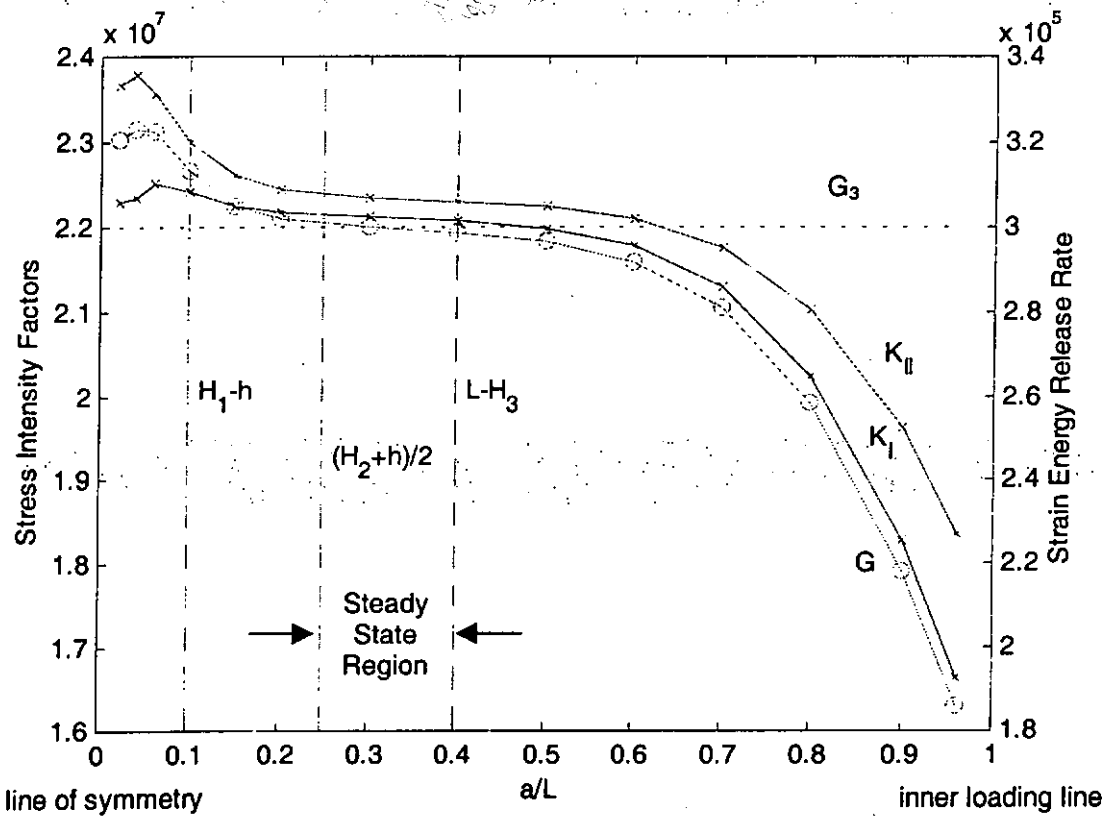

Figure VII.3b Steady State Region (Short) for $E_2/E_1 = 10$, $H_1/H_2 = 0.5$, $h/H_1 = 5/10$

Appendix VIII Tables of Stress Intensity Factors for Subinterface Crack Specimen

The stress intensity factors of the specimen for subinterfacial cracks under steady state cracking, obtained in Section 4.3.4 are kept here.

K_I (×10^6)	h/H_1 =								
H_1/H_2 = 2.0	1/1000	2/1000	5/1000	1/100	2/100	5/100	1/10	2/10	5/10
n = 0.5	914.480	922.563	933.017	931.051	908.893	829.375	717.048	554.404	277.413
n = 1	793.068	790.546	783.050	770.795	747.138	682.341	591.374	454.586	224.125
n = 1.75	674.667	666.850	653.937	640.254	619.677	570.579	502.018	392.116	194.304
n = 2.5	591.534	583.836	571.415	558.996	541.479	501.969	447.190	355.702	179.306
n = 3.4375	517.317	510.856	500.196	489.611	475.042	443.212	399.399	323.872	167.412
n = 5	434.292	429.734	421.692	413.493	402.236	378.092	345.111	286.607	154.185
n = 7	366.208	363.261	357.468	351.258	342.594	324.053	298.849	253.360	142.263
n = 8.5	330.204	328.046	323.387	318.184	310.811	294.975	273.482	234.430	135.162
n = 10	301.988	300.399	296.575	292.124	285.713	271.866	253.086	218.828	129.042
n = 0.5714	10256.9	10033.6	9769.68	9490.71	9046.07	8050.88	6874.73	5281.89	2646.70
n = 0.9143	8960.63	8810.39	8559.93	8296.09	7912.22	7075.17	6053.94	4627.07	2291.58
n = 1.1791	8434.71	8267.49	7996.96	7727.52	7356.75	6583.39	5647.62	4322.16	2135.29
n = 1.4359	6886.05	6864.90	6809.24	6721.34	6550.25	6061.12	5326.01	4138.94	2039.30
n = 2.188	6506.99	6403.18	6230.82	6059.35	5825.40	5330.34	4689.91	3683.18	1842.52
n = 2.5846	5516.94	5480.22	5416.11	5342.24	5220.99	4900.68	4406.85	3531.76	1783.77
n = 2.625	5382.84	5361.24	5317.88	5260.23	5155.80	4858.40	4381.57	3520.15	1779.54
n = 3.2768	5408.98	5339.17	5216.38	5091.26	4920.08	4557.96	4079.74	3284.67	1689.21
n = 3.8571	4814.94	4761.68	4675.44	4589.81	4470.09	4199.94	3814.34	3125.29	1634.70
n = 5.6875	4058.64	4018.70	3947.79	3875.35	3775.76	3561.74	3267.67	2738.30	1497.16
n = 6.4615	3681.67	3649.91	3598.53	3547.59	3476.04	3312.31	3070.85	2609.41	1454.14
n = 7.875	3319.10	3292.33	3248.86	3205.81	3145.58	3008.37	2805.92	2413.74	1382.65

Table VIII.1a K_I values for $H_1/H_2 = 2$

K_I ($\times 10^6$)	h/H_1 =								
H_1/H_2 = 1.5	1/1000	2/1000	5/1000	1/100	2/100	5/100	1/10	2/10	5/10
n = 0.5	638.757	645.930	656.574	659.331	650.133	606.449	537.934	431.526	232.740
n = 1	559.631	558.238	554.091	547.276	533.998	496.778	442.268	354.725	188.848
n = 1.75	476.033	470.634	461.999	453.238	440.585	411.414	370.806	302.843	163.759
n = 2.5	415.849	410.485	402.019	393.836	382.731	358.808	326.434	271.091	150.172
n = 3.4375	361.664	357.155	349.843	342.778	333.382	313.826	287.891	242.959	138.610
n = 5	300.793	297.604	292.066	286.548	279.192	264.145	244.519	210.204	124.953
n = 7	250.795	248.712	244.704	240.502	234.797	223.123	208.027	181.542	112.265
n = 8.5	224.364	222.818	219.578	216.047	211.175	201.156	188.232	165.547	104.724
n = 10	203.676	202.513	199.837	196.807	192.560	183.770	172.443	152.564	98.311
n = 0.5714	6547.00	6411.76	6264.34	6115.34	5878.21	5334.64	4664.36	3711.12	1998.34
n = 0.9143	5731.45	5639.11	5490.59	5340.23	5127.76	4669.59	4098.56	3258.43	1736.42
n = 1.1791	5398.07	5294.37	5130.68	4972.85	4762.37	4333.98	3812.53	3040.01	1620.88
n = 1.4359	4362.60	4351.10	4321.98	4276.88	4189.70	3939.10	3552.21	2888.38	1548.36
n = 2.188	4134.19	4069.62	3964.20	3862.08	3727.18	3452.98	3105.79	2546.31	1393.54
n = 2.5846	3475.74	3452.98	3414.73	3372.69	3306.53	3138.22	2881.90	2413.06	1342.85
n = 2.625	3385.86	3372.78	3347.75	3315.99	3260.42	3106.45	2860.97	2401.81	1338.92
n = 3.2768	3411.04	3367.61	3292.27	3217.18	3117.40	2915.30	2657.70	2227.27	1261.83
n = 3.8571	3018.09	2984.51	2931.15	2879.74	2810.48	2662.00	2458.27	2093.67	1210.91
n = 5.6875	2519.19	2493.95	2449.89	2405.89	2347.16	2226.83	2069.30	1791.33	1081.67
n = 6.4615	2269.49	2249.37	2217.40	2186.54	2144.71	2053.87	1926.40	1687.86	1039.05
n = 7.875	2029.81	2012.84	1985.75	1959.60	1924.22	1847.67	1740.43	1538.49	970.357

Table VIII.1b K_I values for $H_1/H_2 = 1.5$

K_I ($\times 10^6$) $H_1/H_2 = 1.0$	h/H_1 = 1/1000	2/1000	5/1000	1/100	2/100	5/100	1/10	2/10	5/10
n = 0.5	390.424	396.111	405.211	409.955	408.936	391.231	357.419	298.747	175.015
n = 1	347.396	346.766	344.883	341.772	335.655	318.090	291.187	244.705	143.170
n = 1.75	294.160	290.823	285.667	280.694	273.877	258.993	238.751	203.938	122.616
n = 2.5	254.423	251.083	245.936	241.139	234.916	222.300	205.991	178.132	110.080
n = 3.4375	218.344	215.532	211.065	206.876	201.513	190.987	177.786	155.405	98.765
n = 5	177.820	175.818	172.424	169.135	164.892	156.668	146.569	129.596	85.205
n = 7	144.784	143.448	140.975	138.464	135.161	128.735	120.914	107.856	72.985
n = 8.5	127.507	126.489	124.475	122.361	119.538	114.014	107.304	96.136	66.054
n = 10	114.120	113.326	111.647	109.829	107.369	102.523	96.637	86.864	60.393
n = 0.5714	3413.59	3346.60	3280.73	3219.17	3122.62	2896.12	2601.09	2151.74	1255.62
n = 0.9143	2996.34	2949.22	2876.61	2807.00	2713.11	2516.75	2269.23	1884.76	1097.59
n = 1.1791	2821.16	2767.61	2685.51	2609.60	2512.71	2324.04	2097.06	1747.95	1023.61
n = 1.4359	2243.83	2238.77	2226.63	2208.41	2173.78	2074.60	1918.48	1635.23	972.677
n = 2.188	2125.20	2091.76	2038.31	1988.14	1924.40	1801.76	1652.96	1412.73	859.879
n = 2.5846	1760.45	1748.82	1730.00	1710.36	1681.03	1610.38	1506.17	1313.65	817.448
n = 2.625	1710.77	1704.23	1692.32	1678.03	1654.13	1590.75	1492.05	1304.75	813.862
n = 3.2768	1723.91	1701.35	1663.03	1625.87	1578.14	1486.54	1375.90	1194.96	753.425
n = 3.8571	1506.46	1489.05	1461.94	1436.61	1403.82	1337.66	1251.95	1102.33	709.801
n = 5.6875	1229.81	1216.58	1194.07	1172.21	1143.96	1089.08	1021.50	907.347	603.899
n = 6.4615	1093.00	1082.66	1066.52	1051.35	1031.50	990.764	937.002	840.674	568.902
n = 7.875	961.850	953.165	939.550	926.730	909.942	875.537	830.198	748.842	515.440

Table VIII.1c K_I values for $H_1/H_2 = 1.0$

K_I ($\times 10^6$)	h/H_1 =								
$H_1/H_2 = 0.5$	1/1000	2/1000	5/1000	1/100	2/100	5/100	1/10	2/10	5/10
n = 0.5	174.808	178.393	184.294	188.396	190.799	188.594	179.101	157.984	102.517
n = 1	158.427	158.242	157.686	156.763	154.931	149.539	140.876	124.637	82.260
n = 1.75	130.533	128.959	126.617	124.483	121.749	116.260	109.226	97.209	65.919
n = 2.5	109.322	107.750	105.393	103.283	100.683	95.807	89.964	80.378	55.523
n = 3.4375	90.464	89.145	87.108	85.263	83.002	78.860	74.057	66.375	46.564
n = 5	70.102	69.153	67.610	66.171	64.388	61.141	57.447	51.654	36.814
n = 7	54.384	53.728	52.597	51.505	50.129	47.609	44.761	40.342	29.090
n = 8.5	46.552	46.034	45.104	44.187	43.017	40.865	38.435	34.681	25.150
n = 10	40.693	40.270	39.486	38.698	37.684	35.807	33.688	30.424	22.155
n = 0.5714	1059.52	1039.48	1022.31	1008.62	988.417	940.858	874.157	760.431	491.115
n = 0.9143	927.965	912.930	890.972	871.499	847.264	800.357	742.513	648.292	423.393
n = 1.1791	867.620	850.280	824.665	802.257	775.461	727.401	672.582	587.387	386.794
n = 1.4359	667.322	665.996	663.055	658.878	651.203	629.718	595.842	531.845	358.179
n = 2.188	621.208	610.474	593.846	578.857	560.724	528.359	491.958	435.468	296.854
n = 2.5846	497.412	493.874	488.355	482.897	475.218	458.062	434.241	391.333	272.515
n = 2.625	481.049	479.103	475.730	471.915	465.885	450.891	428.667	387.288	270.360
n = 3.2768	481.333	474.063	462.195	451.136	437.534	413.134	385.868	343.852	239.513
n = 3.8571	408.181	402.839	394.726	387.394	378.296	361.161	340.614	306.808	217.118
n = 5.6875	317.002	312.841	306.066	299.735	291.871	277.496	261.078	235.241	168.647
n = 6.4615	273.796	270.755	266.119	261.879	256.521	246.156	233.426	212.099	153.825
n = 7.875	233.623	231.107	227.254	223.720	219.241	210.559	199.886	182.001	132.941

Table VIII.1d K_I values for $H_1/H_2 = 0.5$

K_{II} ($\times 10^6$)	h/H_1 =								
H_1/H_2 = 2.0	1/1000	2/1000	5/1000	1/100	2/100	5/100	1/10	2/10	5/10
n = 0.5	1137.35	1107.71	1059.60	1007.62	931.433	779.008	628.139	465.665	253.265
n = 1	640.634	638.723	633.045	623.763	605.857	556.891	488.357	385.781	212.650
n = 1.75	363.975	375.307	389.519	398.645	404.916	402.701	381.685	326.204	188.853
n = 2.5	239.302	255.503	276.451	291.845	306.193	320.294	318.834	288.393	175.890
n = 3.4375	156.864	175.252	199.284	217.543	235.666	257.903	267.646	254.814	164.826
n = 5	88.702	107.453	132.356	151.543	171.173	197.513	214.494	216.315	151.648
n = 7	48.237	65.843	89.734	108.242	127.431	154.134	173.686	183.602	139.185
n = 8.5	31.658	48.308	71.073	88.774	107.215	133.207	153.076	165.855	131.627
n = 10	20.808	36.560	58.183	75.056	92.687	117.735	137.401	151.746	125.092
n = 0.5714	9028.94	9025.42	8945.75	8755.03	8348.35	7290.22	6044.91	4541.90	2451.94
n = 0.9143	5806.97	5966.84	6136.10	6199.71	6151.49	5761.99	5074.90	3992.33	2179.37
n = 1.1791	4122.76	4392.92	4722.38	4926.17	5051.81	4971.16	4562.73	3717.83	2059.76
n = 1.4359	4931.48	4933.83	4919.54	4884.97	4809.82	4575.50	4181.96	3456.68	1962.20
n = 2.188	2115.57	2382.85	2724.92	2973.00	3199.04	3412.64	3400.49	3037.60	1811.10
n = 2.5846	2963.70	3015.60	3083.80	3133.43	3178.63	3210.45	3145.19	2833.19	1741.20
n = 2.625	3099.06	3122.43	3153.37	3175.47	3194.79	3198.55	3121.95	2811.87	1734.00
n = 3.2768	1229.44	1485.26	1818.30	2067.43	2311.59	2603.20	2731.49	2602.59	1667.88
n = 3.8571	1635.14	1772.29	1953.18	2093.16	2236.10	2422.52	2517.40	2424.81	1605.80
n = 5.6875	793.88	965.71	1195.55	1373.69	1557.90	1811.33	1986.05	2035.36	1469.06
n = 6.4615	1137.90	1229.85	1353.64	1453.98	1563.94	1731.74	1863.61	1911.34	1417.45
n = 7.875	963.95	1046.85	1159.28	1251.30	1353.62	1514.52	1650.57	1729.66	1341.61

Table VIII.2a K_{II} values for $H_1/H_2 = 2$

K_{II} ($\times 10^6$)	h/H_1 =								
H_1/H_2 = 1.5	1/1000	2/1000	5/1000	1/100	2/100	5/100	1/10	2/10	5/10
n = 0.5	825.245	805.359	774.362	742.038	695.141	598.628	496.950	380.254	218.347
n = 1	462.237	461.190	458.072	452.950	442.974	415.042	374.215	308.779	183.336
n = 1.75	260.747	268.845	279.153	286.062	291.430	292.923	283.553	253.508	161.498
n = 2.5	170.590	182.021	196.851	207.850	218.306	229.713	232.284	219.032	148.580
n = 3.4375	111.463	124.331	141.152	153.952	166.705	182.842	191.811	189.342	136.959
n = 5	63.088	76.088	93.310	106.548	120.058	138.287	150.973	156.580	122.736
n = 7	34.782	46.848	63.164	75.760	88.754	106.765	120.389	129.832	109.351
n = 8.5	23.334	34.646	50.074	62.017	74.387	91.699	105.179	115.725	101.418
n = 10	15.915	26.538	41.081	52.375	64.103	80.617	93.712	104.703	94.715
n = 0.5714	5862.48	5866.41	5835.66	5746.57	5543.61	4977.58	4257.26	3320.52	1903.10
n = 0.9143	3745.92	3850.82	3967.90	4023.79	4022.63	3848.98	3494.06	2876.91	1691.54
n = 1.1791	2637.14	2811.40	3027.44	3167.29	3267.44	3273.61	3092.20	2645.88	1595.91
n = 1.4359	3197.87	3201.05	3196.39	3181.15	3145.99	3032.70	2836.29	2450.00	1516.77
n = 2.188	1343.42	1513.56	1732.04	1891.73	2040.40	2196.24	2231.93	2087.69	1383.77
n = 2.5846	1913.88	1947.17	1991.44	2024.49	2056.03	2086.82	2072.14	1939.40	1322.35
n = 2.625	2003.39	2018.75	2039.59	2055.32	2070.41	2082.63	2058.98	1924.83	1316.11
n = 3.2768	778.196	939.548	1149.69	1307.05	1462.06	1653.09	1757.40	1741.47	1250.37
n = 3.8571	1049.66	1135.77	1249.32	1337.23	1427.05	1546.74	1620.36	1611.99	1192.49
n = 5.6875	509.867	616.657	759.036	869.047	982.362	1138.36	1252.12	1315.03	1058.78
n = 6.4615	731.229	787.963	864.151	925.666	992.466	1093.61	1176.72	1229.53	1010.76
n = 7.875	618.947	669.814	738.405	794.276	855.734	951.143	1033.795	1098.266	938.668

Table VIII.2b K_{II} values for $H_1/H_2 = 1.5$

K_{II} (×10^6)	h/H$_1$ =								
H$_1$/H$_2$ = 1.0	1/1000	2/1000	5/1000	1/100	2/100	5/100	1/10	2/10	5/10
n = 0.5	539.572	527.812	510.330	492.956	468.353	416.773	358.439	285.009	172.601
n = 1	299.486	299.015	297.608	295.284	290.713	277.589	257.472	222.593	144.208
n = 1.75	167.112	172.181	178.723	183.273	187.137	189.770	187.073	174.386	123.793
n = 2.5	108.620	115.643	124.780	131.613	138.210	145.924	149.256	145.682	110.662
n = 3.4375	70.787	78.566	88.731	96.476	104.205	114.154	120.435	122.073	98.632
n = 5	40.344	48.058	58.221	66.009	73.925	84.576	92.266	97.263	84.243
n = 7	22.924	29.916	39.302	46.517	53.912	64.054	71.777	77.969	71.447
n = 8.5	16.001	22.449	31.187	37.913	44.829	54.380	61.792	68.142	64.288
n = 10	11.565	17.528	25.653	31.919	38.375	47.331	54.365	60.637	58.499
n = 0.5714	3182.35	3186.99	3180.29	3149.90	3073.64	2842.50	2518.96	2052.44	1253.84
n = 0.9143	2016.57	2072.61	2137.88	2174.33	2188.30	2136.97	2000.44	1730.18	1110.21
n = 1.1791	1408.41	1500.06	1615.26	1692.64	1754.19	1785.57	1732.97	1558.57	1039.42
n = 1.4359	1716.75	1719.33	1719.26	1714.85	1703.11	1662.52	1588.72	1433.09	980.768
n = 2.188	711.549	799.160	911.935	994.872	1073.38	1161.71	1198.48	1166.58	868.320
n = 2.5846	1015.15	1032.36	1055.53	1073.29	1090.88	1111.27	1114.71	1076.68	818.936
n = 2.625	1061.97	1070.11	1081.46	1090.47	1099.72	1110.40	1108.55	1068.45	814.073
n = 3.2768	412.832	494.392	600.585	680.108	758.650	857.243	917.977	936.781	753.961
n = 3.8571	553.743	596.824	653.607	697.596	742.490	802.855	843.877	858.426	706.202
n = 5.6875	272.082	324.448	393.790	447.174	501.862	576.625	632.398	672.509	594.737
n = 6.4615	380.825	408.191	444.840	474.332	506.025	553.246	592.446	623.687	557.824
n = 7.875	320.519	344.648	377.068	403.366	431.940	475.400	512.890	546.233	502.596

Table VIII.2c K_{II} values for $H_1/H_2 = 1.0$

K_{II} ($\times 10^6$)	h/H_1 =								
$H_1/H_2 = 0.5$	1/1000	2/1000	5/1000	1/100	2/100	5/100	1/10	2/10	5/10
n = 0.5	277.862	272.670	265.377	258.579	249.390	230.241	206.997	173.557	111.596
n = 1	150.252	150.109	149.683	148.974	147.565	143.406	136.684	123.902	88.692
n = 1.75	81.566	83.840	86.806	88.924	90.822	92.540	92.336	88.802	69.914
n = 2.5	52.241	55.268	59.207	62.163	65.030	68.463	70.242	69.855	58.194
n = 3.4375	33.881	37.105	41.304	44.496	47.659	51.692	54.287	55.434	48.302
n = 5	19.614	22.658	26.639	29.669	32.713	36.714	39.524	41.443	37.767
n = 7	11.686	14.343	17.840	20.503	23.195	26.780	29.391	31.426	29.588
n = 8.5	8.604	10.986	14.146	16.555	18.996	22.262	24.670	26.632	25.471
n = 10	6.636	8.787	11.657	13.846	16.067	19.047	21.264	23.117	22.366
n = 0.5714	1095.75	1097.59	1097.77	1092.64	1077.51	1026.89	947.603	815.381	536.629
n = 0.9143	682.522	700.133	721.292	734.365	742.465	737.579	710.564	646.183	458.678
n = 1.1791	473.476	501.766	537.637	562.329	583.323	599.801	594.824	559.323	415.991
n = 1.4359	561.141	562.165	562.799	562.415	560.593	553.044	538.040	503.748	382.317
n = 2.188	234.401	260.024	292.979	317.247	340.364	367.198	380.814	379.628	312.430
n = 2.5846	318.687	323.640	330.368	335.611	340.874	347.286	349.680	343.634	285.385
n = 2.625	331.561	333.949	337.340	340.125	343.037	346.673	347.445	340.512	282.851
n = 3.2768	136.773	159.527	189.052	211.065	232.705	259.722	276.803	285.049	248.567
n = 3.8571	172.718	184.406	199.755	211.613	223.588	239.387	250.074	255.276	224.578
n = 5.6875	87.653	101.198	118.950	132.508	146.220	164.453	177.562	187.076	172.448
n = 6.4615	113.321	120.177	129.291	136.574	144.239	155.186	163.749	170.319	157.104
n = 7.875	93.914	99.770	107.571	113.850	120.513	130.187	137.982	144.451	135.221

Table VIII.2d K_{II} values for $H_1/H_2 = 0.5$

Appendix IX The Stress Intensity Plots against the Penetration Ratio

The plots of stress intensity factors K_I and K_{II} , against the penetration ratio h/H_1 are kept here. Figure IX.1a-d shows the values in logscale, while Figure IX.2a-d shows the values in normal scale. For simplicity, only the K-values of modulus ratio 0.5, 1, 2.5, 5, 10 are shown here. Numerical values of the plots are in Appendix VIII. K_I is in solid line while K_{II} is in dashed line. Note that for homogeneous beams, i.e. $E_2/E_1 = 1$, the K-values are almost constant near the 'interface'. For $E_2/E_1 < 1$, K_{II} tends to increase and K_I tends to decrease as the crack in closer to the interface, i.e. smaller h/H_1. Conversely, for $E_2/E_1 > 1$, K_{II} tends to decrease and K_I tends to increase as the crack gets closer to the interface.

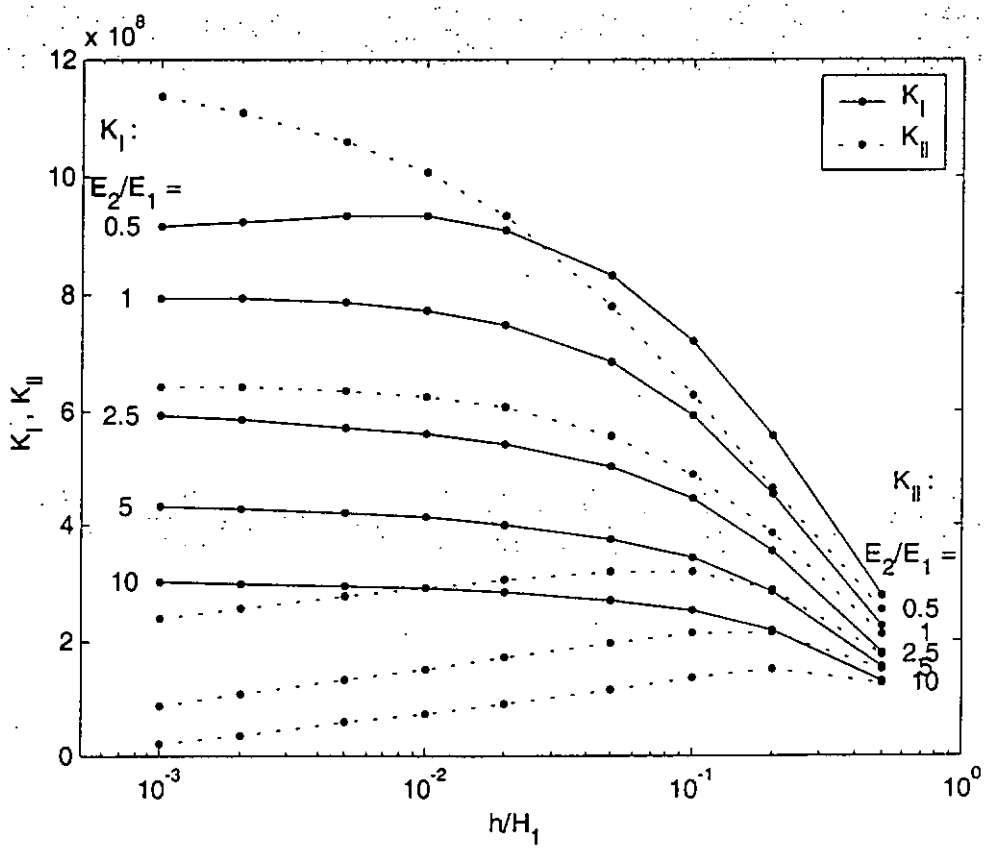

Figure IX.1a Stress Intensity Factors against the penetration ratio h/H_1 for $H_1/H_2 = 2$ (in logscale) .

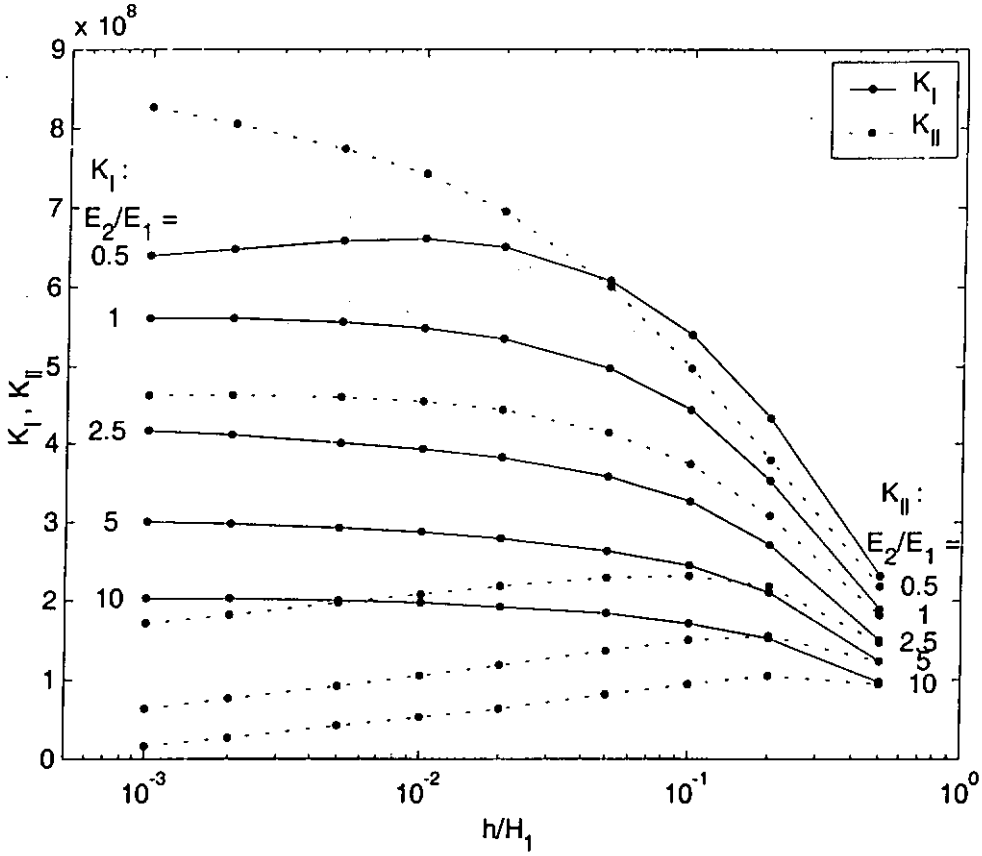

Figure IX.1b Stress Intensity Factors against the penetration ratio h/H_1 for $H_1/H_2 = 1.5$ (in logscale) .

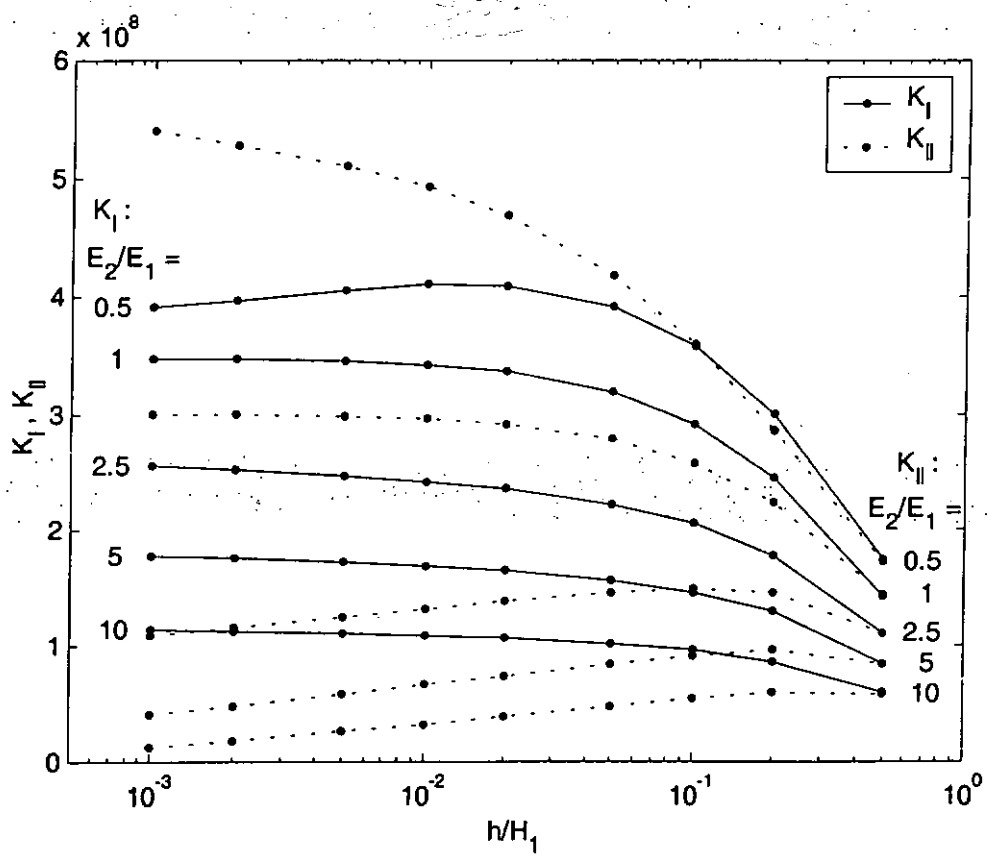

Figure IX.1c Stress Intensity Factors against the penetration ratio h/H_1 for $H_1/H_2 = 1.0$ (in logscale) .

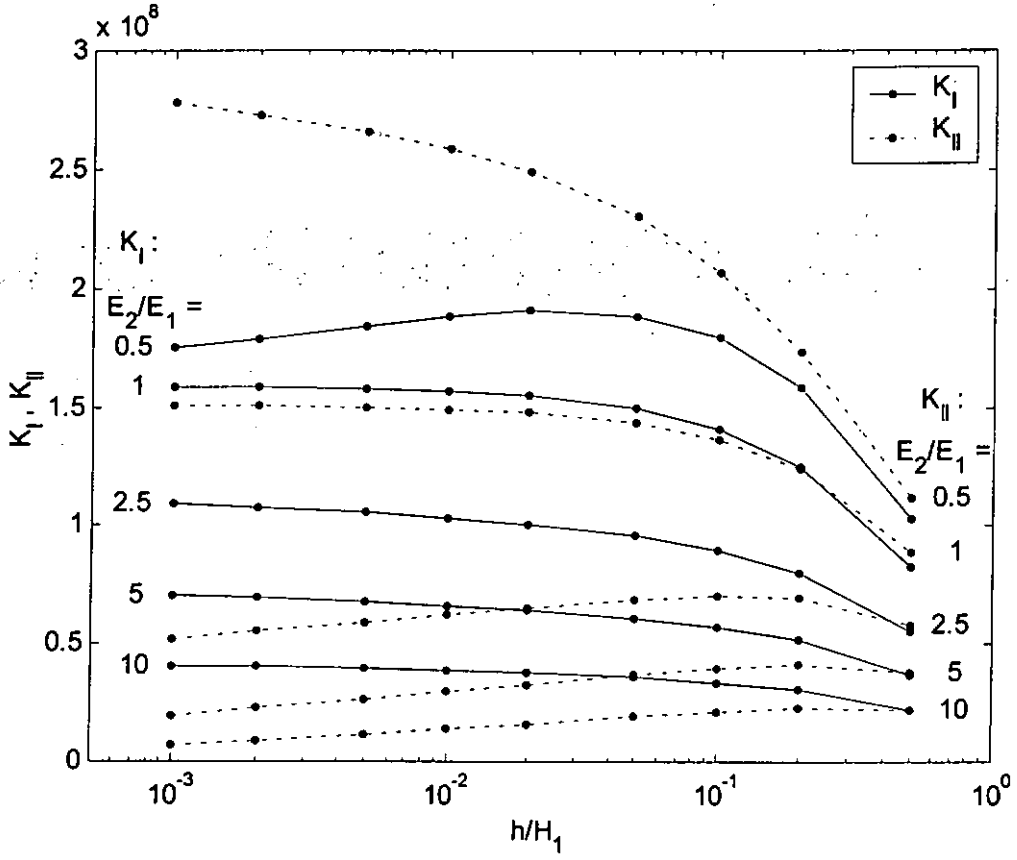

Figure IX.1d Stress Intensity Factors against the penetration ratio h/H_1 for $H_1/H_2 = 0.5$ (in logscale).

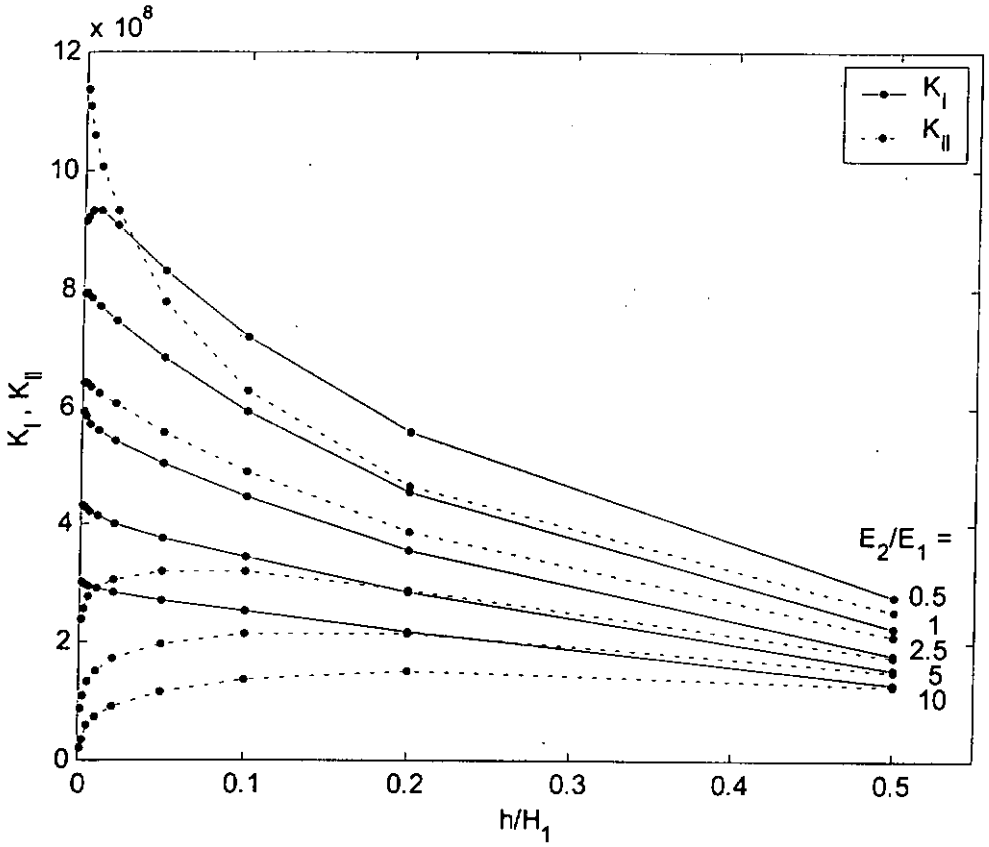

Figure IX.2a Stress Intensity Factors against the penetration ratio h/H_1 for $H_1/H_2 = 2$.

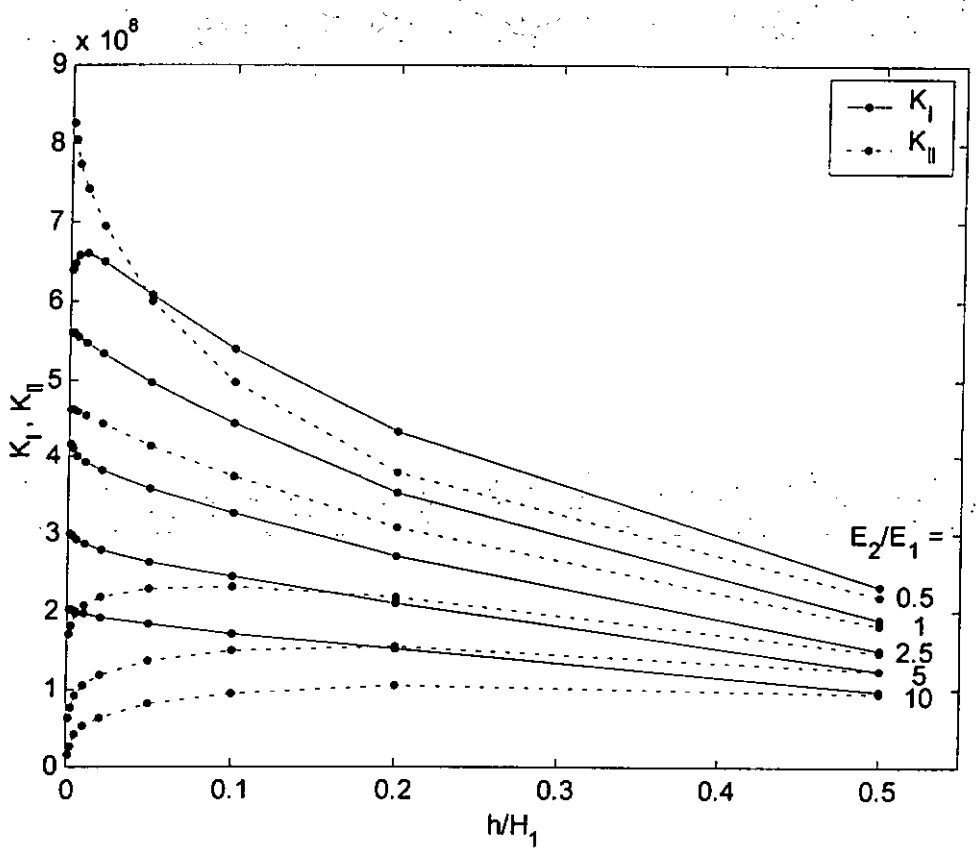

Figure IX.2b Stress Intensity Factors against the penetration ratio h/H_1 for $H_1/H_2 = 1.5$.

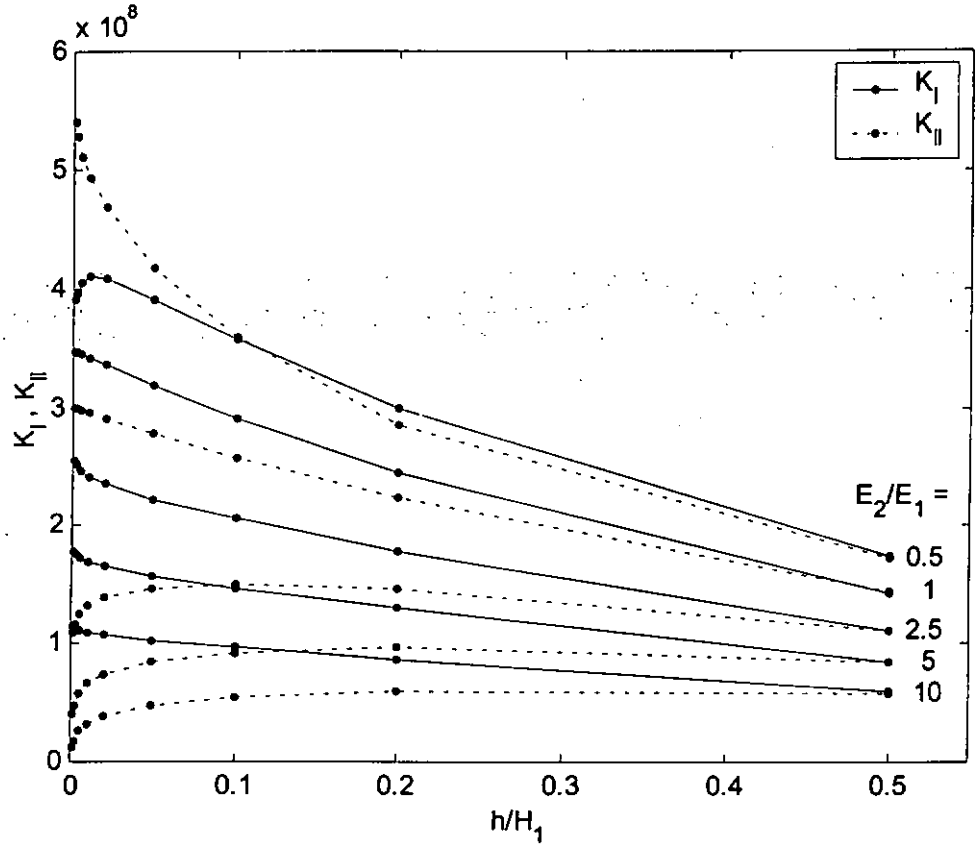

Figure IX.2c Stress Intensity Factors against the penetration ratio h/H_1 for $H_1/H_2 = 1.0$.

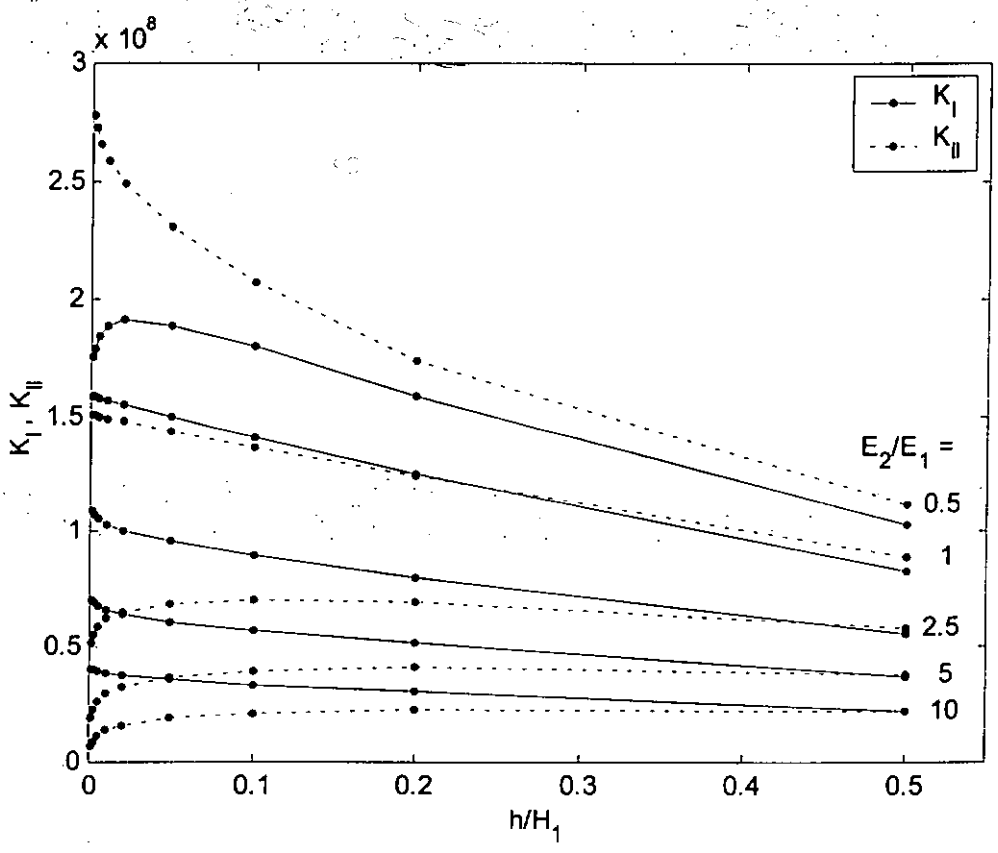

Figure IX.2d Stress Intensity Factors against the penetration ratio h/H_1 for $H_1/H_2 = 0.5$.

Appendix X Table of ϕ and the plots of Section 4.4

The values of ϕ is taken from the interpolation using the values of material constants, the Dundur's parameters α and β, on the following Table X.1 from Hutchinson et al. (1987) :

α :	-0.8	-0.6	-0.4	-0.2	-0.1	0	0.1	0.2	0.4	0.6	0.8
β :											
-0.4	-0.1202	-0.0801	-0.0467	-0.0186	-0.006	0.0058	0.0168	0.0273	0.0468	0.0653	0.081
-0.2	-0.1814	-0.1162	0.0708	-0.0351	-0.0197	-0.0056	0.0075	0.0197	0.0419	0.0618	0.0798
-0.1	-0.2057	-0.1281	-0.0764	-0.0368	-0.0199	-0.0046	0.0096	0.0227	0.0465	0.0675	0.0865
-0.05	-0.2167	-0.1328	-0.0779	-0.0363	-0.0187	-0.0027	0.012	0.0256	0.0501	0.0718	0.0912
-0.02	-0.2229	-0.1354	-0.0785	-0.0356	-0.0176	-0.0012	0.0139	0.0277	0.0527	0.0748	0.0946
0	-0.227	-0.1369	-0.0787	-0.035	-0.0167	0	0.0153	0.0293	0.0547	0.077	0.097
0.02	-0.2309	-0.1384	-0.0788	-0.0343	-0.0156	0.0013	0.0168	0.0311	0.0567	0.0793	0.0995
0.05	-0.2366	-0.1403	-0.0787	-0.033	-0.0138	0.0035	0.0193	0.0339	0.0601	0.083	0.1035
0.1	-0.2456	-0.1431	-0.078	-0.0301	-0.0101	0.0079	0.0243	0.0393	0.0663	0.09	0.111
0.2	-0.262	-0.1468	-0.0744	-0.0219	-0.0003	0.0191	0.0367	0.0528	0.0815	0.1065	0.1287
0.4	-0.2902	-0.1449	-0.0566	0.0055	0.0307	0.0531	0.0733	0.0917	0.1242	0.1522	0.1769

Table X.1 Values of $\phi(\alpha,\beta)$

The plots in FigureX.1a-d show the tendency of K_{II} when the crack gets closer to the interface.

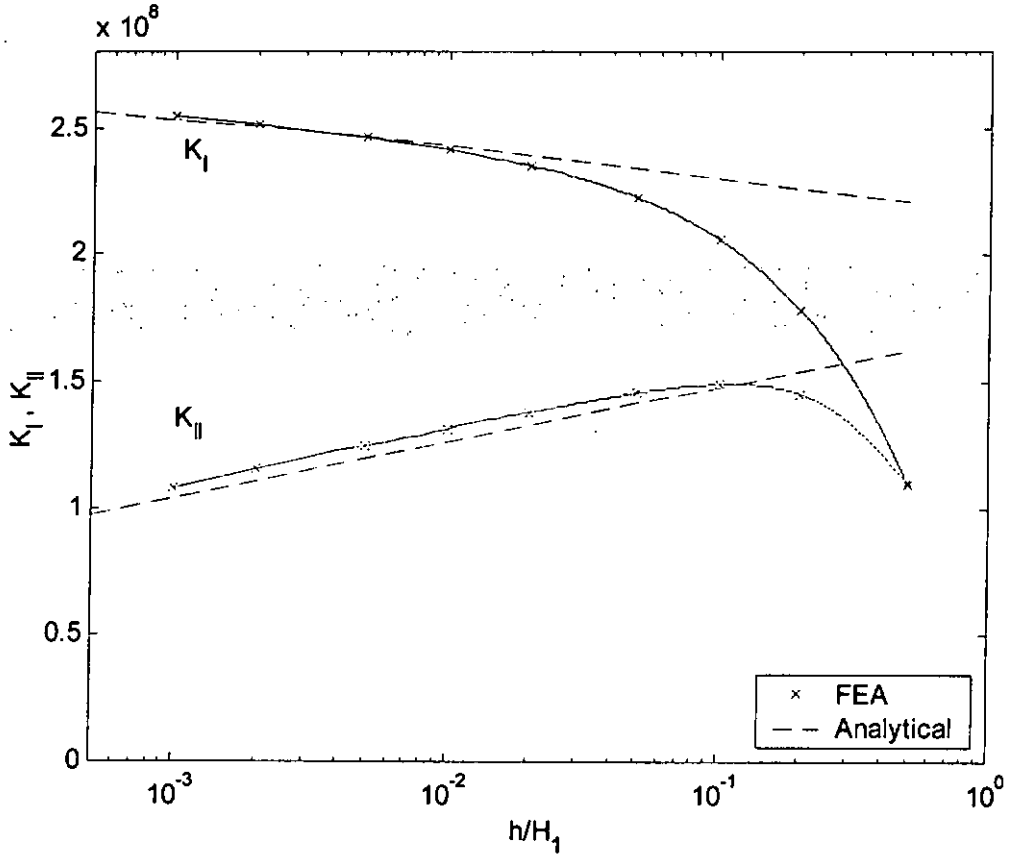

Figure X.1a Comparison of analytical solution and FEA results against relative distance of crack from interface (for $E_2/E_1 = 2.5$, $H_1/H_2 = 1$)

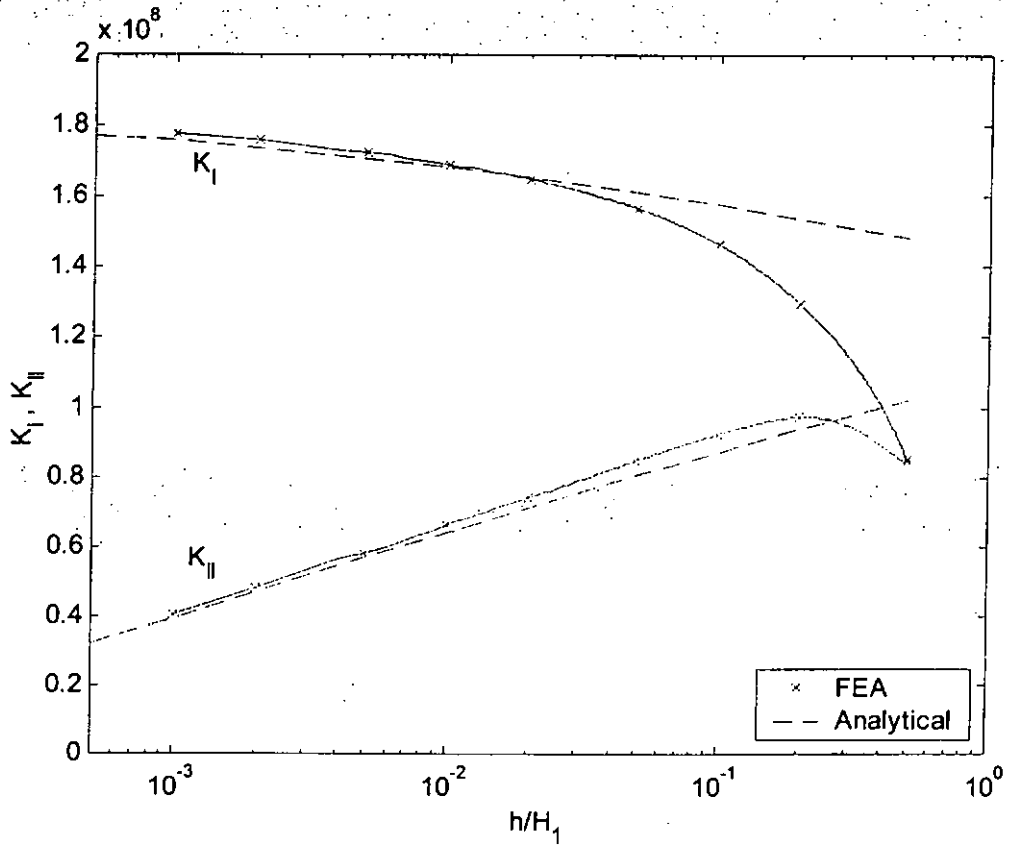

Figure X.1b Comparison of analytical solution and FEA results against relative distance of crack from interface (for $E_2/E_1 = 5$, $H_1/H_2 = 1$)

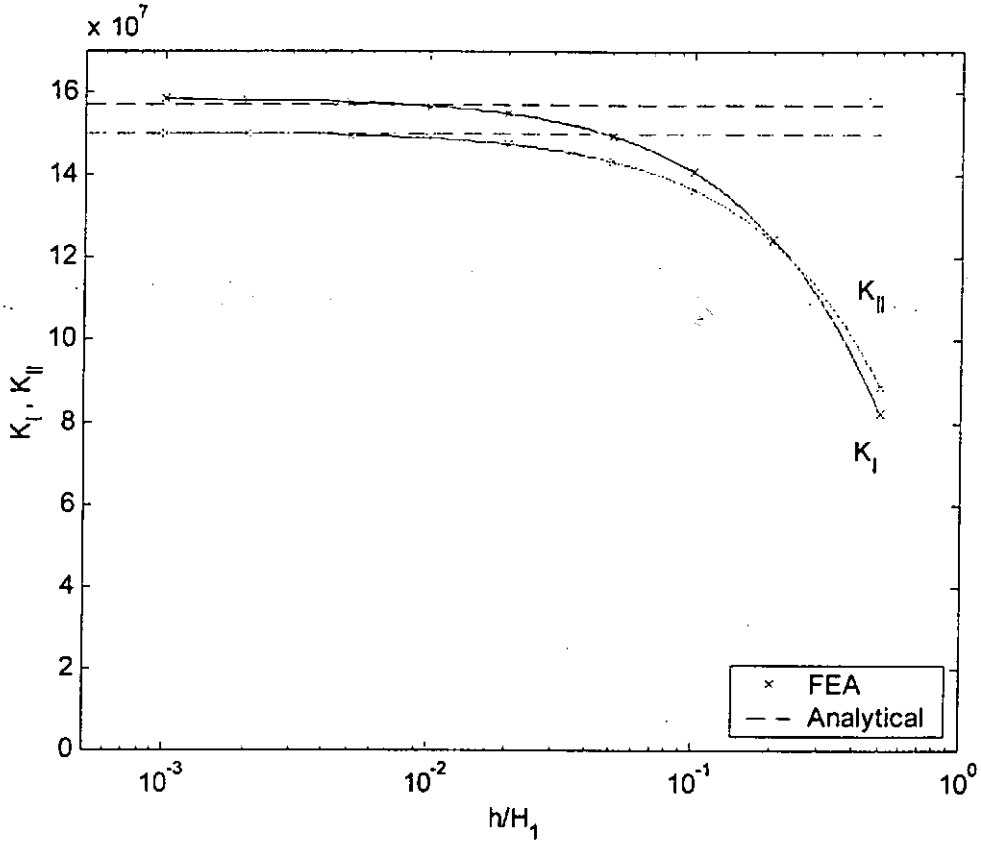

Figure X.1c Comparison of analytical solution and FEA results against relative distance of crack from interface (for $E_2/E_1 = 1$, $H_1/H_2 = 0.5$)

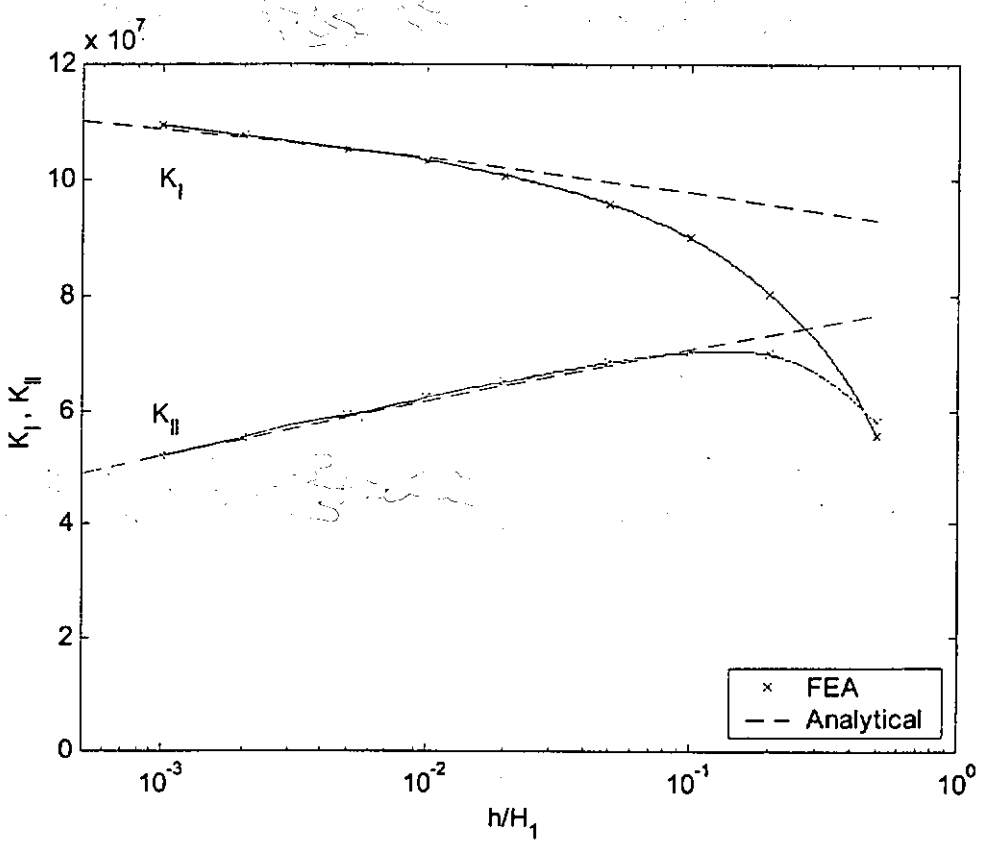

Figure X.1d Comparison of analytical solution and FEA results against relative distance of crack from interface (for $E_2/E_1 = 2.5$, $H_1/H_2 = 0.5$)

	E_2/E_1	1	2.5	5	1	2.5	5
	H_1/H_2	1	1	1	0.5	0.5	0.5
h/H_1							
1/1000		-1.42	-0.51	-1.20	-0.85	-0.48	-0.71
2/1000		-1.24	-0.35	-1.12	-0.73	-0.38	-0.64
5/1000		-0.70	0.04	-0.87	-0.38	-0.08	-0.41
1/100		0.21	0.64	-0.45	0.20	0.38	-0.03
2/100		2.03	1.81	0.37	1.39	1.28	0.71
5/100		7.67	5.36	2.92	5.04	3.95	2.95
1/10		17.61	11.80	7.59	11.50	8.61	6.84
2/10		39.96	26.97	18.72	26.03	19.14	15.56
5/10		139.21	100.31	74.11	90.96	67.63	55.65

Table X.1 Percentage (%) deviation of estimated K_I values by Equation ...(4.18) from the FEA results

	E_2/E_1	1	2.5	5	1	2.5	5
	H_1/H_2	1	1	1	0.5	0.5	0.5
h/H_1							
1/1000		-2.11	-3.90	-2.06	0.00	-0.61	0.00
2/1000		-1.95	-3.83	-2.31	0.09	-0.75	-0.45
5/1000		-1.49	-3.73	-2.70	0.38	-0.90	-0.96
1/100		-0.72	-3.69	-3.25	0.86	-1.05	-1.50
2/100		0.85	-3.55	-4.00	1.82	-1.12	-2.15
5/100		5.61	-2.83	-5.22	4.77	-0.79	-3.02
1/10		13.87	-0.77	-5.77	9.93	0.51	-3.23
2/10		31.71	5.92	-3.79	21.27	4.82	-1.49
5/10		103.30	46.68	21.17	69.41	31.65	16.81

Table X.2 Percentage (%) deviation of estimated K_{II} values by Equation ...(4.18) from the FEA results